arXiv:gr-qc/0209019 v1 6 Sep 2002

Forwarded

(Prof. D.C. Srivastava)
Supervisor
Department of Physics
DDU Gorakhpur University
Gorakhpur

Forwarded

(Prof. C.P.D. Dwivedi)
Head, Department of Physics
DDU Gorakhpur University
Gorakhpur

STUDIES IN GRAVITATIONAL WAVE DATA ANALYSIS

A thesis submitted to the

DDU GORAKHPUR UNIVERSITY

for the degree of

Doctor of Philosophy

IN PHYSICS

by

SANJAY KUMAR SAHAY

Department of Physics
DDU Gorakhpur University
Gorakhpur - 273009

December 2001

TO MY FATHER
LATE SHRI KRISHNA SAHAY

Contents

Acknowledgement **ix**

Declaration **xi**

List of Publications **xii**

Preface **xiii**

1 Introduction: Gravitational Waves, Detectors and Sources **1**

1.1 Gravitational waves 4

1.1.1 Linear field approximation 5

1.1.2 Propagation of gravitational waves 7

1.1.3 The effect of waves on free particles and its polarisation 9

1.1.4 Generation of gravitational wave 12

1.2 Gravitational wave detectors 16

1.2.1 Bar detectors 18

1.2.2 Ground based laser interferometric detectors 23

1.2.3 Laser interferometric space antenna 26

1.3 Sources of gravitational waves 28

1.3.1 Transient sources 29

1.3.2 Continuous gravitational wave 31

1.3.3 Stochastic waves 32

2 Data analysis concept **35**

2.1 Introduction 35

2.2 Gravitational wave antenna sensitivity 36

2.3 Noises in the earth based interferometric detectors 40

2.4 Matched filtering and optimal signal-to-noise ratio 43

2.5 Computational costs 48

2.6 Detection criteria 50

3 Data analysis of continuous gravitational wave: Fourier transform-I **53**

3.1 Introduction 53

3.2 The noise free response of detector: Beam pattern and amplitude modulation 55

3.3 Doppler shift and Frequency modulation 63

3.4 Fourier transform of the complete response 72

3.5 Discussion 81

4 Data analysis of continuous gravitational wave: Fourier transform-II **83**

4.1 Introduction 83

4.2 Fourier transform for one year integration 84

4.2.1 Frequency modulation 84

4.2.2 Complete response 89

4.3 Fourier transform for arbitrary observation time 96

4.4 Spin down 107

4.5 N-component signal 109

4.6 Discussion and conclusions 111

5 All sky search: Study of templates **113**

5.1 Introduction 113

5.2 Matched filter analysis: Templates 115

5.3 Number of Templates 122
5.4 Discussion 127

Appendices **129**

A Source code of the frequency modulated signal: *FM.F* **129**

B Source code of the noise free complete response of the detector: *CR.F* **133**

C Source code for the estimation of templates for all sky search: *TEM.F* **141**

Bibliography **147**

List of Tables

1.1 The existing resonant bar detectors. 22

1.2 Site and orientation of Earth based interferometric gravitational wave detectors. 24

2.1 Analytical fits to noise power spectral densities $S_n(f)$ of ground based interferometers.

5.1 Coefficients of the best fit graphs obtained for the number of templates. 124

List of Figures

1.1 Gravitational wave from binary. 2

1.2 (a) A circle of free particles before a wave travelling in the z direction reaches them. (b

1.3 An idealised gravitational wave detector with two identical masses connected with a sp

1.4 A schematic of resonant bar detector. 21

1.5 A schematic of Earth based laser interferometric gravitational wave detector. 25

1.6 A schematic diagram of the laser interferometric space antenna. 27

3.1 Orientation of the detector. 56

3.2 Earth frame (x', y', z'). 56

3.3 Solar System Barycentre frame (X', Y', Z'). 56

3.4 FT of a FM signal of a source located at $(\pi/36, \pi)$ with a resolution of 1.16×10^{-5}. 69

3.5 FT of a FM signal of a source located at $(\pi/36, \pi)$ with a resolution of 10^{-6}. 70

3.6 FT of a FM signal of a source located at $(\pi/36, \pi)$ with a resolution of 10^{-7}. 71

3.7 Power spectrum of a FM signal of a source located at $(\pi/36, \pi)$ with a resolution of 10

3.8 Power spectrum of the complete response of a Doppler modulated signal of a source lo

3.9 Power spectrum of a Doppler modulated signal at frequencies $f + 2f_{rot}$ of a source loca

3.10 Power spectrum of a Doppler modulated signal at frequencies $f - 2f_{rot}$ of a source loca

3.11 Power spectrum of a Doppler modulated signal at frequencies $f + f_{rot}$ of a source locat

3.12 Power spectrum of a Doppler modulated signal at frequencies $f - f_{rot}$ of a source locat

3.13 Power spectrum of a Doppler modulated signal at frequencies f of a source located at

4.1 FT of a FM signal of a source located at $(\pi/18, 0)$ with a resolution of 3.17×10^{-8}. 87

4.2 Power spectrum of a FM signal of a source located at $(\pi/18, 0)$ with a resolution of 3.17×10^{-8}

4.3 Power spectrum of the complete response of a modulated signal of a source located at $(\pi/18, 0)$

4.4 Power spectrum of a Doppler modulated signal at frequencies $f + 2f_{rot}$ of a source located at (π

4.5 Power spectrum of a Doppler modulated signal at frequencies $f - 2f_{rot}$ of a source located at (π

4.6 Power spectrum of a Doppler modulated signal at frequencies $f + f_{rot}$ of a source located at (π

4.7 Power spectrum of a Doppler modulated signal at frequencies $f - f_{rot}$ of a source located at (π

4.8 Power spectrum of a Doppler modulated signal at frequencies f of a source located at $(\pi/18, 0)$

4.9 FT of a FM signal of a source located at $(\pi/9, \pi/4)$ with a resolution of 9.67×10^{-8}. 98

4.10 FT of the complete response of a Doppler modulated of a source located at $(\pi/9, \pi/4)$ with a re

4.11 Power spectrum of a FM signal of a source located at $(\pi/9, \pi/4)$ with a resolution of $9.67 \times 10^{-}$

4.12 Power spectrum of the complete response of a Doppler modulated signal of a source located at

4.13 Power spectrum of a Doppler modulated signal at frequencies $f + 2f_{rot}$ of a source located at (π

4.14 Power spectrum of a Doppler modulated signal at frequencies $f - 2f_{rot}$ of a source located at (π

4.15 Power spectrum of a Doppler modulated signal at frequencies $f + f_{rot}$ of a source located at (π

4.16 Power spectrum of a Doppler modulated signal at frequencies $f - f_{rot}$ of a source located at (π

4.17 Power spectrum of a Doppler modulated signal at frequencies f of a source located at $(\pi/9, \pi/4$

5.1 Variation of FF with θ_T. 118

5.2 Variation of FF with ϕ_T. 119

5.3 Variation of FF with ϕ_T. 120

5.4 Variation of number of templates with FF for fixed f_o at different T_o.125

5.5 Variation of number of templates with FF for fixed T_o and of frequencies.126

ACKNOWLEDGEMENT

I would like to thank Prof. D.C. Srivastava, my thesis Supervisor whose guidance and constant encouragement throughout the course of the work has been a pleasant, rich and a rewarding experience. I am thankful to my colleague Dr. S.S. Prasad, UNPG College, Padrauna for various useful discussions and comments. A part of the work has been carried out during my various visits at IUCAA, Pune. I have been benefited by the discussions, comments and suggestions of IUCCA Scientists notably of Prof. S.V. Dhurandhar. I am indebted to all of them for their kindness and help. I thankfully acknowledge the local hospitality, financial support, computer and library facilities made available to me during the course of stay. I would like to thank Prof. A.K. Kembhavi, Dean Visitor Academic Programmes and Mrs. S. Shankar, Administrative Officer, Visitor Services, and staff members of IUCAA for their kind cooperation and assistance during the course of stay in IUCAA. In this connection, my heartfelt thanks are also to Prof. J.V. Narlikar, Director, IUCAA for creating such a stimulating research atmosphere in IUCAA.

I am thankful to friends and the staff members of Physics Department for extending me moral support during the work. I would also like to thank Prof. R.M. Misra, Vice-Chancellor, DDU Gorakhpur University for providing requisite facilities for the research work. I am also thankful to the staff of the Computer Centre of the University for providing me necessary facilities.

I would like to thank Drs. B.S. Sathyaprakash and S. Bose, Cardiff, U.K. for various useful suggestions. I also like to thank Prof. A.R. Tharafdar, Convener, Indian Institute of Technology, Kharagpur for local hospitality and computational facility during my visit there.

My heartfelt special thanks are due to my mother and sisters for their love and continuous support.

I gratefully acknowledge the grant of a fellowship from Department of Science and Technology, New Delhi vide research grant number SP/S2/0-15/93.

Place: Gorakhpur (Sanjay Kumar Sahay)
Date:

DECLARATION

Certified that the work incorporated in the thesis ***'Studies in Gravitational Wave Data Analysis'*** submitted by Mr. **Sanjay Kumar Sahay** was carried out by the candidate under my supervision. Such materials as have been obtained from other sources has been duly acknowledged in the thesis.

Place: Gorakhpur
Date:

(Prof. D.C. Srivastava)
Supervisor
Department of Physics
DDU Gorakhpur University
Gorakhpur

LIST OF PUBLICATIONS

1. Srivastava, D.C and Sahay, S.K., *Data analysis of continuous gravitational wave: Fourier transform*, Preprint gr-qc/0009094 (2000).

2. Srivastava, D.C and Sahay, S.K., *Analysis of noise free response of interferometric antenna to Gravitational Radiation I & II*, Proceedings of the Fourth International Conference on Gravitation and Cosmology, Pramana J. Phys. **55**, 589 (2000).

3. Srivastava, D.C and Sahay, S.K., *Data analysis of continuous gravitational wave: Fourier transform-I*, communicated to Monthly Not. RAS (2001).

4. Srivastava, D.C and Sahay, S.K., *Data analysis of continuous gravitational wave: Fourier transform-II*, communicated to Monthly Not. RAS (2001).

5. Srivastava, D.C and Sahay, S.K., *Data analysis of continuous gravitational wave: All sky search and study of templates*, communicated to Monthly Not. RAS (2001).

Preface

This thesis is devoted to the investigations of gravitational wave data analysis from a continuous source e.g. a pulsar, a binary star system. The research in the field of gravitational radiation started after its formulation by Einstein in (1916) as propagating gravitational disturbance described by the linearised field limit of his General Theory of Relativity (GR) but has received serious impetus towards its detection after the announcement of its detection by Weber in 1969 using aluminium bar detectors. This field has now emerged and established itself with General Relativity (GR), Astrophysics and Numerical analysis as its equally important facets. Ofcourse, the technological advancements being employed in the construction of detectors with day by day improving sensitivity have played the crucial role. To date, although the results of Weber could not be confirmed and we do not have as yet any direct detection of gravitational wave (GW) yet it is not a matter of concern. Because on one hand the sensitivity required for the announcement of definite detection of GW bathing earth is yet to be achieved by the detectors whereas on the other hand we have an indirect evidence of the existence of GW observed in 1974 as the slowing down of the binary pulsar PSR 1913 + 16 arising because of back reaction of GW emission. GW Scientists all over the globe are putting more persuasive arguments regarding the feasibility of GW detection in 'near future' and the advantages to be achieved once the "Gravitational Wave Astronomy" as they call it, is established. A huge amount of money is

involved in these projects to the extent that many of the detectors are built in collaboration e.g. American Laser Interferometric Gravitational Wave Observatory (LIGO), Italian French Gravitational Wave Observatory (VIRGO), British-German Observatory (GE0600). As a consequence the literature is full of update reviews on gravitational wave astronomy notably by Thorne (1987), Blair (1991), Schutz (1999), Grishchuk et.al (2000), where the related issues viz., the fall outs, pre-requisites and prospects are discussed and scrutinised with rigour and minute detail.

The thesis starts with two introductory Chapters dealing with gravitational wave and data analysis concepts, respectively. The matter covered in these Chapters are restricted to the extent they are supposed to provide continuity and coherence to the investigations presented in Chapters 3-5. Further, the material presented in these chapters depend heavily on the reviews by Grishchuk (2000), Schutz (1999), Sathyaprakash (1999). Our job have been, frankly speaking, to cut and paste. Let us hope this has not defaced the truth. For the portion describing GR we have adopted notations and conventions of Schutz (1989). The source codes of the numerical computations are relegated to the appendices A-C.

The term "Pulsar" used in the thesis refers to spinning neutron stars. A Pulsar will emit GW signal over extended period of time only when it has long-lived asymmetry. Several mechanisms have been given for such an asymmetry to arise. Some Pulsars emit GW almost monochromatically and are remarkably good clocks as its periods have been measured upto 13 significant digits. However, the GW signals from Pulsars are very weak ($\leq 10^{-25}$) and will be buried in the broadband noise of the detector. In order to detect the signal from the dominant noise one has to analyse the long time observation data of months/years. The output of detector is highly involved function of many

initial parameters. It is usually not possible to obtain the Fourier Transform (FT) analytically. Hence, FT has to be obtained via numerical methods. But it appears to be computationally demanding even for the standard computers expected to be available in near future. Therefore, one will have to work with efficient data analysis techniques, efficient not only in picking weak signal from the noisy data but also in terms of computing-cost requirements. Chapter 2 is on the problem and technique for the data analysis. The noises and sensitivity of the detector has been briefly described. The *Matched Filtering*, a technique of the optimal method for detecting unknown signal and which describes drop in signal-to-noise ratio in terms of *Fitting Factor* (FF), is discussed. The computational cost and detection criteria are also discussed.

The output of detector will be Doppler modulated (both in frequency and in amplitude) due to the motions of Earth and star. To work in Fourier space, one usually employs the numerical method called Fast Fourier Transform (FFT). Fortunately, we have been able to develop analytical FT. We have employed the results to obtain efficient data analysis algorithms for continuous gravitational wave (CGW).

In Chapter 3 we have studied the noise free complete response of Laser Interferometer detector for CGW for its arbitrary location and that of the source. We have taken into account the rotational motion of Earth about its spin axis as well as its orbital motion around Sun. We have developed analytical FT of Frequency modulated output for one day observation time. In Chapter 4 this analysis has been generalised for (i) one year observation time and for (ii) any arbitrary duration of observation data set. The emission of GW from pulsars as such may contain two or more frequencies. Hence, we finally generalise the transform for N-component signal. We also give the method to account for spin down of CGW. The Frequency modulation (FM) smears out

a monochromatic signal into a small bandwidth around the signal frequency. The FT contains double series of Bessel functions and the computational cost depends primarily because of Bessel functions which in turn depends on source location and frequency.

The Amplitude modulation (AM) arises due to the anisotropic response of the detector i.e. the detector possesses a quadrupole antenna pattern. The effect of AM is to split the signal frequency f_o into five lines corresponding to frequencies $f_o \pm 2f_{rot}$, $f_o \pm f_{rot}$ and f_o where f_{rot} represents the rotational frequency of Earth. Hence, for optimal detection of Amplitude modulated signal one will need four additional linear filters. For a 2-component pulsar signal the number of filters will increase further by a factor of 2. The cases of Doppler modulation investigated by us reveal that as a result of the AM the most of the power lies in the frequency band $f + 2f_{rot}$ and the least in the frequency $f - 2f_{rot}$.

An important advantage of our analytical results over FFT arises when one looks for the resolution of the FT. The resolution offered by the FFT is inversely proportional to the observation time, T_o whereas, the analytical FT is independent of T_o. This means that for short observation time the resolution offered by FFT is small whereas for long observation time there would be high computational demands. We have developed, using our analytical FT, a semi-analytical formula to calculate the Doppler shift for one year observation data for any source location and frequency. A monochromatic signal of one kHz frequency from a source located at $\theta = \pi/2$ is found to spread into approximately 3.13 millions Fourier bins. We observe that the number of Fourier bins increases with the source location θ and frequency f_o.

The strategy for the detection of GW signal is to make use of FT to dig out the signal from the noisy output of detectors. To achieve this, one constructs

the templates which are best educated guesses of the expected signal waveform. In Chapter 5 we have applied our results on FT obtained in chapter 4. Applying the technique of *Matched Filtering* we have computed the number of templates required for all sky search problem for a pre-assigned (FF). It is estimated that one would require about 1.44×10^{10}, 3.5×10^{10} and 5.5×10^{10} number of templates for respective data analysis of 30, 120 and 365 days for a FF of 0.97. We have studied the variation of the estimated number of templates with frequency. It is found that the numbers of templates required are approximately 1.22×10^{10}, 2.16×10^{10} and 5×10^{10} for respective signal frequencies 20, 50 and 100 Hz for analysing data of 120 days with a FF of 0.97. In this Chapter we have also studied the variation of the FF with source location $[\theta, \phi]$ and have found a marked symmetry. The FF for any arbitrarily chosen θ, is the same as corresponding to $\pi - \theta$. Similar symmetry have also been observed for ϕ. This symmetry property will reduce the computation burden by a factor of four for all sky search problem. It is not clear whether this symmetry property can be established analytically as well. However the source location, because of this symmetry, becomes uncertain and its exact location determination will require t he use of other methods.

The thesis has been typeset by the candidate in LaTeX.

Chapter 1

Introduction: Gravitational Waves, Detectors and Sources

Gravitational waves (GW) like any other type of waves are propagating perturbations of some flat background space-time. These are identified as small ripples rolling across space-time in the same manner as water waves are on an otherwise flat ocean. These waves originate from the most energetic events in our Universe such as rotating neutron stars, colliding neutron star binaries, supernovae explosions and gravitational collapse in Black Holes. They manifest themselves as strains in space-time that periodically stretch and compress matter. The GW emanating from a binary may be represented as in Fig. (1.1).

Newtonian gravitation does not have the provision for GW. In several Lorentz covariant gravitational theories e.g. scalar, vector, tensor theories the GW arise as the spreading out gravitational influence. The basis of most current thinking of GW is Einstein's theory of General Relativity (GR). In fact, GW was first studied by Einstein in 1916 by applying linear field approximation to GR. However, he was misled to the result that an accelerated spherical mass would emit GW. He corrected his mistake in 1918 and showed that the first order term of GW was quadrupolar. We discuss the properties of GW in the next section.

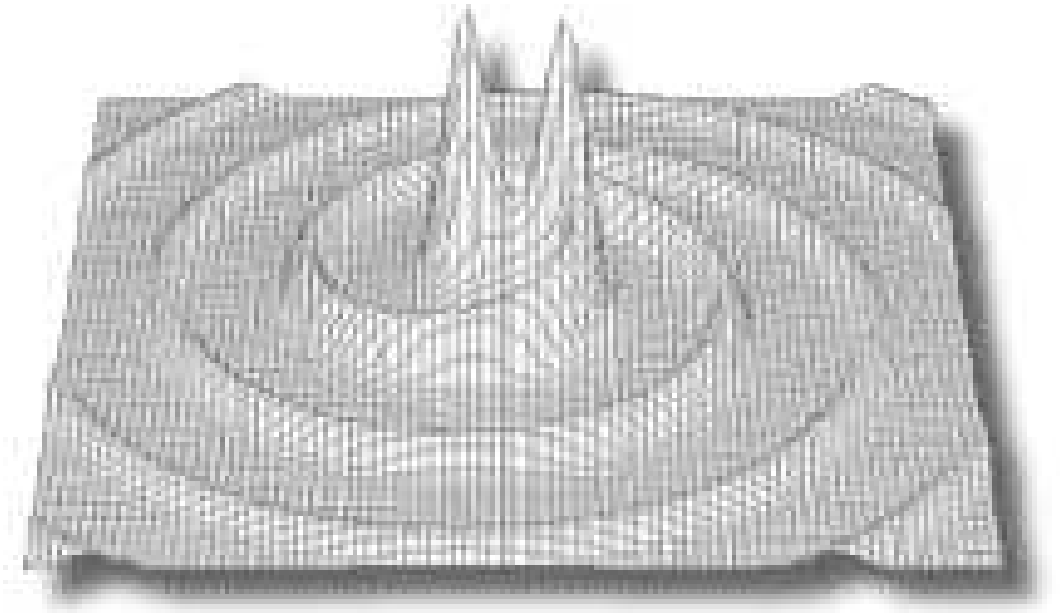

Figure 1.1: Gravitational wave from binary.

The strength of GW is so small that there is no hope of its detection in the manner Hertz demonstrated the existence of electromagnetic waves. The reason may be attributed to the extremely small value of the universal constant of gravitation ($G = 6.7 \times 10^{-11} \mathrm{Nm}^2\mathrm{kg}^{-2}$). The dimensionless amplitude of typical GW reaching the earth is only of the order of 10^{-17}. This put in other words means that such a GW will put a rod of one meter length into a oscillation with an amplitude of one millionth of the radius of a hydrogen atom. Any chance to observe the effects of GW would require acceleration of astrophysical size masses at relativistic speeds. Several GW-detectors are being built at present, or have been proposed for the future, that hope to detect these very small vibrations. The best known of these are the *Laser Interferometer Ground Observatory*; LIGO, and the *Laser Interferometer Space Antenna*; LISA. As the names suggest, the former is a terrestrial observatory and the latter a space based one. Needless to say, what enormous engineering achievements these detectors require to detect the oscillations mentioned

above.

The interaction of GW with matter is also very small and this leads to some profound benefits for astrophysics. The wave will not scatter, so they emanate undisturbed from the regions of their origin viz., densest regions of the Universe, inner cores of imploding stars, the earliest instants of the primeval Universe, and the formation of Black Holes. Hence, they will provide information on the dynamics in these regions about which there are no other means.

A piece of indirect evidence affirming the existence of GW came in 1974 when Joseph Taylor and Russell Hulse studied the pulsar PSR 1913+16 which is a binary partner of compact neutron star and is orbiting around the other in a slowly decreasing eight hour period. The orbital frequency acceleration was observed to be in perfect agreement with what expected from the energy loss arising due to their calculated GW emission (Damour and Taylor, 1992). For their accomplishment, Hulse and Taylor were awarded the 1993 Nobel Prize.

Unfortunately PSR 1913 + 16 is presently emitting GW too feeble for their direct detection on Earth and such a condition will continue until the end of its pas-de-deux inspiral some 350 million years hence. Interestingly, the density of observed binaries in our galaxy is such that a few late stage inspiral events are expected per century to occur. Hence, the study of the orbits of the binary neutron star system and their coalescence have played important role in the setting design criteria for some of the instruments to come into operation in the next few years. To the date we have only the indirect evidence of GW. Yet this has not been of much concern for theoretical physicists because the strength of the postulated GW signals are below the detection threshold currently available.

The quest to detect GW started in its earnest as early as in 1965 with

the pioneering work of J. Weber on resonating bars. These are basically high quality *bells* designed to be rung by transient GW. With this beginning a small GW detection community has arisen and thrived continuing to improve on the original idea. The main effort is directed towards noise reduction by introducing ever lower cryogenic temperature and ever more sensitive displacement sensor to improve detector sensitivity. Many more bars; progressively sophisticated ones have been built. The *Explorer* which is quietly functioning at CERN since 1989, is one such detector worth mention. We discuss GW detectors in section 2.

There is an excellent prospect of detection of GW in the near future. There will emerge what has been called "Gravitational Wave Astronomy". This will provide another window for observing Universe. The expectation is that it will uncover new phenomena as well as add new insights into phenomena already observed in electromagnetic part of the spectrum. GW emanate due to the accelerated motions of mass in the interior of objects. As remarked earlier, these regions are otherwise obscure in electromagnetic, and possibly, even in neutrino astronomy. The GW arise due to the coherent effects of masses moving together rather than individual motions of smaller constituents such as atoms or charged particles which generate the electromagnetic radiation.

1.1 Gravitational waves

The gravitational waves like electromagnetic waves may be defined as time varying gravitational fields in absence of its sources. The gravitation theory, widely believed, is the one proposed by Einstein and famous as GR. In its

mathematical essence it is expressed via the equation known by his name viz.

$$\mathrm{G}_{\alpha\beta} = \mathrm{R}_{\alpha\beta} - \frac{1}{2} g_{\alpha\beta}\mathrm{R} = 8\pi \mathrm{T}_{\alpha\beta}{}^{1} \tag{1.1}$$

The conceptual meaning of this equation is that a localized density distribution characterised by the energy momentum tensor, $T_{\alpha\beta}$ curves the space-time around it. The curvature and other geometrical properties of the space-time are characterised by Ricci curvature tensor $R_{\alpha\beta}$ and the underlying metric tensor $g_{\alpha\beta}$. The curved space-time forces a free mass particle or light to follow the geodesics. These geodesics measure the effect of gravitation. The GR in its weak field limit yields the Newton's theory of gravitation. In this approximation the gravitational field is considered to be represented by a metric with a linear modification of the background Lorentz space-time metric, $\eta_{\alpha\beta}$. It is important to remark that many of the basic concepts of GW theory can be understood in this approximation and were introduced and developed by Einstein himself. At present GW theory; its issues and problems, are dealt in detail in research text books of GR. Due to the limited scope of the thesis we base our discussion on linear field approximation and incorporate few aspects of GW required for understanding of the subject matter presented in the thesis.

1.1.1 Linear field approximation

The metric of the space-time may be expressed as

$$g_{\alpha\beta} = \eta_{\alpha\beta} + h_{\alpha\beta} \ , \qquad |h_{\alpha\beta}| \ll 1 \tag{1.2}$$

It is straight forward to compute Einstein tensor, $G_{\alpha\beta}$ and one obtains

$$G_{\alpha\beta} = -\frac{1}{2}\left[\bar{h}_{\alpha\beta,\,\mu}{}^{,\mu} + \eta_{\alpha\beta}\bar{h}_{\mu\nu}{}^{,\mu\nu} - \bar{h}_{\alpha\mu,\,\beta}{}^{,\mu} - \bar{h}_{\beta\mu,\,\alpha}{}^{,\mu} + O\left(h^2_{\alpha\beta}\right)\right] \tag{1.3}$$

[1]For notations, conventions and basic definitions the reader may refer to Schutz (1989)

where

$$\bar{h}^{\alpha\beta} = h^{\alpha\beta} - \frac{1}{2}\eta^{\alpha\beta}h\,; \qquad h = h^{\alpha}{}_{\alpha} = -\bar{h}^{\alpha}{}_{\alpha} \tag{1.4}$$

We raise and lower the tensor indices using the Lorentz metric. Let us note that the expression for $G_{\alpha\beta}$ would simplify considerably if we could require

$$\bar{h}^{\mu\nu}{}_{,\nu} = 0 \tag{1.5}$$

In fact, there is a gauge freedom available as infinitesimal coordinate transformation defined as

$$x^{\alpha} \longrightarrow x'^{\alpha} = x^{\alpha} + \xi^{\alpha}\left(x^{\beta}\right), \quad |\xi^{\alpha}| \ll 1 \tag{1.6}$$

where ξ^{α} is arbitrary. This gauge transformation preserves (1.2). It can be shown that, in order to achieve the condition (1.5), ξ^{α} has to be chosen as to satisfy

$$\Box\xi^{\mu} = \xi^{\mu\nu}{}_{,\nu} = \bar{h}^{(old)\mu\nu}{}_{,\nu} \tag{1.7}$$

where the symbol $\Box$ is used for the four dimensional Laplacian:

$$\Box f = f^{,\mu}{}_{,\mu} = \eta^{\mu\nu} f_{,\mu\nu} = \left(-\frac{\partial^2}{\partial t^2} + \bigtriangledown^2\right) f \tag{1.8}$$

The gauge condition defined via (1.5) is called Lorentz gauge. We adopt this gauge. In literature harmonic gauge and de Donder gauge are other names for this gauge. The Einstein tensor, to the first order in $h_{\alpha\beta}$ becomes

$$\mathrm{G}^{\alpha\beta} = -\frac{1}{2}\Box\bar{h}^{\alpha\beta} \tag{1.9}$$

Thus the weak-field Einstein equations take the form

$$\Box\bar{h}^{\mu\nu} = -16\pi\mathrm{T}^{\mu\nu} \tag{1.10}$$

In the Newtonian limit where the gravitational fields are too weak to produce velocities near the speed of light,

$$|\mathrm{T}^{oo}| \gg \left|\mathrm{T}^{oj}\right| \gg \left|\mathrm{T}^{ij}\right| \; ; \quad \mathrm{T}^{oo} \simeq \varrho \, , \quad \Box^2 \simeq \bigtriangledown^2 \tag{1.11}$$

Equation (1.10) now results into

$$\bigtriangledown^2 \bar{h}^{oo} = -16\pi\varrho \tag{1.12}$$

This equation may be compared to Newtonian equation for gravitational potential, φ i.e.

$$\bigtriangledown^2 \varphi = -4\pi\varrho \tag{1.13}$$

One obtains, after some calculations

$$h^{oo} = 2\varphi \, , \quad h^{xx} = h^{yy} = h^{zz} = -2\varphi \tag{1.14}$$

and accordingly the space-time metric for a Newtonian gravitational field is represented via

$$ds^2 = -(1+2\varphi)dt^2 + (1-2\varphi)(dx^2 + dy^2 + dz^2) \tag{1.15}$$

1.1.2 Propagation of gravitational waves

The GW in the regions far away from its sources may be described in the weak field approximation. The Einstein equations, in absence of matter and electromagnetic fields ($T_{\alpha\beta} = 0$) take the form

$$\Box \bar{h}^{\mu\nu} = \left(-\frac{\partial^2}{\partial t^2} + \bigtriangledown^2 \right) \bar{h}^{\alpha\beta} = 0 \tag{1.16}$$

This is the three dimensional wave equation and its solution may be taken as

$$\bar{h}^{\alpha\beta} = \mathrm{A}^{\alpha\beta} exp\,(ik_\gamma x^\gamma) \tag{1.17}$$

where $\left\{\mathrm{A}^{\alpha\beta}\right\}$ are constant components of some tensor and $\{k_\alpha\}$ are the constant components of some one form satisfying the equation:

$$\eta^{\mu\nu}k_\mu k_\nu = k^\nu k_\nu = 0 \tag{1.18}$$

This means that (1.17) represents a solution of (1.16) provided k_γ is null one form and the associated four vector k^α is null. The value of $\bar{h}^{\alpha\beta}$ is constant on a hyper surface on which $k_\alpha x^\alpha$ is constant i.e.

$$k_\alpha x^\alpha = k_o t + \mathbf{k}.\mathbf{x} = const.\,; \qquad \mathbf{k} = \{k^i\} \tag{1.19}$$

It is conventional to refer k^o as w, which is called the frequency of wave:

$$k^\alpha : (w, \mathbf{k}) \tag{1.20}$$

The gauge condition (1.5) now requires

$$\mathrm{A}^{\alpha\beta}k_\beta = 0 \tag{1.21}$$

which means that $\mathrm{A}^{\alpha\beta}$ must be orthogonal to k_β.

The solution (1.17) represents a plane wave propagating with velocity of light. In physical applications one has to consider the real part of the solution. Having obtained the solution $\bar{h}^{\alpha\beta}$ one still has the freedom of choosing specific ξ^α with the requirement that it represents some solution of the Eq. (1.7); which in view of (1.16) becomes

$$\left(-\frac{\partial^2}{\partial t^2} + \nabla^2\right)\xi^\alpha = 0 \tag{1.22}$$

Let us take its solution as

$$\xi_\alpha = \mathrm{B}_\alpha \exp(ik_\mu x^\mu) \tag{1.23}$$

where B_α is constant. It can be shown that the freedom available in choosing the values of B_α may be employed such that new $\mathrm{A}_{\alpha\beta}$ satisfy the conditions

$$\mathrm{A}^\alpha{}_\alpha = 0 \tag{1.24}$$

$$\mathrm{A}_{\alpha\beta}\mathrm{U}^\beta = 0 \tag{1.25}$$

where U^α is some fixed four velocity. Eqs. (1.21), (1.24) and (1.25) are called the transverse traceless (TT) gauge conditions. We choose U^α as time basis vector $U^\alpha = \delta^\alpha_0$. Let us take the direction of propagation of the wave as the z axis of the coordinate system. Now using (1.18) and (1.20) we have $k^\mu : (w, 0, 0, w)$. Now Eq. (1.25) in view of (1.21) implies (i) $A_{\alpha 0} = 0$ and (ii) $A_{\alpha z} = 0$ for all α. This is the reason the gauge is called 'transverse' gauge. Further the trace free condition (1.24) require $A_{xx} = -A_{yy}$. Now the non vanishing component of $A_{\alpha\beta}$ may be expressed as

$$A^{TT}_{\mu\nu} = \begin{pmatrix} 0 & 0 & 0 & 0 \\ 0 & A_+ & A_\times & 0 \\ 0 & A_\times & -A_+ & 0 \\ 0 & 0 & 0 & 0 \end{pmatrix} ; \quad A_{xx} = A_+ , \; A_{xy} = A_\times \tag{1.26}$$

Thus there are only two independent components of $A_{\alpha\beta}$; A_+ and $A_\times$. Let us note that traceless condition (1.24) results into

$$\bar{h}^{TT}_{\alpha\beta} = h^{TT}_{\alpha\beta} \tag{1.27}$$

We have considered the plane wave solution of Eq (1.16). We know that any solution of Eqs. (1.21) and (1.16) may be expressed, because of theorems on Fourier analysis, as a superposition of plane waves. Hence if we consider the waves propagating along z axis we can put all such planes waves in the form (1.27). Thus any wave has only two independent components h^{TT}_{xx} and h^{TT}_{xy} represented respectively as h_+ and $h_\times$ corresponding to A_+ and $A_\times$.

1.1.3 The effect of waves on free particles and its polarisation

The independent components h_+ and $h_\times$ represent the polarisation states of the wave. To understand their nature in little detail it is instructive to discuss

the effect of GW as it hits a free particle. Let us choose a background Lorentz frame in which the particle is initially at rest. We may employ the initial four velocity of the particle ($\mathrm{U}^\alpha = \delta^\alpha_{\ 0}$) to define the TT gauge of the wave. A free particle obeys the geodesic equation

$$\frac{d\mathrm{U}^\alpha}{d\tau} + \Gamma^\alpha_{\ \mu\nu}\mathrm{U}^\mu\mathrm{U}^\nu = 0 \tag{1.28}$$

This equation may be used to obtain the initial acceleration of the particle:

$$\left(\frac{d\mathrm{U}^\alpha}{d\tau}\right)_{t=0} = -\Gamma^\alpha_{\ 00} = -\frac{1}{2}\eta^{\alpha\beta}\left(h_{\beta 0,\,0} + h_{0\beta,\,0} - h_{00,\,\beta}\right) \tag{1.29}$$

In view of Eqs. (1.17), (1.26) and (1.27). the initial acceleration of the particle vanishes. This means that the particle will be at rest a moment later and consequently will be there forever. What does it mean ? Is there no effect of the GW on a free particle ? No, the interpretation presented at its face value is quite misleading. The result only means that the choice of the TT gauge employed resulted into a coordinate system for the wave which stays attached to the individual particles.

To get a better measure of the effect of the wave let us consider two nearby particles situated at the origin $(0,0,0)$ and on the x axis, $(\bar{\epsilon},0,0)$ separated by a distance $\bar{\epsilon}$. In view of our above discussion the particles remain at their initial coordinate positions. The proper distance between them is

$$\begin{aligned}
\triangle\, l &= \int \left|ds^2\right|^{1/2} = \int \left|g_{\alpha\beta}dx^\alpha dx^\beta\right|^{1/2} \\
&= \int_0^\epsilon |g_{xx}|^{1/2}\, dx \approx |g_{xx}(x=0)|^{1/2}\,\bar{\epsilon} \\
\triangle l &= \left\{1 + \frac{1}{2}h^{TT}_{xx}(x=0)\right\}\bar{\epsilon}
\end{aligned} \tag{1.30}$$

Thus the proper distance between two particles (as opposed to their coordinate distance) does change with time. The effects of the wave may also be described

in terms of the geodesic deviation of the separation vector, η^α, connecting the two particles. It obeys the equation

$$\frac{d^2}{d\tau^2}\eta^\alpha = \mathrm{R}^\alpha{}_{\mu\nu\beta}\mathrm{U}^\mu\mathrm{U}^\nu\eta^\beta \tag{1.31}$$

It can be shown that for the particles initially having the separation vetor, $\eta^\alpha \longrightarrow (0, \bar{\epsilon}, 0, 0)$ one would get

$$\frac{\partial^2}{\partial t^2}\eta^x = \frac{1}{2}\bar{\epsilon}\frac{\partial^2}{\partial t^2}h^{TT}_{xx}, \quad \frac{\partial^2}{\partial t^2}\eta^y = \frac{1}{2}\bar{\epsilon}\frac{\partial^2}{\partial t^2}h^{TT}_{xy} \tag{1.32}$$

Similarly, for initial separation vector, $\eta^\alpha \longrightarrow (0, 0, \bar{\epsilon}, 0)$ we would get

$$\begin{aligned} \frac{\partial^2}{\partial t^2}\eta^y &= \frac{1}{2}\bar{\epsilon}\frac{\partial^2}{\partial t^2}h^{TT}_{yy} = -\frac{1}{2}\bar{\epsilon}\frac{\partial^2}{\partial t^2}h^{TT}_{xx} \\ \frac{\partial^2}{\partial t^2}\eta^x &= \frac{1}{2}\bar{\epsilon}\frac{\partial^2}{\partial t^2}h^{TT}_{xy} \end{aligned} \tag{1.33}$$

Let us note that in view of the results of the previous section we may write (1.17) as

$$h_{\alpha\beta} = \mathrm{A}_{\alpha\beta}\exp(wt - kz) \tag{1.34}$$

Thus the separation vector η^α of the particles oscillates.

Let us consider a ring of particles initially at rest in the x-y plane as shown in Fig. (1.2-a). Suppose a wave having $h^{TT}_{xx} \neq 0$, $h^{TT}_{xy} = 0$ hits the system of particles. The particles will be moved (in terms of proper distance relative to the one in the centre) in the way shown in Fig. (1.2-b). Similarly, for a wave with $h^{TT}_{xx} = 0 = h^{TT}_{yy}$, $h^{TT}_{xy} \neq 0$ the picture would distort as in Fig. (1.2-c). Since h^{TT}_{xx} and h^{TT}_{xy} are independent, Fig. (1.2-b) and (1.2-c) provide the pictorial representation of the polarisation states of the wave. Let us note that the two polarisation states are simply rotated by 45° relative to each other. This is in contrast to electromagnetic waves where the two polarisation states are at 90° to each other.

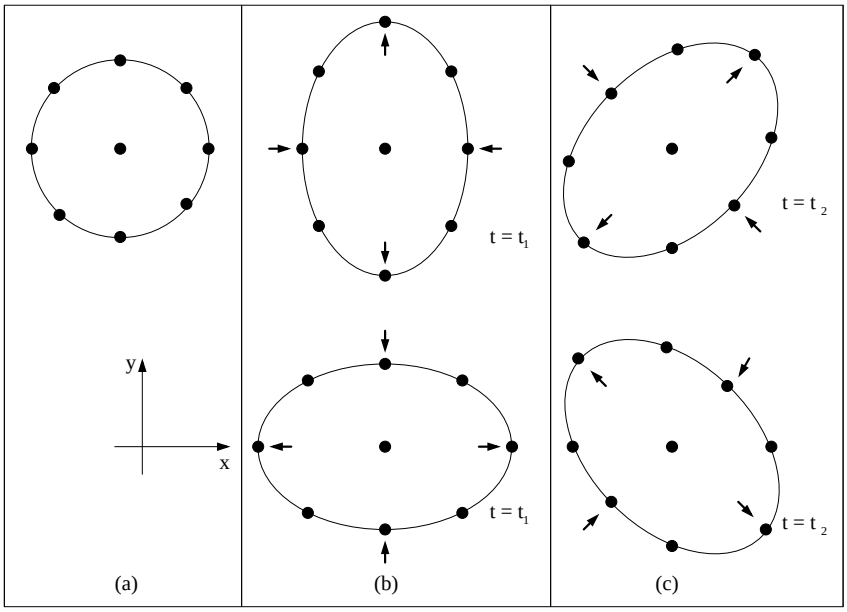

Figure 1.2: (a) A circle of free particles before a wave travelling in the z direction reaches them. (b) and (c) Distortions of the circle by a wave with the '+' and '×' polarisation. The two pictures represent the same wave at phases separated by 180°. Particles are positioned according to their proper distances from one another.

1.1.4 Generation of gravitational wave

To understand the generation of GW it is sufficient to discuss the weak field limit equation (1.10), rewritten as

$$\left(-\frac{\partial^2}{\partial t^2} + \bigtriangledown^2\right) \bar{h}_{\mu\nu} = -16\pi \mathrm{T}_{\mu\nu} \tag{1.35}$$

Let us assume, for sake of simplicity, the time dependence of $\mathrm{T}_{\mu\nu}$ as sinusoidal oscillation of angular frequency ω:

$$\mathrm{T}_{\mu\nu} = \mathrm{S}_{\mu\nu}(x^j)e^{-i\omega t} \tag{1.36}$$

and look for a solution for $\bar{h}_{\mu\nu}$ of the form

$$\bar{h}_{\mu\nu} = \mathrm{B}_{\mu\nu}(x^j)e^{-i\omega t} \tag{1.37}$$

This, in view of Eqs. (1.35) and (1.36), would require $B_{\mu\nu}$ to satisfy

$$\left(\bigtriangledown^2 + \omega^2\right) \mathrm{B}_{\mu\nu} = -16\pi \mathrm{S}_{\mu\nu} \tag{1.38}$$

Outside the source i.e where $S_{\mu\nu} = 0$ we want a solution which would represent outgoing radiation far away. Hence we may take the solution as

$$B_{\mu\nu} = \left(\frac{\mathbb{A}_{\mu\nu}}{r}\right) e^{i\omega r} \tag{1.39}$$

Obviously, $\mathbb{A}_{\mu\nu}$ is to be related to $S_{\mu\nu}$. Under the assumption that the region of the space in which $S_{\mu\nu} \neq 0$ is small compared to $2\pi/\omega$ it can be deduced that

$$\mathbb{A}_{\mu\nu} = 4J_{\mu\nu}\,; \quad J_{\mu\nu} = \int S_{\mu\nu} d^3x \tag{1.40}$$

This assumption is referred to as slow motion approximation since it implies that typical velocity inside the source, which is ω times the size of that region, should be much less than 1. All, except the most powerful sources, satisfy this assumption. Thus we get

$$\bar{h}_{\mu\nu} = \left(\frac{4}{r}\right) J_{\mu\nu} e^{i\omega(r-t)} \tag{1.41}$$

This means that the generated GW has frequency ω. This relation may be expressed in terms of useful quantities with the help of the following results.

(i) The energy momentum satisfies the conservation equation

$$T^{\mu\nu}{}_{,\nu} = 0 \tag{1.42}$$

and obeys the identity:

(ii)

$$\frac{d^2}{dt^2} \int T^{oo} x^l x^m d^3x = 2 \int T^{lm} d^3x \tag{1.43}$$

(iii) The quadrupole moment tensor $\mathbf{I}^{lm}$ is defined as

$$\mathbf{I}^{lm} = \int T^{oo} x^l x^m d^3x \tag{1.44}$$

and which, in view of (1.36), may be expressed as

$$\mathbf{I}^{lm} = \mathrm{D}^{lm} e^{-i\omega t} \tag{1.45}$$

where D^{lm} represents the time independent factor of $\mathbf{I}^{lm}$ (Misner et al., 1973).

The first result gives

$$\mathrm{J}^{\mu o} = 0 \;\Rightarrow\; \bar{h}_{\mu o} \tag{1.46}$$

whereas the others let us write (1.41) as

$$\bar{h}_{jk} = \left(\frac{-2}{r}\right) \omega^2 \mathrm{D}_{jk} e^{i\omega(r-t)} \tag{1.47}$$

We have still freedom of adopting TT gauge and may use it to achieve further simplification. Let us choose z axis along the direction of propagation of the wave. We will then have

$$\bar{h}^{TT}_{zi} = 0 \tag{1.48}$$

$$\bar{h}^{TT}_{xx} = -\bar{h}^{TT}_{yy} = -\omega^2 \left(\mathbb{I}_{xx} - \mathbb{I}_{yy}\right) \left(\frac{e^{i\omega r}}{r}\right) \tag{1.49}$$

$$\bar{h}^{TT}_{xy} = -\left(\frac{2}{r}\right) \omega^2 \mathbb{I}_{xy} e^{i\omega r} \tag{1.50}$$

where $\mathbb{I}_{jk}$ represent the trace free part of quadrupole moment tensor i.e.

$$\mathbb{I}_{jk} = \mathbf{I}_{jk} - \frac{1}{3}\delta_{jk}\mathbf{I}^i{}_i \tag{1.51}$$

As an application of our results let us determine the amplitude of GW generated by a laboratory source.

Laboratory generator (Bar)

Let us take a system of two equal mass points capable of oscillating about their mean position, such as shown in Figure (1.3). Let the system oscillates

longitudinally with angular frequency w about its mean position i.e.

$$\left.\begin{aligned} x_1 &= -\tfrac{1}{2}l_o - \mathrm{A}\cos \mathrm{w}t \\ x_2 &= \tfrac{1}{2}l_o + \mathrm{A}\cos \mathrm{w}t \end{aligned}\right\} \tag{1.52}$$

where l_o is the normal separation between the mass points and A represents the amplitude of oscillation. Now it is straight-forward to compute $\mathbf{I}_{jk}$. The only non-zero component is

$$\left.\begin{aligned} \mathbf{I}_{xx} &= \mathrm{m}\left[(x_1)^2 + (x_2)^2\right] \\ &= const. + \mathrm{mA}^2\cos 2\mathrm{w}t + 2\mathrm{m}l_o\mathrm{A}\cos \mathrm{w}t \end{aligned}\right\} \tag{1.53}$$

For purpose of wave generation the constant term is irrelevant. We may obtain the non-vanishing components of $\mathbb{I}_{jk}$ as

$$\left.\begin{aligned} \mathbb{I}_{xx} &= \tfrac{4}{3}\mathrm{m}l_o\mathrm{A}e^{-i\mathrm{w}t} + \tfrac{2}{3}\mathrm{m}l_o\mathrm{A}^2e^{-2i\mathrm{w}t} \\ \mathbb{I}_{yy} &= \mathbb{I}_{zz} = -\tfrac{2}{3}\mathrm{m}l_o\mathrm{A}e^{-i\mathrm{w}t} - \tfrac{1}{3}\mathrm{m}l_o\mathrm{A}^2e^{-2i\mathrm{w}t} \end{aligned}\right\} \tag{1.54}$$

Finally one obtains after taking the real part

$$\left.\begin{aligned} \bar{h}^{TT}_{xx} &= -\bar{h}^{TT}_{xy} = -\left[2\mathrm{mw}^2 l_o\mathrm{A}\cos(\mathrm{w}(r-t)) + \right. \\ &\qquad \left. 4\mathrm{mw}^2\mathrm{A}^2\cos(2\mathrm{w}(r-t))\right]/r \\ \bar{h}^{TT}_{xy} &= 0 \end{aligned}\right\} \tag{1.55}$$

For a laboratory generator, let us take

$$\mathrm{m} = 10^3\ kg\,, \quad l_o = 1\ m\,, \quad \mathrm{A} = 10^{-4}\ m\,, \quad \mathrm{w} = 10^{-4}\ s^{-1} \tag{1.56}$$

The data chosen represents a typical bar detector. Substituting the values after converting them into geometrised units (G = 1 = c) the amplitude of generated wave is about $10^{-34}/r$

$$|h| \simeq 10^{-34}/r\,; \qquad \textit{Laboratory source} \tag{1.57}$$

This demonstrates that laboratory generators are unlikely to produce useful GW for its demonstration. For sake of comparison, let us conclude this subsection by making an estimate of the strength of waves from strongest astrophysical sources.

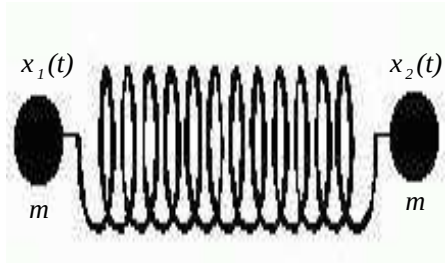

Figure 1.3: An idealised gravitational wave detector with two identical masses connected with a spring.

Astrophysical sources

For a strong GW we should have $h_{\mu\nu} = O(1)$. This would occur near the source where the Newtonian potential would be of the order 1. For a source of mass M this should be at a distance of order M. As we have seen the amplitude of GW falls off as r^{-1} far from the source. This means that the largest amplitude expected to be incident on earth would be $\sim$ M/R where R is the distance of the source from earth. For the formation of 10 $M_\odot$ black hole in a supernova explosion in a nearby galaxy 10^{23} away this is about 10^{-17}. Thus

$$|h|_{max} \simeq 10^{-17}\,; \qquad \textit{Astrophysical sources} \tag{1.58}$$

Thus is in fact an upper limit and less violent events will lead to very much smaller amplitudes.

1.2 Gravitational wave detectors

Equation (1.30) may be recast as

$$\frac{\triangle l - \bar{\epsilon}}{\bar{\epsilon}} = \frac{1}{2} h_{xx}^{TT} \tag{1.59}$$

This means that the strain produced due to the hitting of a GW in two mass points separated by $\bar{\epsilon}$ is of the order of h. In view of Eq. (1.58) let us note that

even a strong GW signal would produce a space strain of the order of 10^{-17}, an unbelievably small effect which would jerk masses spaced at one kilometer by a mere 10^{-20}-one thousand of the diameter of a proton!

Josheph Weber (1960) who pioneered the direct detection of GW constructed an instrument consisting of massive cylinders of aluminium so-called "bar" detectors. These detectors exploit the sharp resonance of the cylinder to get their sensitivity which is normally confined to a narrow bandwidth (one or a few Hz) around the resonant frequency.

Despite their great potential sensitivity the primary drawback of resonant bars is that they are by definition resonant. They are sensitive mainly to the signal with a frequency corresponding to the bar mechanical ringing frequency of the order of 1 kHz. A bar would respond to the hammer blow of the asymmetrical supernova explosion by simply ringing at its own bell tones and would be excited by a twin neutron star inspiral only in that brief instant when the two stars crib up through the bell tone frequency.

Bar detectors continue to be developed, and have until very recently had a sensitivity to broadband bursts. However, the best hope for the first detection of GW lies with large-scale interferometers. Within ten years from now, we may see the launch of space-based interferometer, LISA, to search for signals at frequencies lower than those that are accessible from the ground. To measure the strain produced by GW to bar or interferometric detector, one must fight against the different sources of noises.

An interesting additional twist is given by the fact that the gravitational wave may be accompanied by gamma ray bursts. The GW detectors will then work in coincidence not only with themselves and GW bar antennas, but also with conventional high-energy physics detectors like the underground neutrino experiments and the orbital gamma rays burst monitors.

In this section we review, in brief, these developments. In subsection (1.2.1) the underlying physical principles of the bar detectors have been described. Subsection (1.2.2) deals with large-scale interferometers. Finally subsection (1.2.3) describe the space-based project LISA, the exciting prospects for the long-term future of GW detection in space. For details, one may refer to Thorne (1987, 1995), Saulson (1994).

1.2.1 Bar detectors

A bar detector, in its simplest form, may be idealised as a system of two mass points coupled to a spring and may be depicted as shown in Fig. (1.3). Let the system lies on the x axis of our TT coordinate system with the masses at coordinate positions x_1 and x_2. The force free oscillation of the system, in flat space time, may be expressed via

$$\left.\begin{aligned} \mathrm{m}x_{1,00} &= -\kappa(x_1 - x_2 + l_o) - \nu(x_1 - x_2)_{,0} \\ \mathrm{m}x_{2,00} &= -\kappa(x_2 - x_1 + l_o) - \nu(x_2 - x_1)_{,0} \end{aligned}\right\} \tag{1.60}$$

where l_o, κ and ν represent respectively unstretched length of the spring, spring constant and damping constant. We can combine these equations to obtain the usual damped harmonic oscillator equation

$$\xi_{,00} + 2\gamma\xi_{,0} + w_o^2\xi = 0 \tag{1.61}$$

by introducing

$$\xi = x_2 - x_1 - l_o\,, \quad w_o^2 = 2\kappa/\mathrm{m}\,, \quad \gamma = \nu/m \tag{1.62}$$

Let us recall that the TT coordinate system is not convenient for discussion of the dynamics of such system because in this frame a free particle always (before the arrival and after the passage of the wave) remains at rest. However,

this fact is useful in assigning a local inertial frame $\left\{x^{\alpha'}\right\}$ at some TT coordinate. Suppose that the only motions in the system are those produced by the wave then masses velocities will be very small and we may apply Newton's equations of motion for the masses:

$$\mathrm{m}x^{j'}_{,0'0'} = \mathrm{F}^{j'} \tag{1.63}$$

where $\left\{\mathrm{F}^{j'}\right\}$ are the components of any non gravitational forces on the mass. Further as the coordinates $\left\{x^{j'}\right\}$ differ negligibly to the order of $h_{\mu\nu}$ from that of its value $\{x^j\}$ in TT coordinate system, we may write this equation with negligible error:

$$\mathrm{m}x^{j}_{,00} = \mathrm{F}^{j} \tag{1.64}$$

The only non gravitational force on each mass is due to the spring. The spring will exert a force proportional to its instantaneous proper extensions. If the proper length of the spring is l and the direction of propagation of the wave, for simplicity, is assumed to be along z axis then

$$l(t) = \int_{x_1(t)}^{x_2(t)} \left[1 + h^{TT}_{xx}(t)\right]^{1/2} dx \approx \left[1 + \frac{1}{2}h^{TT}_{xx}(t)\right](x_2 - x_1) \tag{1.65}$$

(refer to (1.30)). Hence, equation of motion of the system after hitting of the wave is given via

$$\left.\begin{aligned} \mathrm{m}x_{1,00} &= -\kappa(l_o - l) - \nu(l_o - l)_{,0} \\ \mathrm{m}x_{2,00} &= -\kappa(l - l_o) - \nu(l - l_o)_{,0} \end{aligned}\right\} \tag{1.66}$$

Let us define

$$\xi = l - l_o = \left[1 + \frac{1}{2}h^{TT}_{xx}\right](x_2 - x_1) - l_o \tag{1.67}$$

leading to

$$x_2 - x_1 \simeq (\xi + l_o)\left(1 - \frac{1}{2}h^{TT}_{xx}\right) = \xi + l_o - \frac{1}{2}h^{TT}_{xx}l_o + O\left(|h_{\mu\nu}|^2\right) \tag{1.68}$$

Using this equation, we may obtain from Eq. (1.66)

$$\xi_{,00} + 2\gamma\xi_{,0} + w_o^2\xi = \frac{1}{2}l_o h_{xx,00}^{TT} \tag{1.69}$$

correct to first order in h_{xx}^{TT}. This is the fundamental equation governing the response of the detector to the GW. It has the simple form of a forced, damped harmonic oscillator .

Let a GW of frequency ω described via

$$h_{xx}^{TT} = \mathrm{A}\cos\omega t \tag{1.70}$$

hits the detector then the steady solution for ξ may be taken as

$$\left.\begin{aligned} \xi &= \mathrm{R}\cos(\omega t + \varphi)\,; \\ \mathrm{R} &= \tfrac{1}{2}l_o\omega^2\mathrm{A}/\left[(w_o-\omega)^2 + 4\omega^2\nu^2\right]^{1/2}\,, \\ \tan\varphi &= 2\nu\omega/\left(w_o^2-\omega^2\right) \end{aligned}\right\} \tag{1.71}$$

The average energy of oscillation of the detector over one period, $2\pi/\omega$:

$$\langle \mathrm{E}\rangle = \frac{1}{8}\mathrm{m}\mathrm{R}^2(w_o^2+\omega^2) \tag{1.72}$$

If we wish to detect a specific source whose frequency ω is known, then we should adjust w_o equal to ω for maximum response (resonance). The resonance amplitude and energy of the detector will be

$$\mathrm{R}_{resonant} = \frac{1}{4}l_o\mathrm{A}\omega/\gamma \tag{1.73}$$

$$\mathrm{E}_{resonant} = \frac{1}{64}\mathrm{m}l_o^2\omega^2\mathrm{A}^2(\omega/\gamma)^2 \tag{1.74}$$

The ratio (ω/γ) is related to what is called the quality factor Q.

$$\mathrm{Q} = \omega/2\gamma \tag{1.75}$$

$$\mathrm{E}_{resonant} = \frac{1}{16}\mathrm{m}l_o^2\omega^2\mathrm{A}^2\mathrm{Q}^2 \tag{1.76}$$

The bar detectors are massive cylindrical bars; its elasticity provides the function of the spring. When waves hit the bar broadside, they excite its longitudinal modes of vibration. The first detectors built by Weber were aluminium

bars of mass 1.4×10^3 kg, length $l_o = 1.5$ m, resonant frequency $w_o = 10^4\, s^{-1}$ and Q about 10^5. This means that a strong resonant GW of A = 10^{-20} will excite the bar to an energy of the order of 10^{-20} J. The resonant amplitude given by (1.73) is only about 10^{-15} m, roughly the diameter of an atomic nucleus.

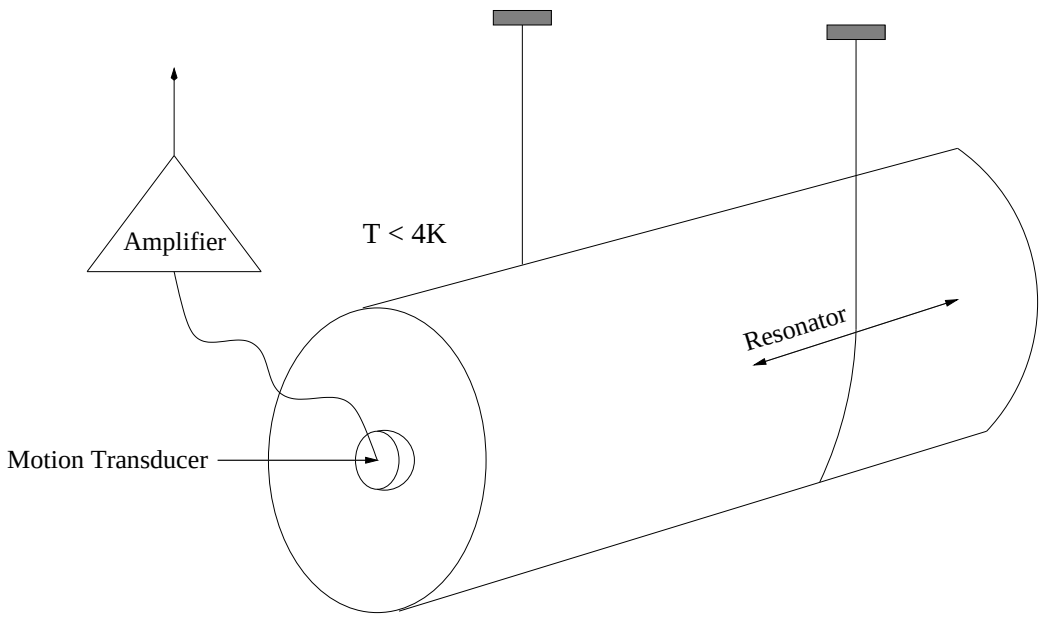

Figure 1.4: A schematic of resonant bar detector.

Clearly, the detections of such small levels of excitations will be hampered by random noise in the oscillator. For example, thermal noise in any oscillator induces random vibration with a mean energy of kT; k the Boltzmann constant having value 1.38×10^{-23} J/K. At room temperature (T $\sim$ 300K) the thermal noise amounts to the energy $\sim 4 \times 10^{-21}$ J. Other sources of noise such as vibrations from passing vehicles and every day seismic disturbances could be considerably larger than this, so the apparatus has to be carefully isolated.

A typical "bar" detector consists of a cylinder of aluminium with a length $l_o \sim 3$ m, a resonant frequency of order $w_o \sim 500$ Hz to 1.5 kHz, and a mass

Detector	Location	Taking data since
NAUTILUS	Frascati, Rome	1993
EXPLORER	Cern (Rome group)	1990
ALLEGRO	Louisiana, USA	1991
AURIGA	Padua, Italy	1997
NIOBE	Perth, Australia	1993

Table 1.1: The existing resonant bar detectors.

$\sim$ 1000 kg whose mechanical oscillations are driven by GW [Fig. (1.4)]. A transducer converts mechanical vibrations of the bar into an electrical signal, which is then amplified by an amplifier and recorded.

Currently there are a number of bar detectors in operation [see Table (1.1)]. Some of these operate at room temperature and some others at cryogenic temperature. Some detectors (NAUTILUS & EXPLORER) may be cooled down to ultra cryogenic temperature. They can detect signal amplitudes $h \sim 10^{-20}$ in a band width of 10-20 Hz around a central frequency of 1 kHz. Asymmetric supernovae in our Galaxy are the best candidates for these detectors. For example, a supernova collapse in our galaxy at a distance of 10 kpc emits GW of the amplitude $h \sim 10^{-17}$. At present this sensitivity has been achieved by some of the bar detector. They may also see continuous radiation emitted by a neutron star if the frequency happens to lie in their sensitivity band.

1.2.2 Ground based laser interferometric detectors

The effect of GW is to produce a transverse shear strain and this fact makes the Michelson interferometer an obvious candidate for a detector. The Michelson interferometers must have kilometric arms, constituted by "high fineness" Fabry Perot cavities to trap the light for long period and to increase the sensitivity. Laser standing power measured in KW will be stored within the cavities. Beam losses at the level of 10^{-6} per passages are required. Mirrors must be 20 or 30 cm in diameter just to hold diffraction losses, and coating with parts per million reflection losses have been developed. Vacuum pipe with diameters of the order of a meter are necessary just to contain the diffraction limited laser beams and vacuum exceeding 10 torr is required to prevent the introduction of spurious signal by refraction index fluctuations. The list of ground based laser interferometric detector site and orientation are shown in Table (1.2).

Interferometric detectors currently under construction will increase our ability to directly observe GW. The Japanese TAMA-300 meter interferometric detector having sensitivity 10^{-20} is already operational and some initial hours of data has been analysed. Several other projects are now nearing to completion: The British-German collaboration is constructing a 600 m interferometer (GEO) in Hannover, Germany, the French-Italian collaboration is building a 3 km detector (VIRGO) near Pisa, Italy and the Americans are building two 4 km antennas (LIGO), one in Livingston and the other in Hanford in the USA which will have the sensitivity 10^{-21}. These detectors will start taking data between 2002 and 2003. The larger of these detectors, LIGO and VIRGO, are likely to be upgraded in sensitivity by an order of magnitude with a better low-frequency performance in 2005. These ground based interferometers will eventually be sensitive to sources in the frequency range from 10 Hz to several

Detector	*Location*	*Length* (m)	*Corner Location*	*Arm 1*	*Arm 2*
Glasgow	Glasgow, GBR	10	55.87°N – 4.28°W	77.00°	167.00°
CIT	Pasadena, CA, USA	40	34.17°N – 118.13°W	180.00°	270.00°
MPQ	Garching, GER	30	48.24°N – 11.68°W	329.00°	239.00°
ISAS-100	Tokyo, JPN	100	35.57°N – 139.47°W	42.00°	135.00°
TAMA-20	Tokyo, JPN	20	35.68°N – 139.54°W	45.00°	315.00°
Glasgow	Glasgow, GBR	10	55.87°N – 4.28°W	62.00°	152.00°
TAMA-300	Tokyo, JPN	300	35.68°N – 139.54°W	90.00°	180.00°
GEO-600	Hannover, GER	600	52.25°N – 9.81°W	25.94°	291.61°
VIRGO	Pisa, ITA	3000	43.63°N – 10.5°W	71.50°	341.50°
LIGO	Hanford, WA, USA	4000	46.45°N – 119.41°W	36.80°	126.80°
LIGO	Livingston, LA, USA	4000	30.56°N – 90.77°W	108.00°	198.00°

Table 1.2: Site and orientation of Earth based interferometric gravitational wave detectors.

kHz.

When a GW, with frequencies high compared to the masses ~ 1 Hz pendulum frequency, passes through the detector of arm length l_o then one arm of the detector get stretched in one direction whereas the other arm gets compressed. If the total change in the the arm-length is δl, then the response $R(t)$ of the detector which is defined as $\frac{\delta l}{l_o}$ may be given via

$$R(t) = \frac{\delta l}{l_o} = F_+ h_+(t) + F_\times h_\times(t) \tag{1.77}$$

where, h_+, $h_\times$ are two polarisations of the signal and F_+, $F_\times$ are beam pattern functions arising because of transformation equations relating to the wave frame and the detector frame [refer to Eq. (1.31)]. Let the detector frame (x, y, z) and the wave frame (X, Y, Z) are related via transformation matrix $\mathbf{A}$ i.e

$$\xi^i = \mathbf{A}^i_R \xi^R\,, \quad \xi^k = \mathbf{A}^k_j \xi^j \tag{1.78}$$

where capital latin letters refers to wave frame quantities and lower case for the detector frame quantities. It can be shown that the response of the detector

may be expressed as

$$\frac{\delta l}{l_o} = -\sin 2\Omega \left[\left(\mathbf{A}_X^x \mathbf{A}_Y^y - \mathbf{A}_Y^x \mathbf{A}_Y^y \right) h_+ + \left(\mathbf{A}_X^x \mathbf{A}_Y^y + \mathbf{A}_Y^x \mathbf{A}_X^y \right) h_\times \right] \tag{1.79}$$

where 2Ω is the angle between the arms of the detector, normally kept equal to 90° [Schutz and Tinto (1987)].

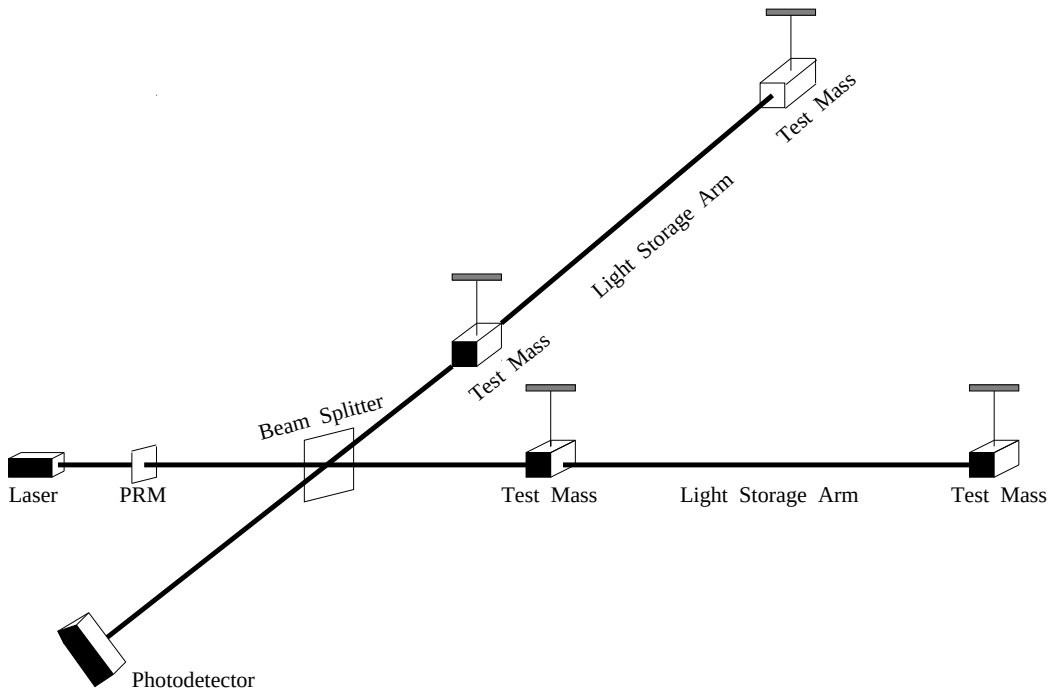

Figure 1.5: A schematic of Earth based laser interferometric gravitational wave detector.

A laser interferometric detector consists of four test masses/mirrors that hang from vibration isolated supports as shown in Fig. (1.5). The mirrors facing each other on each arm form a Fabry-Perot cavity. A beam splitter splits a carefully prepared laser beam in two, and directs the resulting beams down the two arms. Each beams penetrates through the mass, and through the dielectric coating (the mirror). The length of the arm's of the Fabry-Perot cavity is adjusted to be nearly an integral number of half wave-length of light.

The cavity's end mirror has much higher reflectivity than its corner mirror, so the trapped light leaks back out through the corner mirror, and then hits the beam splitter where it recombines with light from the other arm. Most of the recombined light goes back toward the laser (where it can be returned to the interferometer by a "power recycled mirror" labeled PRM, but a tiny portion goes toward the photo-diode.

When a GW hits the detector and moves the masses, thereby changing the lengths of the arms of the two cavities, it shifts each cavity's resonant frequency slightly relative to the laser frequency, and the phase of the light that exists from the cavity toward the beam splitter. Correspondingly, the relative phase of the two beams returning to the splitter is altered by an amount $\triangle\Phi \propto \delta l$, and this relative phase shift causes a change in the intensity of the recombined light at photo-diode, $\triangle I_{pd} \propto \triangle\Phi \propto \delta l \propto R(t)$. Thus, the change of photo-diode output current is directly proportional to the GW strain.

Scientists are now studying the technologies that may be needed for a further improvement of the sensitivity of the next-generation detectors. This may involve cooling mirrors, using ultra-massive mirrors of special materials, using purely non-transmissive optics, and even circumventing the quantum limit in interferometers, as has been studied for bars. The goal of next-generation detectors would be limited just by gravity-gradient noise and quantum effects.

1.2.3 Laser interferometric space antenna

Gravity-gradient noise on Earth is much larger than the amplitude of any expected waves from astronomical sources at frequencies below about 1 Hz, but this noise falls off a $1/r^3$ as one moves away from the Earth. A detector in space would not notice the Earth's noisy environment. The Laser inter-

ferometric space antenna (LISA) project, efforts underway by both European Space Agency (ESA) and NASA with a view toward a collaborative mission around 2010, would open up the frequency window between 0.1 mHz and 0.1 Hz.

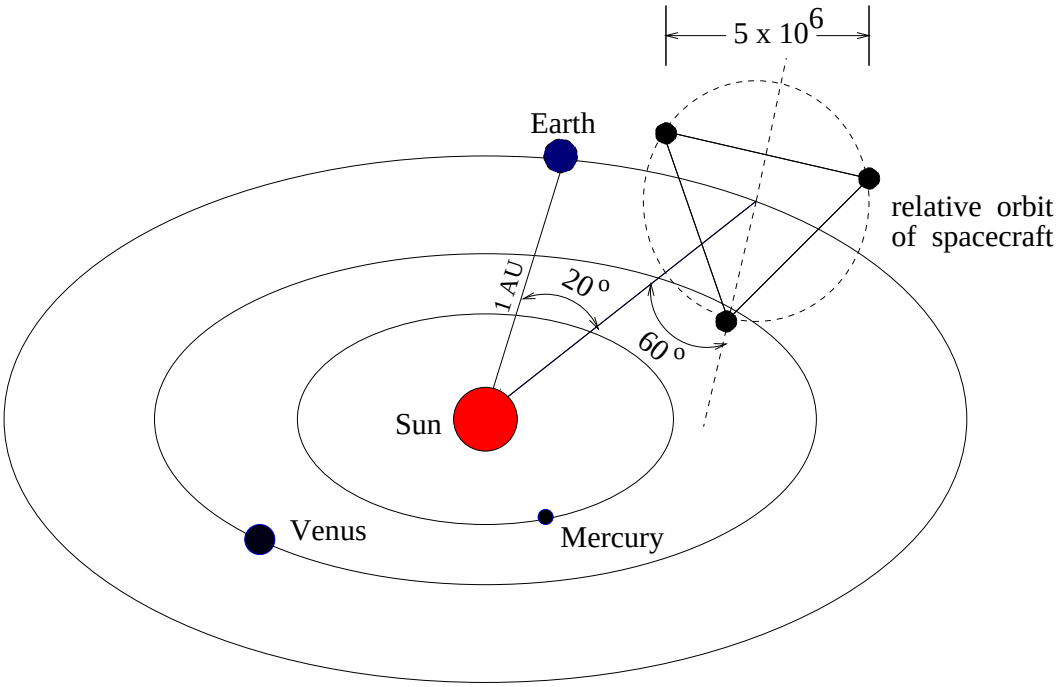

Figure 1.6: A schematic diagram of the laser interferometric space antenna.

A concept of the project is shown in Fig. (1.6). Three spacecraft are placed in solar orbit at 1 A.U, about 20 degrees behind the Earth in it orbit. The spacecraft are located at the corners of an equilateral triangle with 5×10^6 km-long sides. Two arms of the triangle comprise a Michelson interferometer with vertices at the corners. The third arm permits another interferometric observable to be measured, which can determine a second polarization. The interferometers use one micron light as the terrestrial detectors but need only a single pass in the arms to gain the desired sensitivity. The end points of

the interferometers are referenced to proof masses free-floating within and shielded by the spacecraft. The spacecraft is incorporated in a feedback loop with precision thrust control to follow the proof masses.

The main environmental disturbances to LISA are the forces from the Sun.: fluctuations in solar radiation pressure and pressure from the solar wind. To minimize these, LISA incorporates drag-free technology. Interferometry is referenced to an internal proof mass that falls freely, not attached to the spacecraft. The job of the spacecraft is to shield this mass from external disturbances. It does this by sensing the position of the mass and firing its own jets to keep itself (the space craft) stationary relative to the proof mass. To do this, it needs thrusters of very small thrust that have accurate control. The availability of such thrusters, of the accelerometers needed to sense disturbances to the spacecraft, and of lasers capable of continuously emitting 1 W infrared light for years, have enabled the LISA mission.

LISA is supposed to see many exciting sources for example the coalescences of giant black holes in the centre of galaxies. LISA will see such events with extraordinary sensitivity, recording typical signal-to-noise-ratios of 1000 or more for events at redshift 1.

1.3 Sources of gravitational waves

Astronomical observations have led to the belief that luminous matter constitutes a small fraction of the total matter content of the Universe. More than 90% of the mass in the Universe is electro-magnetically silent. The presence of dark matter is inferred from the gravitational influence it causes on luminous matter. It is possible that some fraction of this dark matter is a strong emitter of GW. There are many reviews on GW sources (Thorne, 1987; Blair,

1991; Schutz, 1989, 1993, 1999, Sathyaprakash, 1999 and Grishchuk, et. al., 2000). The discussion on the GW sources in this section is introductory and for details one may refer to these reviews. The anticipated GW sources can be classified into (i) Transients (ii) Continuous and (iii) Stochastic.

1.3.1 Transient sources

Supernovae and inspiralling compact stars in binary systems are prime examples of sources of this type. These sources last for a duration of about $10^{-3} - 10^{4}$ seconds.

Supernovae explosions

The type II Supernovae explosions, which are believed to occur as a result of the core collapse of an evolved massive ($> 9M_{\odot}$) star and which are associated with violent mass ejection with velocities of order 0.03 with formation of a compact remnant—neutron star or a black hole–may emit significant amount of GW depending upon how asymmetric the collapse is. The emission occurs essentially during the rotational core collapse, bounce and oscillations, rotation-induced bars and convective instabilities set up in the core of the new born neutron star.

Rapid rotation flattens the collapsing core inducing large quadrupole moment; thus generating GW. Study of a wide range of rotational core collapse models suggests that the largest signals are produced by models which are (i) initially slowly rotating and have a stiff equation of state or (ii) initially rapidly rotating and have a soft equation of state. In the first case bounce occurs at densities above nuclear matter density, with a fast deceleration of the collapsing core resulting in the emission of GW signals. In the second

case, the quadrupole moment is large due to rapid rotation which facilitates emission of GW. However, in either case the signals are not strong enough to be interesting sources for the first generation detectors.

When the core's rotation is *high enough* it may cause the core to flatten before it reaches nuclear density leading to an instability which transforms the flattened core into a bar-like configuration spinning about its transverse axis. Some of these instabilities could also fragment the core into two or more pieces which then rotate about each other. Both are efficient ways of losing energy in the form of GW.

Instabilities in the core of the newly born neutron star, which last for about a second after the collapse, are likely to produce GW due to anisotropic mass distribution and motion.

Inspiraling compact binaries

The binary systems whose either member is a compact star e.g. neutron star (NS) and black hole (BH) are the most promising transient sources of GW during the phase of their coalescence. The well known binary pulsar PSR 1913 + 16 is such a system but it will coalesce in a time scale of 10^9 years from now — not a right candidate. However, there are binaries in our galaxy with coalescence time scale much shorter than this. Further, statistical analysis of binary pulsars estimates three NS-NS coalescence per year out to a distance of 200 Mpc (Phinney, 1991; Narayanan et. al 1991). The initial LIGO/VIRGO interferometers have a fair chances to see the inspiral events. Compact inspiraling binaries emit quasi-periodic GW with a frequency that sweeps upward toward a maximum frequency. The maximum frequency may be of the order of 1 KHz for neutron stars. In the lower frequency regime the wave form is

easily computed from the quadrupole formalism. At higher frequencies Post-Newtonian corrections would be required (Thorne, 1987; Krolak, 1989). In view of the strong potentialities of such sources the various aspects related to the emission of GW has been dealt extensively in full details and one may refer to Sathyprakash, 1999 and Grischuk, et al. 2000.

1.3.2 Continuous gravitational wave

The continuous gravitational wave (CGW) sources are of prime interest because such sources can be observed again and again and hence single interferometer is sufficient to confirm its detection. However, one can't expect a source to be continuous as well as strong. For emission of GW from pulsars, there should be some asymmetry in it. There are several mechanisms which may lead to deformations of the star, or to precession of its rotation axis. The characteristic amplitude of GW from pulsars scales as

$$h \sim \frac{\mathrm{I} f_o^2 \varepsilon}{r} \tag{1.80}$$

where I is the moment of inertia of the pulsar, f_o is the GW frequency, ε is a measure of deviation from axissymmetry and r is the distance of the pulsar.

As remarked earlier, pulsars are born in supernovae explosions. The outer layers of the star crystallizes as the newborn star pulsar cools by neutrino emission. Estimates, based on the expected breaking strain of the crystal lattice, suggest that anisotropic stresses, which build up as the pulsar looses rotational energy, could lead to $\varepsilon \leq 10^{-5}$; the exact value depends on the breaking strain of the neutron star crust as well as the neutron star's "geological history", and could be several orders of magnitude smaller. Nonetheless, this upper limit makes pulsars a potentially interesting source for kilometer scale interferometers.

Large magnetic fields trapped inside the super fluid interior of a pulsar may also induce deformation of the star. This mechanism has been explored recently, indicating that the effect is extremely small for standard neutron star models ($\varepsilon \leq 10^{-9}$).

Another plausible mechanism for the CGW is the Chandrasekhar-Friedman-Schutz (CFS) instability, which is driven by GW back reaction. It is possible that newly-formed neutron stars may undergo this instability spontaneously as they cool soon after formation. The frequency of the emitted wave is determined by the frequency of the unstable normal mode, which may be less than the spin frequency.

Accretion is another way to excite neutron stars. There is also the Zimmermann - Szedinits mechanism where the principal axes of moment inertia are driven away from the rotational axes by accretion from a companion star. Accretion can in principle produce relatively strong wave since the amplitude is related to the accretion rate rather than to structural effects in the star.

1.3.3 Stochastic waves

Catastrophic processes in the early history of Universe, as well as the astrophysical sources distributed all over the cosmos, generate stochastic background of GW. A given stochastic background will be characteristic of the sources that are responsible for it and it may be possible to discriminate different backgrounds provided their spectral characteristics are sufficiently different.

Primordial background: It is believed that similar to cosmic microwave background (CMBR) the GW background was also produced at the same

time as a result of quantum fluctuations in the early Universe (Grischuk, 1997). Primordial background radiation would freely travel to us from almost the very moment of creation because GW couples very weakly with matter. Hence, its detection would help us to get a picture of the first moments after the big bang. The COBE data have set limits on the strength of the GW background. The strength are far too weak to be detected by any planned ground-based detectors. However, advanced LIGO detectors may observe the background generated by the collisions of a cosmic string network (for details one may refer to Allen, 1997).

Phase transitions in the early Universe, inspired by fundamental particle physics theories, and cosmological strings and domain walls are also sources of a stochastic background. These processes are expected to generate a background which has a different spectrum and strength than the primordial one. Future ground-based detectors will achieve good enough sensitivity to measure this background GW and such measurements will prove to be a good test bed for these cosmological models.

Supernovae background: Even though an individual supernova may not be detectable out to a great distance, the background produced by all supernovae within the Hubble radius might indeed be detected (Blair & Ju, 1996). The coincidence between an advanced interferometer and a resonant bar within 50 km of the interferometer will enable the detection of this background. These studies may shed light on the history of star formation rate, a subject of vigorous debate amongst astrophysicists.

Galactic binary background: Binaries with orbital periods $P \sim 10^{-4} - 10^{-2} s$ will be observable in space-based detectors. A large number of them are present

in our galaxy but they will not be identifiable separately because they are at a large distances and consequently have a feeble amplitude. However they would contribute to background GW. In addition to binaries of compact stars, there are also other binaries consisting of white dwarfs, cataclysmic variables, etc., which will also contribute to the background radiation produced by compact binaries. The net effect is that these sources will appear as a background noise in space interferometers. By studying the nature of this background one can learn a lot about binary population in our Galaxy.

Galactic pulsar background The CGW from pulsars could also produce background of radiation which will limit the sensitivity of the ground-based laser interferometers (Giazotto, Gourgoulhon and Bonazzola, 1997). There are about 10^9 neutron stars in our Galaxy of which about 2×10^5 will contribute to the background radiation. This background radiation will be prominent, and observable in the LIGO/VIRGO detectors, in the frequency range of 5-10 Hz, at an rms amplitude of $h_{rms} \sim 2 \times 10^{-26}$, where the rms is computed over 10^5 sources. At frequency of 10 Hz, wavelength of GW will be around 30,000 Km. Hence, it would be possible to cross-correlate data from two distant detectors, such as two LIGOs, or LIGO and VIRGO, and discriminate the background against other sources of noise.

Chapter 2

Data analysis concept

2.1 Introduction

The GW data analysis strategy is different in many ways from conventional astronomical data analysis. This is due to the following:

- GW antennas are essentially omni-directional with their response better than 50% of the average over 75% of the sky. Hence our data analysis systems will have to carry out all-sky searches for the sources.

- Interferometers are typically broad-band covering 3 to 4 orders of magnitude in frequency. While this is obviously to our advantage, as it helps to track sources whose frequency may change rapidly, it calls for searches to be carried over a wide-band of frequencies.

- In contrast to electromagnetic (EM) radiation, most astrophysical GWs are tracked in phase and the signal-to-noise ratio (SNR) is built up by coherent superposition of many wave cycles emitted by a source. Consequently, the SNR is proportional to the amplitude and only falls off, with the distance to the source r, as $1/r$. Therefore, the number of sources of a limiting SNR increases as r^3 for a homogeneous distribution of sources in a flat Universe, as opposed to EM sources that increase only as $r^{3/2}$.

- The GW antennas acquire data continuously for many years at the rate of several mega-bytes per second. It is expected that about a hundredth of this data will have to pass through our search analysis systems. Unless on-line processing can be done we cannot hope to make our searches. This places huge demands on the speed of our data analysis hardware. A careful study of our search algorithms with a view to making them as optimal (maximum SNR) and efficient (least search times) as one possibly can is required.

2.2 Gravitational wave antenna sensitivity

The performance of a GW detector is characterised by the one sided *power spectral density* (PSD) of its noise background. The analytical fits to noise power spectral densities $S_n(f)$ of ground based interferometers are given in Table (2.1) where S_o and f_{n_o} represent respectively the value of minimum noise and the corresponding frequency. At the lower-frequency cutoff f_l and the high-frequency cutoff f_u, $S_n(f)$ can be treated as infinite. One can construct the noise PSD as follows:

A GW detector output represents a dimensionless data train, say $x(t)$. In the absence of any GW signal. The detector output is just an instance of noise $n(t)$, that is, $x(t) = n(t)$. The noise auto-correlation function c is defined as

$$\mathrm{c}(t_1, t_2) \equiv \langle n(t_1) n(t_2) \rangle, \tag{2.1}$$

where $\langle \quad \rangle$ represents the average over an ensemble of noise realisations. In general, c depends both on t_1 and t_2. However, if the detector output is a stationary noise process, i.e. its performance is, statistically speaking, independent of time, then c depends only on $\tau \equiv t_2 - t_1$. We shall, furthermore,

Detector	Fit to noise power spectral density	S_o $(Hz)^{-1}$	f_{n_o} (Hz)	f_l (Hz)	f_u (Hz)
LIGO I	$S_o/3\ \left[(f_{n_o}/f)^4 + 2(f/f_{n_o})^2\right]$	8.0×10^{-46}	175	40	1300
LIGO II	$S_o/11\ \left\{2(f_{n_o}/f)^{9/2} + 9/2[1 + (f/f_{n_o})^2]\right\}$	7.9×10^{-48}	110	25	900
LIGO III	$S_o/5\ \left\{(f_{n_o}/f)^4 + 2[1 + (f/fn_o)^2]\right\}$	2.3×10^{-48}	75	12	625
VIRGO	$S_o/4\ \left[290(f_s/f)^5 + 2(f_{n_o}/f) + 1 + (f/f_{n_o})^2\right]$	1.1×10^{-45}	475	16	2750
GEO600	$S_o0/5\ \left[4(f_{n_o}/f)^{3/2} - 2 + 3(f/f_{n_o})^2\right]$	6.6×10^{-45}	210	40	1450
TAMA	$S_o/32\ \left\{(f_{n_o}/f)^5 + 13(f_{n_o}/f) + 9[1 + (f/f_{n_o})^2]\right\}$	2.4×10^{-44}	400	75	3400

Table 2.1: Analytical fits to noise power spectral densities $S_n(f)$ of ground based interferometers.

assume that $\mathrm{c}(\tau) = \mathrm{c}(-\tau)$. For data from real detectors the above average can be replaced by a time average under the assumption of ergodicity:

$$\mathrm{c}(\tau) = \frac{1}{T}\int_{-T/2}^{T/2} n(t)n(t-\tau)dt. \tag{2.2}$$

The assumption of stationarity is not strictly valid in the case of real GW detectors; however, if their performance does not vary greatly over time scales much larger than typical observation time scales, stationarity could be used as a working rule. While this may be good enough in the case of binary inspiral and coalescence searches, it is a matter of concern for the observation of continuous and stochastic GW. Under such an assumption the one-sided noise PSD, defined only at positive frequencies, is the Fourier transform (FT) of the noise auto-correlation function:

$$\begin{aligned} S_n(f) &\equiv \frac{1}{2}\int_{-\infty}^{\infty} \mathrm{c}(\tau)e^{-2\pi i f\tau}d\tau, \quad f \geq 0, \\ &\equiv 0, \quad f < 0, \end{aligned} \tag{2.3}$$

where a factor of 1/2 is included by convention because it has been assumed that $\mathrm{c}(\tau)$ is an even function. This equation implies that $S_n(f)$ is real. It is straightforward to show that

$$\langle \tilde{n}(f)\tilde{n}^*(f')\rangle = S_n(f)\delta(f-f'), \tag{2.4}$$

where $\tilde{n}(f)$ represents the Fourier transform of $n(t)$ and * denotes complex conjugation. The above identity implies that $S_n(f)$ is positive definite.

The autocorrelation function $\mathrm{c}(\tau)$ at $\tau = 0$ can be expressed as an integral over $S_n(f)$. Indeed, it is easy to see that

$$\langle n^2(t)\rangle = 2\int_0^{\infty} S_n(f)df. \tag{2.5}$$

The above equation justifies the name *power spectral density* given to $S_n(f)$. It is obvious that $S_n(f)$ has dimensions of time but it is conventional to use,

instead, the dimensions of Hz^{-1} since it is a quantity defined in the frequency domain. The square-root of $S_n(f)$ is the noise amplitude, $\sqrt{S_n(f)}$, and has dimensions of *per root Hz.* It is often useful to define the dimensionless quantity $h_n^2(f) \equiv fS_n(f)$, called the *effective noise.* In GW interferometer literature one also comes across the *displacement noise* or *strain noise* defined as $h_{l_o}(f) \equiv l_o h_n(f)$, and the corresponding noise spectrum $S_{l_o}(f) \equiv l_o^2 S_n(f)$, where l_o is the arm length of the interferometer. The displacement noise gives the smallest strain $\delta l/l_o$ in the arms of an interferometer which can be measured at a given frequency.

Sensitivity vs source amplitudes

One compares the GW amplitudes of astronomical sources with the instrumental sensitivity and assesses what sort of sources will be observable in the following way. Firstly, as comparisons are almost always made in the frequency-domain it is important to note that the Fourier component $\tilde{h}(f)$ of a deterministic signal $h(t)$ has dimensions of Hz^{-1} and the quantity $f|\tilde{h}(f)|$, is dimensionless. It is this last quantity that should be compared with $h_n(f)$ to deduce the strength of a source relative to detector noise. Secondly, it is quite common also to compare the amplitude spectrum per logarithmic bin of a source, $\sqrt{f}|\tilde{h}(f)|$, with the amplitude spectrum of noise, $\sqrt{S_n(f)}$, both of which have dimensions of per root Hz. For monochromatic sources, one compares the effective noise in a long integration period with the expected "instantaneous" amplitudes in the following way: A monotonic wave of frequency f_o observed for a time T_o is simply a narrow line in a frequency bin of width $\Delta f \equiv 1/T_o$ around f_o. The noise in this bin is $S_n(f)\Delta f = S_n(f)/T_o$. Thus the SNR after a period of observation T_o is

$$\frac{S}{N} = \frac{h_o}{\sqrt{S_n(f_o)/T_o}}. \tag{2.6}$$

One, therefore, computes this dimensionless noise spectrum for a given duration of observation, $S_n(f)/T_o$, to assess the detectability of a continuous GW. Surely, if the observation time is T_o then the total *energy* (that is, the integrated power spectrum) of both the signal and noise must increase in proportion to T_o^2. Then how does the SNR for a continuous wave improve with the duration of observation? The point is that while the signal energy is all concentrated in one bin, the noise is distributed over the entire frequency band. As T_o increases, the frequency resolution improves as $1/T_o$ and the number of frequency bins increase in proportion to T_o. Consequently, the noise intensity *per frequency bin* increases only as T_o. Now, the signal intensity is concentrated in just one bin since the signal is assumed to be monochromatic. Therefore, the power SNR increases as T_o, or, the amplitude SNR increases as $\sqrt{T_o}$.

2.3 Noises in the earth based interferometric detectors

As mentioned in the earlier section the performance of GW detector is characterised by the one-sided PSD. The sensitivity of ground based detectors is limited at frequencies less than a Hertz by the time-varying local gravitational field caused by a variety of different noise sources, e.g. low frequency seismic vibrations, density variation in the atmosphere due to winds, etc. Thus, for data analysis purposes, the noise PSD is assumed to be essentially infinite below a certain lower cutoff f_s. The effective noise $h_n(f)$ expected in these detectors is equal to $\sqrt{fS_n(f)}$. Type of noises that one have to fight to detect the signals are:

Ground vibration: External mechanical vibrations are a problem for bar detectors, too, but are more serious for interferometers, not least because interferometers bounce light back and forth between the mirrors, and so each reflection introduces further vibrational noise. Suspension/isolation systems are based on pendula. A pendulum is a good mechanical filter for frequencies above its natural frequency. By hanging the mirrors on pendula of perhaps 0.5 m length, one achieves filtering below a few Hz. Since the spectrum of ground noise falls at higher frequencies, this provides suitable isolation. But these systems can be very sophisticated; the GEO600 detector has a three-stage pendulum and other vibration isolation components. The most ambitious isolation system is being developed for the VIRGO detector.

Thermal noise: Vibrations of the mirrors and of the suspending pendulum can mask gravitational waves. As with vibrational noise, this is increased by the bouncing of the light between the mirrors. Unlike bars, interferometers measure only at frequencies far from the resonant frequency, where the amplitude of vibration is smaller. Thus, the pendulum suspensions have thermal noise at a few Hz, but measurements will be made above 20 or 30 Hz in the first detectors. Internal vibrations of the mirrors have natural frequencies of several kilohertz. By ensuring that both kinds of oscillations have very high Q, one can confine most of the vibration energy to a small bandwidth around the resonant frequency, so that at the measurement frequencies the vibration amplitudes are small. This allows interferometers to operate at room temperature. But mechanical Qs of 10^7 or higher are required, and this is technically demanding.

Shot noise: The photons that are used to do interferometry are quantized, and so they arrive at random and make random fluctuations in the light

intensity that can look like a gravitational wave signal. The more photons one uses, the smoother will be the interference signal. As a random process, the error improves with the square-root of the number N of photons. Using infrared light with a wavelength $\lambda \sim 1\ \mu$m, one can expect to measure to an accuracy of

$$\triangle \mathrm{L}_{shot} \sim \lambda/(2\pi\sqrt{\mathrm{N}})$$

To measure at a frequency f, one has to make at least $2f$ measurements per second i.e. one can accumulate photons for a time $1/2f$. With light power P and GW amplitude h one gets $\mathrm{N} = \mathrm{P}/(hc/\lambda)/(2f)$ photons. In order that $\triangle \mathrm{L}_{shot}$ should be below 10^{-16} m one needs large light power, far beyond the output of any continuous laser.

Light-recycling techniques overcome this problem by using light efficiently. An interferometer actually has two places where light leaves. One is where the interference is measured. The other goes back towards the input laser. Normally one arranges that no light goes to the interference sensor, so that only when a gravitational wave passes does a signal register there. This means that all the light normally returns to the mirror, apart from small losses at the mirrors. Since mirrors are of good quality, only one part in 10^3 or less of the light is lost during a 1 ms storage time. By placing a power-recycling mirror in front of the laser, one can reflect this wasted light back in, allowing power to build up in the arms until the laser merely resupplies the mirror losses. This can dramatically reduce the power requirement for the laser. The first interferometers will work with laser powers of 5-10 W. This is attainable with modern laser technology.

Quantum effects: Shot noise is a quantum noise, but in addition there are effects like bar detectors face: zero-point vibrations of mirror surfaces and

so on. These are small compared to present operating limits of detectors, but they may become important in 5 years or so. Practical schemes to reduce this noise have already been demonstrated in principle, but they need to be improved considerably. They can be reduced by making the mirror masses large, since the amplitude of vibration scales inversely as the square-root of the mass.

Gravity gradient noise: One noise which cannot be screened out is that arises due to changes in the local Newtonian gravitational field on the time scale of the measurements. A gravitational wave detector will respond to tidal forces from local sources just as well as to gravitational waves. Environmental noise comes not only from man-made sources, but even more importantly from natural ones: seismic waves are accompanied by changes in the gravitational field, and changes in air pressure are accompanied by changes in air density. The spectrum falls steeply with increasing frequency, so for first-generation interferometers this will not be a problem, but it may limit the performance of detectors a decade from now. And it is the primary reason that detecting gravitational waves in the low-frequency band around 1 mHz must be done in space.

2.4 Matched filtering and optimal signal-to-noise ratio

Matched filtering is a data analysis technique that efficiently searches for a signal of known shape buried in noisy data (Helstrom, 1968). The technique consists in correlating the noisy output of each interferometer data with a set of theoretical waveform templates. If the maximum of the correlation exceeds a preset threshold, a detection is announced. However, even if a signal is present

in the data, the accompanying noise can mask its presence by preventing such crossing of the threshold in some cases. Thus a signal can be detected with only a certain probability, called its detection probability. Also, there will be a non-zero probability, called the false alarm probability, of a false detection due to noise alone. A formalism to choose the optimal set of templates using a criterion was first given by Sathyaprakash and Dhurandhar (1991) and Dhurandhar and Sathyaprakash (1994) known as the S-D formalism.

These search templates will be discrete subset of a continuous, multi parameter family, each of which approximate a possible signal. Given a signal $h(t)$ buried in noise $n(t)$, the task is to find an 'optimal' template $q(t)$ that would produce, on the average, the best possible SNR. The enhancement in the signal-to-noise ratio not only increases the number of detectable events but, more importantly, it also allows a more accurate determination of signal parameters—the error in the estimation of parameter being inversely proportional to the signal-to-noise ratio.

If the functional form of the template is identical to that of the signal, the mean signal-to-noise ratio in the presence of a signal is highest possible for any linear data processing technique, which is why matched filtering is also known as optimal filtering (Helstrom, 1968). A *matched filter*, in the frequency domain, is a best-guess template of the expected signal waveform divided by the interferometer's spectral noise density.

In order to take full advantage of matched filtering it is essential that the phase of the waveform be known to a very high degree of accuracy to accumulate the SNR (Cutler et al. 1993). This is referred to as coherent integration of the signal, where the SNR grows $\sqrt{T_o}$. This is in contrast with incoherent methods, such as *stacking* and *tracking* (Brady, et. al. 1998, 2000), where one disregards the phase information and the SNR does not accumulate

as quickly. *Tracking* involves tracking of lines in the time-frequency plane built from the FT of short (around 40 minutes long) stretches of data. The other *stacking* involves dividing the data into shorter (around a day long) stretches, searching each stretch for signals, and enhancing the detectability by incoherently summing the FT of data stretches.

There are several questions that must be answered in order to determine the feasibility of a matched filtering search strategy and, if feasible, to implement it. Which parameters significantly affect the wave form ? How should the spacing of the template parameters (lattice points) be chosen? Is there a parameterization that is in some sense preferred by the template waveforms? How many templates are needed to cover a given region of interest in the parameter space and how much computing power and memory will it cost to process the data through them? In the case of modulated Pulsar signal we must also ask what approximation to the true wave form is good enough?

Ambiguity function, well known in statistical theory of signal detection (Helstrom, 1968), is a very powerful tool in signal analysis. It helps to access the number of templates required to span the parameter space of the signal. However, Apostolatos (1995) defined a term called *Fitting Factor* (FF) which quantitatively describes the closeness of the true signals to the template manifold in terms of the reduction in SNR due to cross correlation of a signal outside the manifold with all the templates lying inside the manifold.

Fitting factor

One of the standard measure for deciding what class of wave form is good enough is the *Fitting Factor* and has already been used by various earlier authors (Sathyaprakash and Dhurandhar, 1991 and Dhurandhar and Sathyaprakash,

1994) as a measure of adequateness of a template family, but previous discussions have not shown explicitly how this intuitively well-formed function is connected with detectability. Previously FF has sometimes been called the "correlation", a number that is often used in so many different ways. The name comes from the fact that, by maximising the quantity FF, the parameters of the templates can be adjusted to best fit the true waveform.

Let us consider a detector receiving almost monochromatic GW signals from a pulsar. The signal will be Doppler modulated due to the motion of Earth and stars, represented by $S(t)$. The detector's output $X(t)$ of the detector will be

$$X(t) = S(t) + n(t) \tag{2.7}$$

If the search template is the exact waveform $h(t)$, then we would achieve the highest possible signal-to-noise ratio given as

$$\left(\frac{S}{N}\right)_{max} = \langle S(f)|S(f)\rangle^2 \tag{2.8}$$

where the inner product of two waveforms $\langle h_1|h_2\rangle$ is defined as

$$\begin{aligned} \langle h_1|h_2\rangle &= 2\int_0^\infty \frac{\tilde{h}_1^*(f)\tilde{h}_2(f) + \tilde{h}_1(f)\tilde{h}_2^*(f)}{S_n(f)}df \\ &= 4\int_0^\infty \frac{\tilde{h}_1^*(f)\tilde{h}_2(f)}{S_n(f)}df \end{aligned} \tag{2.9}$$

The SNR ratio will be reduced below $(S/N)_{max}$ whenever the template is not the exact waveform but some other approximate one. If search is performed with some family of templates $S_T(f;\vec{\xi})$ for a signal vector $\vec{\xi}$ (The signal is considered a vector in parameter space). Then the SNR will be given by

$$\left(\frac{S}{N}\right) = \overset{max}{\vec{\xi}} \frac{\langle X(f)|S_T(f;\vec{\xi})\rangle}{rms\langle n|S_T(f;\vec{\xi})\rangle} \tag{2.10}$$

For an ensemble of realizations of the detector noise, the expectation values $\langle n|S_T(f;\vec{\xi})\rangle$ and $\langle n|S_T(f;\vec{\xi})\rangle\langle n|S_T(f;\vec{\xi})\rangle$ are zero and $\langle S_T(f;\vec{\xi})|S_T(f;\vec{\xi})\rangle$,

respectively. Thus the ensemble-averaged signal-to-noise ratio turns out to be

$$\begin{aligned}\left(\frac{S}{N}\right) &= \overset{max}{\vec{\xi}} \frac{\langle S(f)|S_T(f;\vec{\xi})\rangle}{\sqrt{\langle S_T(f;\vec{\xi})|S_T(f;\vec{\xi})\rangle}} \\ &= \left[\overset{max}{\vec{\xi}} \frac{\langle S(f)|S_T(f;\vec{\xi})\rangle}{\sqrt{\langle S_T(f;\vec{\xi})|S_T(f;\vec{\xi})\rangle\langle S(f)|S(f)\rangle}}\right]\left(\frac{S}{N}\right)_{max} \qquad (2.11)\end{aligned}$$

The name *Fitting Factor* is given to the reduction in signal-to-noise ratio that results because of using the chosen template family, rather than the true signal h, in the search:

$$\begin{aligned}FF(\vec{\xi}) &= \overset{max}{\vec{\xi}} \frac{\langle S(f)|S_T(f;\vec{\xi})\rangle}{\sqrt{\langle S_T(f;\vec{\xi})|S_T(f;\vec{\xi})\rangle}} \\ &= \overset{max}{\vec{\xi}} \frac{\langle S(f)|S_T(f;\vec{\xi})\rangle}{\sqrt{\langle S_T(f;\vec{\xi})|S_T(f;\vec{\xi})\rangle\langle S(f)|S(f)\rangle}} \qquad (2.12)\end{aligned}$$

Therefore, if the family of search template used at the detection stage does not contain the true signal waveform, then the reduction in the signal-to-noise ratio will be given by

$$\left(\frac{S}{N}\right) = FF(\vec{\xi}) \times \left(\frac{S}{N}\right)_{max} \qquad (2.13)$$

The spacing of the grid of filters is decided by the fractional loss due to to the imperfect match that can be tolerated. Given the parameters space that one needs to scan, it is then easy to estimate the total number of filters required to carry out the search for the signal. The signal strength scales inversely with distance, the fraction of event rate retained is approximately FF^3. Therefore it has become conventional to regard $FF = 0.9$ as the lowest acceptable FF value for some template family to be considered adequate. Since a reduction in SNR by 10% means a 27% loss in the event rate. On the other hand a 10% reduction in SNR is equivalent to roughly 10% shortening of the detectors arms.

2.5 Computational costs

Matched filtering places stringent demands on the knowledge of the signal's phase evolution which depends on two things: (1) our modelling of the signal and (2) the parameters characterising the signal. If our signal model is inaccurate or if the signal's parameters are unknown, there could be a loss in the SNR extracted. For instance, in the case of inspiral signals, a mismatch of one cycle in 10^4 cycles leads to a drop in the SNR by more than a factor of two, losing a factor of eight in the number of potentially detectable events. Recall that the SNR is inversely proportional to the distance to a source; thus an SNR loss by a factor a will reduce the span of a detector by the same factor, resulting in a decrease in the volume of observation, and hence the number of events, by a factor a^3. Moreover, since the parameters of a signal will not be known in advance, it is necessary to filter the data with a family of templates located at various points in the parameter space e.g., placed on a lattice such that any signal will lie close enough to at least one of the templates to have a good cross-correlation with that template. The number of such templates is typically very large. This places a great demand on the computational resources needed to make an on-line search.

The search problem for continuous waves from spinning neutron stars is the most computer-intensive job in gravitational wave data analysis. Today, there is little hope that all-sky searches lasting for a year or more, can be made. It is easy to see why this is such an intensive job: Firstly, the data has to be collected continuously for months together and at a good sensitivity. Secondly, though a neutron star emits a periodic signal in its rest frame, save for the neutron star spin-down which indeed induces some modulation in the waveform, because of Earth's acceleration relative to the source, the detector

does not see a periodic wave. The wave is both frequency and amplitude modulated. One can, fortunately, de-modulate these effects since Earth's motion is known quite accurately, and hence recover the original periodic signal. But de-modulation requires a knowledge of the source's direction and its frequency, which are unknown in a blind search. The angular resolution one obtains in a year's integration is $\Delta\theta = \lambda/D$, where λ is the wave length of radiation and D is the baseline of the detector in a year's integration, namely 1 A.U. Thus, for $f = 1$ kHz we have $\Delta\theta = 10^{-6}$ rad or about two arcsec. Now, assuming that the source may be in any one of the 4 arcsec^2 patches on the sky we get the number of patches in the sky for which we will have to try out a de-modulation correction to be $4\pi/(\Delta\theta)^2 = 4\pi 10^{12}$. It is quite an impossible task to apply Doppler de-modulation to the detector output for each of these $\sim 10^{13}$ patches and compute as many Fourier transforms.

One, therefore, asks the question given a compute power what is the best possible search one can do? Is there any advantage in going from a one-step search to a two or multi-step hierarchical search? What about directional searches? These are some of the problems for which we have some answer; but a great deal of work is needed and is currently under progress, to improve and optimise search algorithms.

The differential geometric studies shows that with a TFLOPS-class computer, the number of days of data can be analysed on-line and we can carry out a blind search. Unfortunately, the longest data we can integrate on-line, for neutron stars with spin frequencies $f \leq 100$ Hz and spin-down rates less than 1000 years, is about 18 days. This yields a SNR lower by a factor of 5 as compared to a year's worth of observing. On-line searches for neutron stars with $f \leq 500$ Hz (largest observed frequencies of millisecond pulsars) and spin-down rates of 40 years (shortest observed spin-down rates), can only

be made for a data set lasting for a duration of 20 hours or less. If source's position is known in advance, but not its frequency, then one can carry out an on-line search, again with a TFLOPS-class computer, for the frequency of the source in a data set that is worth 3 months long. This is good news since there are many known pulsars and X-ray binary systems that are potential sources of radiation. In addition, the obvious targeted search locations are the centre of the Galaxy and globular clusters.

There have been efforts to study the effectualness of a two-step hierarchical method for a blind search. Here the basic idea is to construct Fourier transforms of data sets of duration smaller than the period in which Doppler modulations will be important and to stack spectral densities obtained in this way and to add them all up. This is an incoherent way of building the signal since one adds spectral densities that have no phase information. Therefore, one gains in SNR less than what an optimal matched filtering method is able to achieve. However, this does not matter since (i) the targeted SNR's are quite high ~ 10 and (ii) candidate events can always be followed-up using coherent integration methods. These methods afford an on-line all-sky blind search for continuous gravitational waves for a period of 4 months or less using a 20 GFLOPS computer. Detector groups are planning to build computers of this kind to aid in their search for continuous GW.

2.6 Detection criteria

A signal needs to be above the noise experienced in the instrument and environment. However, this alone is insufficient to establish it as a gravitational wave in the terrestrial detectors. The most satisfying circumstance is that a gravitational wave observation be made in a set of widely distributed detectors

[the Gravitational Wave Network (GWN)] and the resorted wave forms allow the solutions for the polarization of the wave and the position of the source. Armed with this information an electromagnetic (or neutrino) search could be attempted in the error circle of the gravitational wave detection: a time honored approach bringing gravitational wave of observation into the main stream of Astrophysics. The strategy would apply to all classes of sources: impulsive chirps, quasiperiodic and periodic.

The confident detection of impulsive sources is most difficult, while the periodic and quasiperiodic detection will have confidence limits based on quasi-stationary system noise (the signals last long enough to take a meaningful sample of the noise spectrum), the impulsive signals especially if rare, will be particularly dependent of the non-Gaussian component of the noise; the noise most difficult to reduce and control in a signal detectors. The technique of multiple coincidence of several detectors is one of the best means to gain confidence. The coincidence must occur within a time window to permit a consistent solution for a location in the sky. If the general character of the source can be guessed in advance (for example, a binary coalescence chirp, or a black-hole normal mode oscillation), the signal is filtered prior to the coincidence measurement to improve the sensitivity. The more detectors involved, the greater the confidence assigned to the detection.

There is still a possibility of coincidence due to environmental or anthropogenic causes. The various sites throughout the world are far enough apart that most environmental perturbations should not correlate between them. The acoustic noise, the seismic noise, and the power line (especially if the network includes detectors in a different power grids and significantly different time zones) will be uncorrelated. There are correlations in the magnetic field fluctuations (thunderstorms) and in radio frequency emittions. As part

of the detection strategy a large number of environmental parameters will be measured along with the gravitational wave signals at each site. One of the requirements for the authenticity of impulsive sources will be the lack of correlation with environmental perturbations and other ancillary internal signals developed to monitor the performance of the instruments.

Chapter 3

Data analysis of continuous gravitational wave: Fourier transform-I

3.1 Introduction

The first generation of long-baseline laser interferometers and ultra cryogenic bar detectors will start collecting data very soon. The network of detectors will not only confirm the existence of GWs but will also yield information about its important parameters viz; amplitude, frequency and phase. In addition, a careful monitoring of the signal will also provide the information about the structure and the dynamics of its source. At the present stage, the data analysis depends largely upon the study of the expected characteristic of its potential sources and the waveforms. The majority of the experimental searches are focussed on the detection of burst and *chirp* signals. However, the interest in the data analysis for CGW signals is growing. A prime example of sources of this type is a spinning neutron star. Many research groups around the globe are working extensively on the data analysis for spinning neutron stars [Jaranwoski, et.al (1998, 1999, 2000), Brady et. al. (1998, 2000), Królak (1999)].

Our Galaxy is expected to have, on logistic grounds, at least 10^8 spinning

neutron stars; with a birth rate of one in every 30 years. However, a very insignificant fraction of them are observed—the number of known pulsars has gone up to 1100. There are compelling arguments that nearby millisecond pulsars can provide a detectable source of CGW. Hence, there is a strong case for searching all sky for the presence of neutron stars with the philosophy that they are emitting GWs but otherwise unknown optically. This study will help us to understand the pulsar population in our Galaxy.

The detection of GW signals in the output has its own problems, not the least of which is the sheer volume of data analysis. Bar detectors have essentially the same problems as interferometers in reference to CGW sources. The possibility that these detectors are capable to search for different kinds of signals makes them very versatile, but also complicates the data analysis. Each detector produces a single data stream that may contain many kinds of signals. Detectors don't point, but rather sweep their broad quadrupolar beam pattern across the sky as the earth moves. So possible sources could be anywhere on the sky and accordingly the data analysis algorithms need to accommodate signals from any arbitrary location of its source.

In this and the next Chapter we present analysis of FT of the output data of a ground based laser interferometer. The output data has prominently dominant broad band noise and the signal is to be extracted out of it. For this, one has to enhance SNR. This is achieved by analyzing long observation time data as SNR is directly proportional to the square root of observation time $\sqrt{T_o}$. However, in a data for long duration, the monochromatic signal gets Doppler modulated due to (i) orbital motions of Earth around Sun and (ii) spin of Earth. The Frequency modulation (FM) will spread the signal in a very large number of bins depending on the source location and the frequency. In addition there is Amplitude modulation (AM). As we will see in the sequel

the amplitude of the detector output consists of simple harmonic terms with frequencies w_{rot} and $2w_{rot}$ where, w_{rot} stands for angular rotational frequency of Earth. Accordingly, the AM results in splitting of FT into frequencies $\pm w_{rot}$ and $\pm 2w_{rot}$.

In the next section, we present the noise free response of the laser interferometric detector and obtain the explicit beam pattern functions. In section 3, we discuss the Doppler effect and obtain the FT of the FM signal for arbitrary source and detector locations taking into account Earth's rotational motion about its axis and its revolution around Sun. In section 4, the FT of the Doppler modulated complete response of the detector has been obtained. In the last section we discuss the results of the Chapter.

3.2 The noise free response of detector: Beam pattern and amplitude modulation

Let a plane GW falls on a laser interferometer and produces changes in the arms of the detector. In order to express these changes quantitatively we would require to specify the wave and the detector. Let XYZ and xyz represent respective frames characterising wave and detector. We assume the direction of propagation of the wave to be the Z axis and the vertical at place of detector to be the z axis [see Fig. (3.1)]. In view of our discussion in subsection (1.2.2), the difference of the changes δl in the arm lengths of the detector is given via

$$R(t) = \frac{\delta l}{l_o} = -\sin 2\Omega \left[\left(\mathbf{A}_X^x \mathbf{A}_X^y - \mathbf{A}_Y^x \mathbf{A}_Y^y \right) h_+ + \left(\mathbf{A}_X^x \mathbf{A}_Y^y + \mathbf{A}_Y^x \mathbf{A}_X^y \right) h_\times \right] \quad (3.1)$$

where l_o is the normal length of the arms of the detector and 2Ω express the angle between them (Schutz and Tinto, 1987). The matrix $\left(\mathbf{A}_K^j\right)$ represents

Figure 3.1: Orientation of the detector.

Figure 3.2: Earth frame (x', y', z').

Figure 3.3: Solar System Barycentre frame (X', Y', Z').

the transformation expressing the rotations to bring the wave frame (X, Y, Z) to the detector frame (x, y, z). The direction of the source may be expressed in any of the coordinates employed in Spherical Astronomy. However, we find it convenient to define it in Solar System Barycentre (SSB) frame (X', Y', Z') [see Fig. (3.3)]. This SSB frame is nothing but astronomer's ecliptic coordinate system. Let θ and ϕ denote the celestial colatitude and celestial longitude of the source. These coordinates are related to right ascension $\bar{\alpha}$ and declination $\bar{\delta}$ of the source via

$$\left.\begin{aligned} \cos\theta &= \sin\bar{\delta}\cos\epsilon - \cos\bar{\delta}\sin\epsilon\sin\bar{\alpha} \\ \sin\theta\cos\phi &= \cos\bar{\delta}\cos\bar{\alpha} \\ \sin\theta\sin\phi &= \sin\bar{\delta}\sin\epsilon + \cos\bar{\delta}\cos\epsilon\sin\bar{\alpha} \end{aligned}\right\} \tag{3.2}$$

where ϵ represents obliquity of the ecliptic. We choose x axis as the bisector of the angle between the arms of the detector. At this stage the orientation of the detector in the horizontal plane is arbitrary. It is assigned with the help of the angle γ which x axis makes with the local meridian. The location of the detector on earth is characterised by the angle α, colatitude and β, the local sidereal time expressed in radians. The transformation matrix $\left(\mathbf{A}_K^j\right)$ may be expressed as

$$\mathbf{A} = \mathbf{DCB} \tag{3.3}$$

where

B : rotation required to bring XYZ to $X'Y'Z'$

C : rotation required to bring $X'Y'Z'$ to $x'y'z'$

D : rotation required to bring $x'y'z'$ to xyz

Here $x'y'z'$ represents the frame associated with earth [see Figs. (3.1-3.2)]. The Euler angles defining the corresponding rotation matrices (Goldstein, 1980) are

given via

$$\left.\begin{array}{lcl} \mathbf{B} & : & (\theta, \phi, \psi) \\ \mathbf{C} & : & (0, \epsilon, 0) \\ \mathbf{D} & : & (\alpha, \beta + \pi/2, \gamma - \pi/2) \end{array}\right\} \tag{3.4}$$

where ψ is a measure of the polarisation of the wave. Let us express Eq. (3.1) as

$$R(t) = \frac{\delta l}{l_o} = -\sin 2\Omega \left[F_+ h_+ + F_\times h_\times\right] \tag{3.5}$$

The functions F_+ and $F_\times$ involve the angles $\theta, \phi, \psi, \epsilon, \alpha, \beta, \gamma$ and express the effect of the interaction of the wave and detector. These are called antenna or beam patterns. After a straight forward calculation one obtains (Jotania and Dhurandhar, 1994)

$$\begin{aligned} F_+(t) \;=\; & \frac{1}{2}\left[\left\{(\cos\psi\cos\phi - \cos\theta\sin\phi\sin\psi)^2 - (\cos\psi\sin\phi + \cos\theta\cos\phi\sin\psi)^2\right\}\right. \\ & \times \left\{2(\cos\alpha\cos\beta\cos\gamma - \sin\beta\sin\gamma)(-\cos\alpha\cos\beta\sin\gamma - \sin\beta\cos\gamma)\right\} \\ & + \left\{(-\sin\psi\cos\phi - \cos\theta\sin\phi\cos\psi)^2 - (\cos\theta\cos\phi\cos\psi - \sin\psi\sin\phi)^2\right\} \\ & \times \left[\cos^2\epsilon\left\{2(\cos\alpha\sin\beta\cos\gamma + \cos\beta\sin\gamma)(\cos\beta\cos\gamma - \cos\alpha\sin\beta\sin\gamma)\right\}\right. \\ & - \sin^2\epsilon\sin^2\alpha\sin 2\gamma + \sin 2\epsilon\left\{(\cos\alpha\sin\beta\cos\gamma + \cos\beta\sin\gamma)\sin\alpha\sin\gamma\right. \\ & - \left.(\cos\beta\cos\gamma - \cos\alpha\sin\beta\sin\gamma)\sin\alpha\cos\gamma\right\}] \\ & - (\sin^2\theta\cos 2\phi) \\ & \times \left[\sin^2\epsilon\left\{2(\cos\alpha\sin\beta\cos\gamma + \cos\beta\sin\gamma)(\cos\beta\cos\gamma - \cos\alpha\sin\beta\sin\gamma)\right\}\right. \\ & - \cos^2\epsilon\sin^2\alpha\sin 2\gamma - \sin 2\epsilon\left\{(\cos\alpha\sin\beta\cos\gamma + \cos\beta\sin\gamma)\sin\alpha\sin\gamma\right. \\ & - \left.\left.(\cos\beta\cos\gamma - \cos\alpha\sin\beta\sin\gamma)\sin\alpha\cos\gamma\right\}\right]] \\ & + \left\{(\cos\psi\cos\phi - \cos\theta\sin\phi\sin\psi)(-\sin\psi\cos\phi - \cos\theta\sin\phi\cos\psi)\right. \\ & - \left.(\cos\psi\sin\phi + \cos\theta\cos\phi\sin\psi)(\cos\theta\cos\phi\cos\psi - \sin\psi\sin\phi)\right\} \end{aligned}$$

$$
\begin{aligned}
&\times\ [\cos\epsilon\,\{(\cos\beta\cos\gamma-\cos\alpha\sin\beta\sin\gamma)(\cos\alpha\cos\beta\cos\gamma-\sin\beta\sin\gamma)\\
&-\ (\cos\alpha\sin\beta\cos\gamma+\cos\beta\sin\gamma)(\cos\alpha\cos\beta\sin\gamma+\sin\beta\cos\gamma)\}\\
&+\ \sin\epsilon\,\{(\cos\alpha\cos\beta\cos\gamma-\sin\beta\sin\gamma)(\sin\alpha\sin\gamma)\\
&+\ (\cos\alpha\cos\beta\sin\gamma+\sin\beta\cos\gamma)(\sin\alpha\cos\gamma)\}]\\
&+\ \{(\cos\psi\cos\phi-\cos\theta\sin\phi\sin\psi)(\sin\theta\sin\phi)\\
&+\ (\cos\psi\sin\phi+\cos\theta\cos\phi\sin\psi)(\sin\theta\cos\phi)\}\\
&\times\ [-\sin\epsilon\,\{(\cos\beta\cos\gamma-\cos\alpha\sin\beta\sin\gamma)(\cos\alpha\cos\beta\cos\gamma-\sin\beta\sin\gamma)\\
&-\ (\cos\alpha\sin\beta\cos\gamma+\cos\beta\sin\gamma)(\cos\alpha\cos\beta\sin\gamma+\sin\beta\cos\gamma)\}\\
&+\ \cos\epsilon\,\{(\cos\alpha\cos\beta\cos\gamma-\sin\beta\sin\gamma)(\sin\alpha\sin\gamma)\\
&+\ (\cos\alpha\cos\beta\sin\gamma+\sin\beta\cos\gamma)(\sin\alpha\cos\gamma\}]\\
&+\ \{(-\sin\psi\cos\phi-\cos\theta\sin\phi\cos\psi)(\sin\theta\sin\phi)\\
&+\ (\cos\theta\cos\phi\cos\psi-\sin\psi\sin\phi)(\sin\theta\cos\phi)\}\\
&\times\ [-(\cos\epsilon\sin\epsilon)\,\{2(\cos\alpha\sin\beta\cos\gamma+\cos\beta\sin\gamma)\\
&\quad(\cos\beta\cos\gamma-\cos\alpha\sin\beta\sin\gamma)+\sin^2\alpha\sin 2\gamma\}\\
&+\ \cos 2\epsilon\,\{(\cos\alpha\sin\beta\cos\gamma+\cos\beta\sin\gamma)(\sin\alpha\sin\gamma)\\
&-\ (\cos\beta\cos\gamma-\cos\alpha\sin\beta\sin\gamma)(\sin\alpha\cos\gamma)\}]\ ;
\end{aligned}
\tag{3.6}
$$

$$
\begin{aligned}
F_\times(t)\ =\ & 2(\cos\psi\cos\phi-\cos\theta\sin\phi\sin\psi)(\cos\psi\sin\phi+\cos\theta\cos\phi\sin\psi)\\
&\times(\cos\alpha\cos\beta\cos\gamma-\sin\beta\sin\gamma)(-\cos\alpha\cos\beta\sin\gamma-\sin\beta\cos\gamma)\\
&+(-\sin\psi\cos\phi-\cos\theta\sin\phi\cos\psi)(\cos\theta\cos\phi\cos\psi-\sin\psi\sin\phi)\\
&\times\big[\cos^2\epsilon\,\{2(\cos\alpha\sin\beta\cos\gamma+\cos\beta\sin\gamma)(\cos\beta\cos\gamma-\cos\alpha\sin\beta\sin\gamma)\}\\
&-\ \sin^2\epsilon\sin^2\alpha\sin 2\gamma+\sin 2\epsilon\,\{(\cos\alpha\sin\beta\cos\gamma+\cos\beta\sin\gamma)\sin\alpha\sin\gamma\\
&-\ (\cos\beta\cos\gamma-\cos\alpha\sin\beta\sin\gamma)\sin\alpha\cos\gamma\}]\\
&-\frac{1}{2}(\sin^2\theta\sin 2\phi)
\end{aligned}
$$

$$
\begin{aligned}
&\times \left[\sin^2\epsilon\,\{2(\cos\alpha\sin\beta\cos\gamma+\cos\beta\sin\gamma)(\cos\beta\cos\gamma-\cos\alpha\sin\beta\sin\gamma)\}\right.\\
&-\cos^2\epsilon\sin^2\alpha\sin 2\gamma-\sin 2\epsilon\,\{(\cos\alpha\sin\beta\cos\gamma+\cos\beta\sin\gamma)\sin\alpha\sin\gamma\\
&-\ (\cos\beta\cos\gamma-\cos\alpha\sin\beta\sin\gamma)\sin\alpha\cos\gamma\}]\\
&+\{(\cos\psi\cos\phi-\cos\theta\sin\phi\sin\psi)(-\sin\psi\sin\phi+\cos\theta\cos\phi\cos\psi)\\
&-\ (\cos\psi\sin\phi+\cos\theta\cos\phi\sin\psi)(\cos\theta\sin\phi\cos\psi+\sin\psi\cos\phi)\}\\
&\times[\cos\epsilon\,\{(\cos\beta\cos\gamma-\cos\alpha\sin\beta\sin\gamma)(\cos\alpha\cos\beta\cos\gamma-\sin\beta\sin\gamma)\\
&-\ (\cos\alpha\sin\beta\cos\gamma+\cos\beta\sin\gamma)(\cos\alpha\cos\beta\sin\gamma+\sin\beta\cos\gamma)\}\\
&+\sin\epsilon\,\{(\cos\alpha\cos\beta\cos\gamma-\sin\beta\sin\gamma)(\sin\alpha\sin\gamma)\\
&+\ (\cos\alpha\cos\beta\sin\gamma+\sin\beta\cos\gamma)(\sin\alpha\cos\gamma)\}]\\
&+\{-(\cos\psi\cos\phi-\cos\theta\sin\phi\sin\psi)(\sin\theta\cos\phi)\\
&+\ (\cos\psi\cos\phi+\cos\theta\cos\phi\sin\psi)(\sin\theta\sin\phi)\}\\
&\times[-\sin\epsilon\,\{(\cos\beta\cos\gamma-\cos\alpha\sin\beta\sin\gamma)(\cos\alpha\cos\beta\cos\gamma-\sin\beta\sin\gamma)\\
&-\ (\cos\alpha\sin\beta\cos\gamma+\cos\beta\sin\gamma)(\cos\alpha\cos\beta\sin\gamma+\sin\beta\cos\gamma)\}\\
&+\cos\epsilon\,\{(\cos\alpha\cos\beta\cos\gamma-\sin\beta\sin\gamma)(\sin\alpha\sin\gamma)\\
&+\ (\cos\alpha\cos\beta\sin\gamma+\sin\beta\cos\gamma)(\sin\alpha\cos\gamma\}]\\
&+\{(-\sin\psi\sin\phi+\cos\theta\cos\phi\cos\psi)(\sin\theta\sin\phi)\\
&+\ (\cos\theta\sin\phi\cos\psi+\sin\psi\cos\phi+)(\sin\theta\cos\phi)\}\\
&\times[-(\cos\epsilon\sin\epsilon)\,\{2(\cos\alpha\sin\beta\cos\gamma+\cos\beta\sin\gamma)\\
&\quad(\cos\beta\cos\gamma-\cos\alpha\sin\beta\sin\gamma)+\sin^2\alpha\sin 2\gamma\}\\
&+\cos 2\epsilon\,\{(\cos\alpha\sin\beta\cos\gamma+\cos\beta\sin\gamma)(\sin\alpha\sin\gamma)\\
&-\ (\cos\beta\cos\gamma-\cos\alpha\sin\beta\sin\gamma)(\sin\alpha\cos\gamma)\}]\ ;
\end{aligned}
\tag{3.7}
$$

It is easy to understand the structure of the above complicated looking expressions for F_+ and $F_\times$ by introducing following abbreviations

$$\left.\begin{aligned}
U &= \cos\alpha\cos\beta\cos\gamma - \sin\beta\sin\gamma\,, \\
V &= -\cos\alpha\cos\beta\sin\gamma - \sin\beta\cos\gamma\,, \\
X &= \cos\alpha\sin\beta\cos\gamma + \cos\beta\sin\gamma\,, \\
Y &= -\cos\alpha\sin\beta\sin\gamma + \cos\beta\cos\gamma
\end{aligned}\right\} \tag{3.8}$$

$$\left.\begin{aligned}
L &= \cos\psi\cos\phi - \cos\theta\sin\phi\sin\psi\,, \\
M &= \cos\psi\sin\phi + cos\theta\cos\phi\sin\psi\,, \\
N &= -\sin\psi\cos\phi - cos\theta\sin\phi\cos\psi\,, \\
P &= -\sin\psi\sin\phi + cos\theta\cos\phi\cos\psi\,, \\
Q &= \sin\theta\sin\phi\,, \qquad R \;=\; \sin\theta\cos\phi\,,
\end{aligned}\right\} \tag{3.9}$$

$$\left.\begin{aligned}
A &= 2XY\cos^2\epsilon - \sin^2\epsilon\sin^2\alpha\sin 2\gamma + \sin 2\epsilon(X\sin\alpha\sin\gamma \\
&\quad - Y\sin\alpha\cos\gamma)\,, \\
B &= 2XY\sin^2\epsilon - \cos^2\epsilon\sin^2\alpha\sin 2\gamma - \sin 2\epsilon(X\sin\alpha\sin\gamma \\
&\quad - Y\sin\alpha\cos\gamma)\,, \\
C &= \cos\epsilon(YU + XV) + \sin\epsilon(U\sin\alpha\sin\gamma - V\sin\alpha\cos\gamma)\,, \\
D &= -\sin\epsilon(YU + XV) + \cos\epsilon(U\sin\alpha\sin\gamma - V\sin\alpha\cos\gamma]\,, \\
E &= -2XY\cos\epsilon\sin\epsilon - \cos\epsilon\sin\epsilon\sin^2\alpha\sin 2\gamma \\
&\quad + \cos 2\epsilon(X\sin\alpha\sin\gamma - Y\sin\alpha\cos\gamma)
\end{aligned}\right\} \tag{3.10}$$

One obtains:

$$\begin{aligned}
F_+(t) &= \frac{1}{2}\left[2(L^2 - M^2)UV + (N^2 - P^2)A \;+ (Q^2 - R^2)B\right] + (LN - MP)C \\
&\quad + (LQ + MR)D + (NQ + PR)E\,, \qquad (3.11) \\
F_\times(t) &= 2LMUV + NPA - \frac{1}{2}B\sin^2\theta\sin 2\phi \;+ (LP + MN)C \\
&\quad + (MQ - LR)D + (PQ - NR)E \qquad (3.12)
\end{aligned}$$

The compactification achieved here is because of the fact that these abbreviations find places in the transformation matrices as:

$$\mathbf{B} = \begin{pmatrix} L & N & Q \\ M & P & -R \\ \sin\theta\sin\psi & \sin\theta\cos\psi & \cos\theta \end{pmatrix} \tag{3.13}$$

$$\mathbf{C} = \begin{pmatrix} 1 & 0 & 0 \\ 0 & \cos\epsilon & \sin\epsilon \\ 0 & -\sin\epsilon & \cos\epsilon \end{pmatrix} \tag{3.14}$$

$$\mathbf{D} = \begin{pmatrix} U & V & \sin\alpha\cos\beta \\ X & Y & \sin\alpha\sin\beta \\ -\sin\alpha\cos\gamma & \sin\alpha\sin\gamma & \cos\alpha \end{pmatrix} ; \tag{3.15}$$

After algebraic manipulation Eqs. (3.11) and (3.12) may be expressed as

$$F_+(t) = F_{1_+}\cos 2\beta + F_{2_+}\sin 2\beta + F_{3_+}\cos\beta + F_{4_+}\sin\beta + F_{5_+} ; \tag{3.16}$$

$$F_\times(t) = F_{1_\times}\cos 2\beta + F_{2_\times}\sin 2\beta + F_{3_\times}\cos\beta + F_{4_\times}\sin\beta + F_{5_\times} \tag{3.17}$$

where F_{i_+} and $F_{i_\times}$ $(i = 1, 2, 3, 4, 5)$ are time independent expressions given via

$$\left.\begin{aligned} F_{1_+} &= -2G\cos\alpha\cos 2\gamma + \tfrac{H\sin 2\gamma}{2}(\cos^2\alpha + 1)\,, \\ F_{2_+} &= H\cos\alpha\cos 2\gamma + G\sin 2\gamma(\cos^2\alpha + 1)\,, \\ F_{3_+} &= I\sin\alpha\cos 2\gamma + J\sin 2\alpha\sin 2\gamma\,, \\ F_{4_+} &= 2J\sin\alpha\cos 2\gamma - \tfrac{I}{2}\sin 2\alpha\sin 2\gamma\,, \\ F_{5_+} &= \tfrac{3\sin^2\alpha\sin 2\gamma}{2}[H + L^2 - M^2]\,, \end{aligned}\right\} ; \tag{3.18}$$

$$\left.\begin{aligned} G &= \tfrac{1}{2}[(LQ + MR)\sin\epsilon - (LN - MP)\cos\epsilon]\,, \\ H &= \tfrac{1}{2}[(N^2 - P^2)\cos^2\epsilon - (L^2 - M^2) + (Q^2 - R^2)\sin^2\epsilon \\ &\quad - (NQ + PR)\sin 2\epsilon]\,, \\ I &= \tfrac{1}{2}[(Q^2 - R^2)\sin 2\epsilon - (N^2 - P^2)\sin 2\epsilon - \\ &\quad 2(NQ + PR)\cos 2\epsilon]\,, \\ J &= \tfrac{1}{2}[(LN - MP)\sin\epsilon + (LQ + MR)\cos\epsilon] \end{aligned}\right\} \tag{3.19}$$

Let us note that $F_{i_\times}$ is related to F_{i_+} via

$$F_{i_\times}(\theta, \phi, \psi, \alpha, \beta, \gamma, \epsilon) = F_{i_+}(\theta, \phi - \frac{\pi}{4}, \psi, \alpha, \beta, \gamma, \epsilon) ; \tag{3.20}$$
$$i = 1, 2, 3, 4, 5$$

This symmetry is representative of the quadrupolar nature of the detector and the wave. A detector in different orientations will record different amplitudes in the response. The explicit beam pattern functions may be computed easily for any instant of time. Due to symmetries involved in F_+ and $F_\times$ it is sufficient to discuss either of the beam pattern.

The amplitude modulation of the received signal is a direct consequence of the non-uniformity of the sensitivity pattern. The antenna response is not peaked in any direction but is anisotropic. As remarked earlier they are fairly complicated function of their arguments. Equations. (3.16) and (3.17) reveal that the monochromatic signal frequency will split, due to AM, into five lines. This results in the distribution of energy in various frequencies and consequent reduction of the amplitude of the signal. The periodicity of the beam patterns F_+ and $F_\times$ with a period equal to one sidereal day is due to the diurnal motion of Earth.

3.3 Doppler shift and Frequency modulation

The frequency of a monochromatic signal will be Doppler shifted due to the translatory motion of the detector, acquired from the motions of Earth. Let us consider a CGW signal of constant frequency f_o. The frequency f' received at the instant t by the detector is given by

$$f'(t) = f_o\gamma_o\left(1 + \frac{\mathbf{v}.\mathbf{n}}{c}(t)\right) \quad ; \quad \gamma_o = \left(1 - \frac{v^2}{c^2}\right)^{-1/2} \tag{3.21}$$

where $\mathbf{n}$ is the unit vector from the antenna to source, $\mathbf{v}$ is the relative velocity of the source and the antenna, and c is the velocity of light. The unit vector $\mathbf{n}$ from the antenna to the source, because of the fact that the distance of the

source is very large compared to the average distance of the centre of the SSB frame and the detector, may be taken parallel to the unit vector drawn from the centre of the SSB frame to the source. Hence,

$$\mathbf{n} \quad = \quad (\sin\theta\cos\phi \quad , \quad \sin\theta\sin\phi \quad , \quad \cos\theta) \tag{3.22}$$

As $\mathbf{v}$ keeps on changing continuously both in its amplitude and direction f' is a continuous function of t. Further, since $v \ll c$ we take $\gamma_o = 1$.
The radius vector $\mathbf{r}(t)$ in the SSB frame is given by

$$\begin{aligned}\mathbf{r}(t) \quad = \quad & [R_{se}\cos(w_{orb}t) + R_e\sin\alpha\cos\beta \ , \\ & R_{se}\sin(w_{orb}t) + R_e\sin\alpha\sin\beta\cos\epsilon - R_e\cos\alpha\sin\epsilon\,, \\ & R_e\sin\alpha\sin\beta\sin\epsilon + R_e\cos\alpha\cos\epsilon] \ ;\end{aligned} \tag{3.23}$$

$$\beta = \beta_o + w_{rot}t \tag{3.24}$$

where R_e, R_{se} and w_{orb} represent respectively Earth's radius, average distance between Earth's centre from the centre of SSB frame and the orbital angular velocity of Earth. Here, t represents the time in seconds elapsed from the instant Sun is at the Vernal Equinox and β_o is local sidereal time at that instant. The Doppler shift is now given via

$$\begin{aligned}\frac{f'-f_o}{f_o} \quad = \quad \frac{\mathbf{v}.\mathbf{n}}{c}(t) \quad = \quad \frac{\dot{\mathbf{r}}_\mathbf{t}.\mathbf{n}}{c} \quad = \quad & \frac{R_{se}w_{orb}}{c}\sin\theta\sin(\phi - w_{orb}t) + \\ & \frac{R_e w_{rot}}{c}\sin\alpha\,[\sin\theta\{\cos\beta\cos\epsilon\sin\phi - \\ & \cos\phi\sin\beta\} + \cos\beta\sin\epsilon\cos\theta]\end{aligned} \tag{3.25}$$

The phase $\Phi(t)$ of the received signal is given by

$$\begin{aligned}\Phi(t) \quad &= \quad 2\pi\int_0^t f'(t')dt' \\ &= \quad 2\pi f_o\int_0^t \left[1 + \frac{\mathbf{v}.\mathbf{n}}{c}(t')\right]dt'\end{aligned} \tag{3.26}$$

Here, we assume the initial phase of the wave to be zero. After a straight forward calculation we obtain

$$
\begin{aligned}
\Phi(t) &= 2\pi f_o \Bigg[t + \frac{R_{se}}{c} \sin\theta \cos\phi' + \\
&\quad \frac{R_e}{c} \sin\alpha \{ \sin\theta (\sin\beta \cos\epsilon \sin\phi + \cos\phi \cos\beta) + \\
&\quad \sin\beta \sin\epsilon \cos\theta \} - \frac{R_{se}}{c} \sin\theta \cos\phi - \\
&\quad \frac{R_e}{c} \sin\alpha \{ \sin\theta (\sin\beta_o \cos\epsilon \sin\phi + \cos\phi \cos\beta_o) + \\
&\quad \sin\beta_o \sin\epsilon \cos\theta \}] \\
&= 2\pi f_o t + \mathcal{Z} \cos(w_{orb} t - \phi) + \mathcal{P} \sin(w_{rot} t) + \mathcal{Q} \cos(w_{rot} t) - \mathcal{R} - \mathcal{Q} \\
&= 2\pi f_o t + \mathcal{Z} \cos(a \xi_{rot} - \phi) + \mathcal{N} \cos(\xi_{rot} - \delta) - \mathcal{R} - \mathcal{Q} \qquad (3.27)
\end{aligned}
$$

where

$$
\left.
\begin{aligned}
\mathcal{P} &= 2\pi f_o \tfrac{R_e}{c} \sin\alpha (\cos\beta_o (\sin\theta \cos\epsilon \sin\phi + \cos\theta \sin\epsilon) \\
&\quad - \sin\beta_o \sin\theta \cos\phi) \,, \\
\mathcal{Q} &= 2\pi f_o \tfrac{R_e}{c} \sin\alpha (\sin\beta_o (\sin\theta \cos\epsilon \sin\phi + \cos\theta \sin\epsilon) \\
&\quad + \cos\beta_o \sin\theta \cos\phi) \,, \\
\mathcal{N} &= \sqrt{\mathcal{P}^2 + \mathcal{Q}^2} \,, \\
\mathcal{Z} &= 2\pi f_o \tfrac{R_{se}}{c} \sin\theta \,, \\
\mathcal{R} &= \mathcal{Z} \cos\phi \,,
\end{aligned}
\right\} \qquad (3.28)
$$

$$
\left.
\begin{aligned}
\delta &= \tan^{-1} \tfrac{\mathcal{P}}{\mathcal{Q}} \,, \\
\phi' &= w_{orb} t - \phi \,, \\
\xi_{orb} &= w_{orb} t \;=\; a \xi_{rot}; \quad a \;=\; w_{orb}/w_{rot} \;\approx\; 1/365.26 \,, \\
\xi_{rot} &= w_{rot} t
\end{aligned}
\right\} \qquad (3.29)
$$

The two polarisation states of the signal can be taken as

$$h_+(t) = h_{o_+} \cos[\Phi(t)] \qquad (3.30)$$

$$h_\times(t) = h_{o_\times} \sin[\Phi(t)] \,; \qquad (3.31)$$

h_{o_+}, $h_{o_\times}$ are the time independent amplitude of $h_+(t)$, and $h_\times(t)$ respectively.

To understand the nature of the FM, let us consider the FT of $h_+(t)$ and $h_\times(t)$. We may begin by considering the function

$$h(t) = \cos[\Phi(t)] \tag{3.32}$$

and analysing the data for one day observation time. The FT is given via

$$\left[\tilde{h}(f)\right]_d = \int_0^T \cos[\Phi(t)] e^{-i2\pi f t} dt \; ; \tag{3.33}$$

$$T = \text{one sideral day} = 86164 \text{ sec.}$$

This may be splitted into two terms as

$$\left[\tilde{h}(f)\right]_d = I_{\nu_-} + I_{\nu_+} \; ; \tag{3.34}$$

$$I_{\nu_-} = \frac{1}{2w_{rot}} \int_0^{2\pi} e^{i[\xi\nu_- + \mathcal{Z}\cos(a\xi-\phi) + \mathcal{N}\cos(\xi-\delta) - \mathcal{R} - \mathcal{Q}]} d\xi \, , \tag{3.35}$$

$$I_{\nu_+} = \frac{1}{2w_{rot}} \int_0^{2\pi} e^{-i[\xi\nu_+ + \mathcal{Z}\cos(a\xi-\phi) + \mathcal{N}\cos(\xi-\delta) - \mathcal{R} - \mathcal{Q}]} d\xi \, , \tag{3.36}$$

$$\nu_\pm = \frac{f_o \pm f}{f_{rot}}; \quad \xi = \xi_{rot} = w_{rot} t \tag{3.37}$$

Numerical result shows that I_{ν_+} oscillates very fast and contributes very little to $\left[\tilde{h}(f)\right]_d$. Hence, hereafter, we drop I_{ν_+} from Eq. (3.34) and write ν in place of ν_-. Using the identity

$$e^{\pm i\kappa\cos\vartheta} = J_o(\pm\kappa) + 2\sum_{l=1}^{l=\infty} i^l J_l(\pm\kappa)\cos l\vartheta \tag{3.38}$$

we obtain

$$\begin{aligned}\left[\tilde{h}(f)\right]_d \simeq & \frac{1}{2w_{rot}} e^{i(-\mathcal{R}-\mathcal{Q})} \int_0^{2\pi} e^{i\nu\xi} \left[J_o(\mathcal{Z}) + 2\sum_{k=1}^{k=\infty} J_k(\mathcal{Z}) i^k \cos k(a\xi - \phi)\right] \\ & \times \left[J_o(\mathcal{N}) + 2\sum_{m=1}^{m=\infty} J_m(\mathcal{N}) i^m \cos m(\xi - \delta)\right] d\xi \end{aligned} \tag{3.39}$$

where J stands for the Bessel function of first kind of integral order. After performing the integration we get

$$\left[\tilde{h}(f)\right]_d \simeq \frac{\nu}{2w_{rot}} \sum_{k=-\infty}^{k=\infty} \sum_{m=-\infty}^{m=\infty} e^{i\mathcal{A}} \mathcal{B}[\mathcal{C} - i\mathcal{D}] \; ; \tag{3.40}$$

$$\left.\begin{aligned}
\mathcal{A} &= \tfrac{(k+m)\pi}{2} - \mathcal{R} - \mathcal{Q} \\
\mathcal{B} &= \tfrac{J_k(\mathcal{Z}) J_m(\mathcal{N})}{\nu^2 - (ak+m)^2} \\
\mathcal{C} &= \sin 2\nu\pi \cos(2ak\pi - k\phi - m\delta) - \\
&\quad \tfrac{ak+m}{\nu} \{\cos 2\nu\pi \sin(2ak\pi - k\phi - m\delta) + \sin(k\phi + m\delta)\} \\
\mathcal{D} &= \cos 2\nu\pi \cos(2ak\pi - k\phi - m\delta) + \\
&\quad \tfrac{ka+m}{\nu} \sin 2\nu\pi \sin(2ak\pi - k\phi - m\delta) - \cos(k\phi + m\delta)
\end{aligned}\right\} \tag{3.41}$$

The FT of the two polarisation states of the wave can now be written as

$$\begin{aligned}
\left[\tilde{h}_+(f)\right]_d &= h_{o_+} \left[\tilde{h}(f)\right]_d \\
&\simeq \frac{\nu h_{o_+}}{2w_{rot}} \sum_{k=-\infty}^{k=\infty} \sum_{m=-\infty}^{m=\infty} e^{i\mathcal{A}} \mathcal{B}[\mathcal{C} - i\mathcal{D}] \; ;
\end{aligned} \tag{3.42}$$

$$\begin{aligned}
\left[\tilde{h}_\times(f)\right]_d &= -ih_{o_\times} \left[\tilde{h}(f)\right]_d \\
&\simeq \frac{\nu h_{o_\times}}{2w_{rot}} \sum_{k=-\infty}^{k=\infty} \sum_{m=-\infty}^{m=\infty} e^{i\mathcal{A}} \mathcal{B}[\mathcal{D} - i\mathcal{C}]
\end{aligned} \tag{3.43}$$

The FT of the FM signal contains the double series Bessel functions. The Bessel functions has contributions due to the rotational as well as the orbital motion of the earth. It is remarked that Jotania et al. (1996) have analysed FT of FM signal for one day observation time. They have taken specific detector as well as source location. They have also neglected the orbital motion. Our analysis generalizes their results. We may now compute $\left[\tilde{h}(f)\right]_d$ and may plot its behaviour. To achieve this we have made use of *Mathematica* software. Fig. (3.4) represents such a plot for

$$\left.\begin{array}{lll} f_o = 80\ Hz\,, & h_o = h_\times = 1 & \\ \alpha = \pi/3\,, & \beta_o = \pi/4\,, & \gamma = 2\pi/5\,, \\ \theta = \pi/36\,, & \phi = \pi\,, & \psi = \pi/6. \end{array}\right\} \tag{3.44}$$

with the resolution equal to $1/T_o = 1.16 \times 10^{-5}$ Hz. Figures (3.5) and (3.6) represent the plot of the FT at resolution 10^{-6} Hz and 10^{-7} Hz. A careful look at these plots reveals that the resolution of Fig. (3.4) does not represent the details of dominant peaks around f_o, whereas, Fig. (3.6) does not give any new behaviour as compared to Fig. (3.5). Hence, we may say that a resolution of about 10^{-6} Hz is required to understand the correct behaviour of the FT for one day observation time data analysis. In this reference let us recall that the data analysis for Fast Fourier Transform (FFT) limits the resolution to $1/T_o$. However, detector output may provide us higher resolution. Thus the semi-analytical analysis presented here may provide more information as compared to FFT. Further, in order to see the distribution of amplitudes at various frequencies we plot power spectrum in Fig. (3.7).

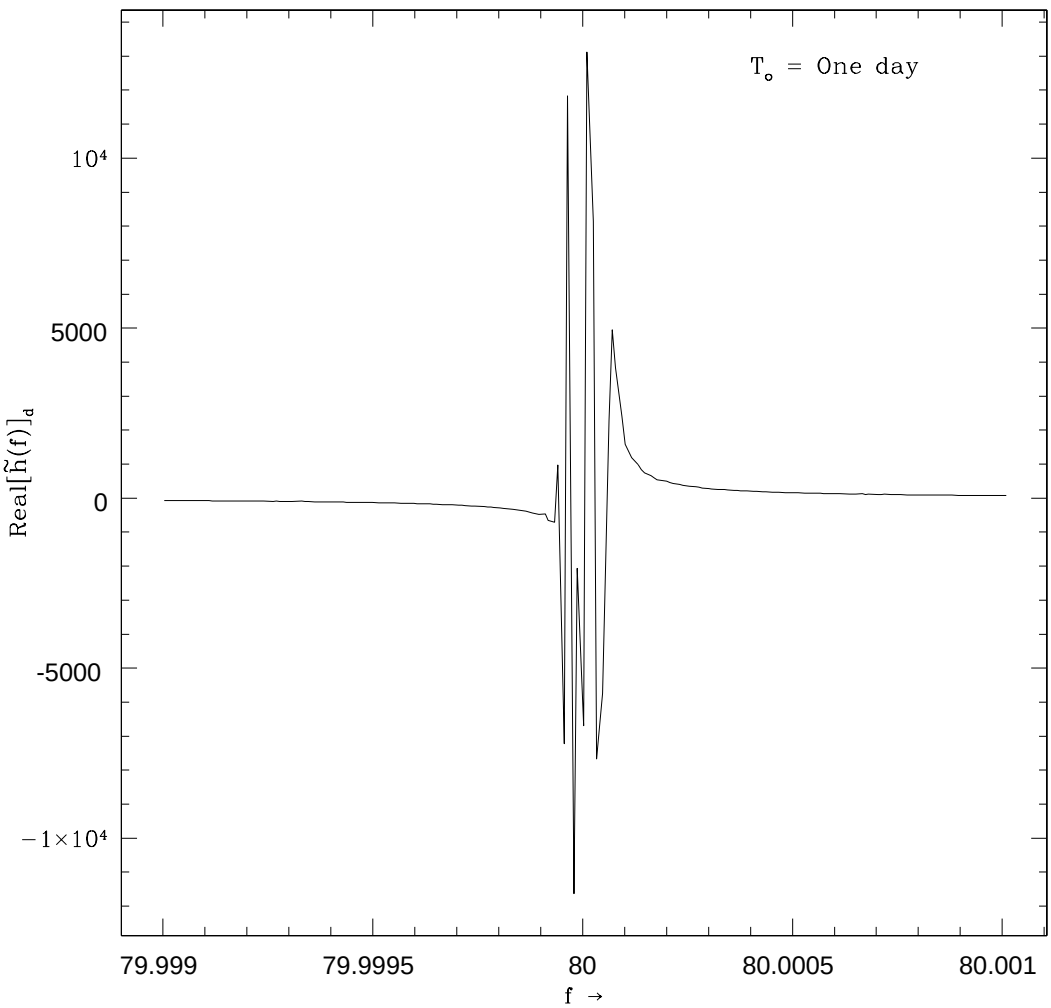

Figure 3.4: FT of a FM signal of a source located at $(\pi/36, \pi)$ with a resolution of 1.16×10^{-5}.

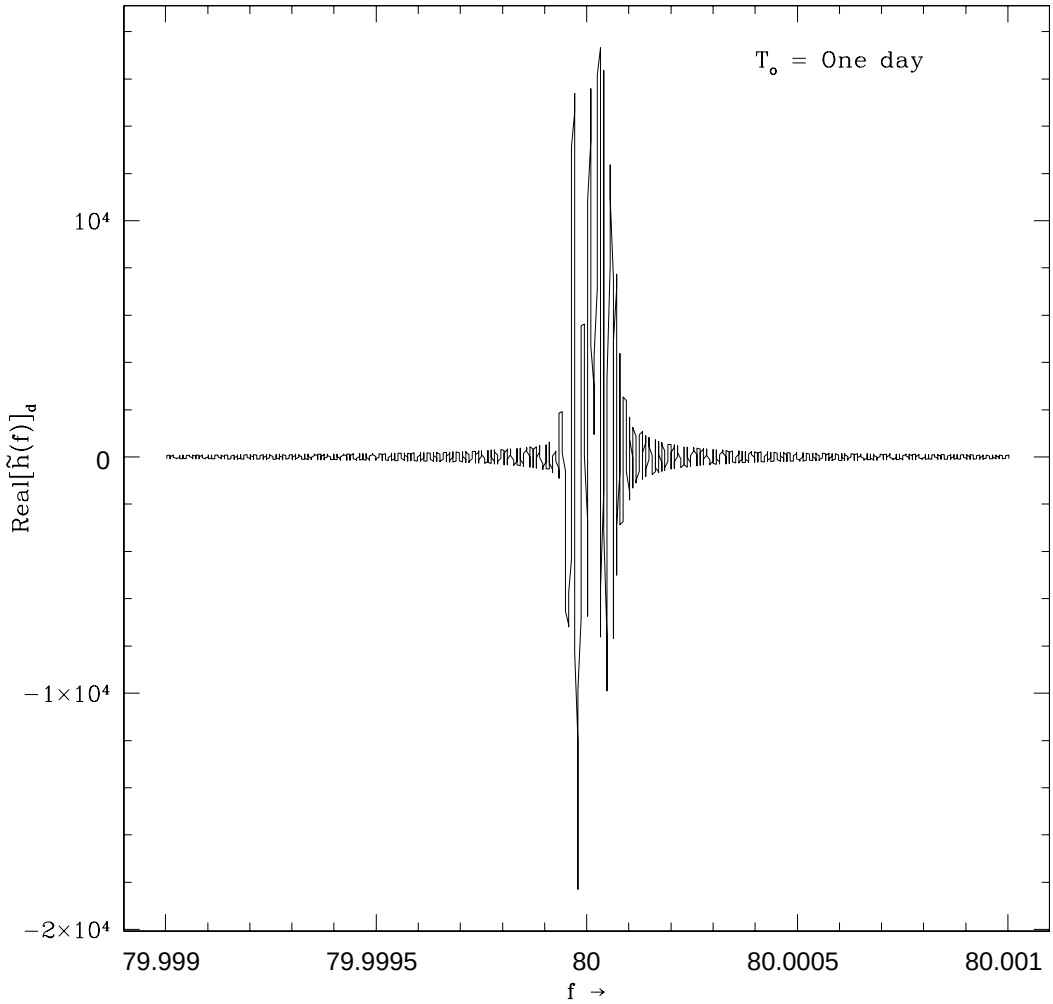

Figure 3.5: FT of a FM signal of a source located at $(\pi/36, \pi)$ with a resolution of 10^{-6}.

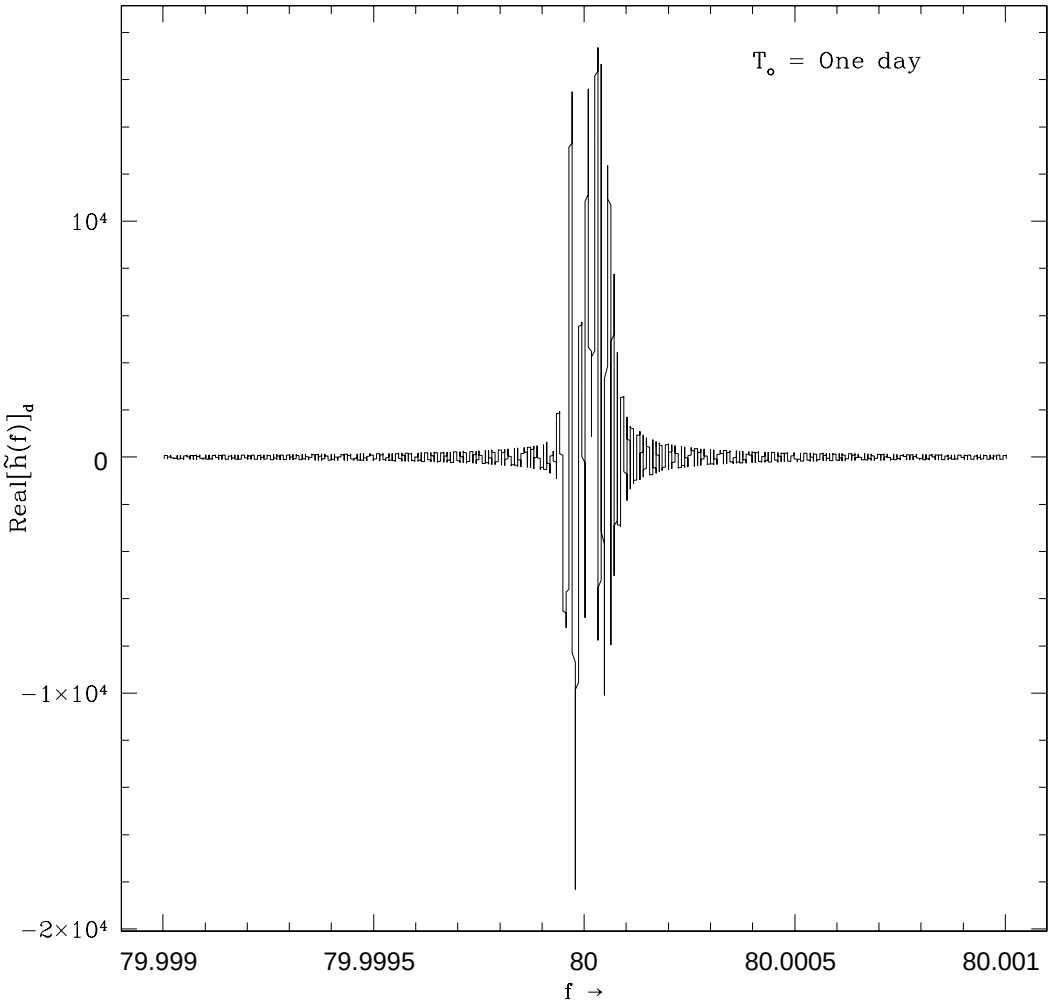

Figure 3.6: FT of a FM signal of a source located at $(\pi/36, \pi)$ with a resolution of 10^{-7}.

3.4 Fourier transform of the complete response

The complete response $R(t)$, in view of Eqs. (3.5), (3.16), (3.17), (3.30) and (3.31) may be written as

$$R(t) = R_+(t) + R_\times(t) \; ; \tag{3.45}$$

$$\begin{aligned} R_+(t) &= h_{o_+} \left[F_{1_+} \cos 2\beta + F_{2_+} \sin 2\beta + F_{3_+} \cos \beta + \right. \\ &\quad \left. F_{4_+} \sin \beta + F_{5_+} \right] \cos[\Phi(t)] \, , \end{aligned} \tag{3.46}$$

$$\begin{aligned} R_\times(t) &= h_{o_\times} \left[F_{1_\times} \cos 2\beta + F_{2_\times} \sin 2\beta + F_{3_\times} \cos \beta + \right. \\ &\quad \left. F_{4_\times} \sin \beta + F_{5_\times} \right] \sin[\Phi(t)] \end{aligned} \tag{3.47}$$

Here we have taken for simplicity the angles between the arms of the detector to be $\pi/2$ i.e. $\Omega = \pi/4$. Now the FT of the complete response may be expressed as

$$\tilde{R}(f) = \tilde{R}_+(f) + \tilde{R}_\times(f) \tag{3.48}$$

To evaluate these let us substitute β as given by (3.24). One obtains

$$\begin{aligned} R_+(t) &= h_{o_+} \left[\frac{1}{2} \left\{ e^{-i2\beta_o} (F_{1_+} + iF_{2_+}) e^{-i2w_{rot}t} + e^{i2\beta_o} (F_{1_+} - iF_{2_+}) e^{i2w_{rot}t} + \right. \right. \\ &\quad \left. e^{-i\beta_o} (F_{3_+} + iF_{4_+}) e^{-iw_{rot}t} + e^{i\beta_o} (F_{3_+} - iF_{4_+}) e^{iw_{rot}t} \right\} \\ &\quad \left. + \; F_{5_+} \right] \cos[\Phi(t)] \end{aligned} \tag{3.49}$$

and similar expression for $R_\times(t)$. Now it is straight forward to obtain the expression for $\tilde{R}_+(f)$ and $\tilde{R}_\times(f)$. We get

$$\begin{aligned} \left[\tilde{R}_+(f) \right]_d &= h_{o_+} \left[e^{-i2\beta_o} (F_{1_+} + iF_{2_+}) \left[\tilde{h}(f + 2f_{rot})/2 \right]_d + \right. \\ &\quad e^{i2\beta_o} (F_{1_+} - iF_{2_+}) \left[\tilde{h}(f - 2f_{rot})/2 \right]_d + \\ &\quad e^{-i\beta_o} (F_{3_+} + iF_{4_+}) \left[\tilde{h}(f + f_{rot})/2 \right]_d + \\ &\quad \left. e^{i\beta_o} (F_{3_+} - iF_{4_+}) \left[\tilde{h}(f - f_{rot})/2 \right]_d + F_{5_+} \left[\tilde{h}(f) \right]_d \right] \end{aligned} \tag{3.50}$$

Similarly we have

$$\begin{aligned}\left[\tilde{R}_\times(f)\right]_d &= h_{o_\times}\left[e^{-i2\beta_o}(F_{2_\times}-iF_{1_\times})\left[\tilde{h}(f+2f_{rot})/2\right]_d+\right.\\ &\quad -e^{i2\beta_o}(F_{2_\times}+iF_{1_\times})\left[\tilde{h}(f-2f_{rot})/2\right]_d+\\ &\quad e^{-i\beta_o}(F_{4_\times}-iF_{3_\times})\left[\tilde{h}(f+f_{rot})/2\right]_d+\\ &\quad \left.-e^{i\beta_o}(F_{4_\times}+iF_{3_\times})\left[\tilde{h}(f-f_{rot})/2\right]_d-iF_{5_\times}\left[\tilde{h}(f)\right]_d\right] \quad (3.51)\end{aligned}$$

Collecting our results the FT of the complete response of the detector for one day integration will be

$$\begin{aligned}\left[\tilde{R}(f)\right]_d &= e^{-i2\beta_o}\left[\tilde{h}(f+2f_{rot})/2\right]_d\left[h_{o_+}(F_{1_+}+iF_{2_+})+h_{o_\times}(F_{2_\times}-iF_{1_\times})\right]+\\ &\quad e^{i2\beta_o}\left[\tilde{h}(f-2f_{rot})/2\right]_d\left[h_{o_+}(F_{1_+}-iF_{2_+})-h_{o_\times}(F_{2_\times}+iF_{1_\times})\right]+\\ &\quad e^{-i\beta_o}\left[\tilde{h}(f+f_{rot})/2\right]_d\left[h_{o_+}(F_{3_+}+iF_{4_+})+h_{o_\times}(F_{4_\times}-iF_{3_\times})\right]+\\ &\quad e^{i\beta_o}\left[\tilde{h}(f-f_{rot})/2\right]_d\left[h_{o_+}(F_{3_+}-iF_{4_+})-h_{o_\times}(F_{4_\times}+iF_{3_\times})\right]+\\ &\quad \left[\tilde{h}(f)\right]_d\left[h_{o_+}F_{5_+}-ih_{o_\times}F_{5_\times}\right] \quad (3.52)\end{aligned}$$

This shows that due to AM every Doppler modulated FM signal will split in four additional lines at $f \pm 2f_{rot}$ and $f \pm f_{rot}$, where f_{rot} is the rotational frequency of Earth ($f_{rot} \approx 1.16 \times 10^{-5}$ Hz). In terms of dimensionless scaled frequency ν the power of the signal will be at $\nu \pm 2a$, $\nu \pm a$ & ν.

We have plotted in Fig. (3.8) the power spectrum of the noise free complete response of the signal for its various parameters as given by (3.44). The contribution in the power spectrum of modulation at frequencies $f+2f_{rot}$, $f-2f_{rot}$, $f+f_{rot}$ and $f-f_{rot}$ and f are represented in Figs. (3.9), (3.10), (3.11), (3.12) and (3.13). It is observed that the most of the power will be at $f+2f_{rot}$ and least power will be in $f-f_{rot}$.

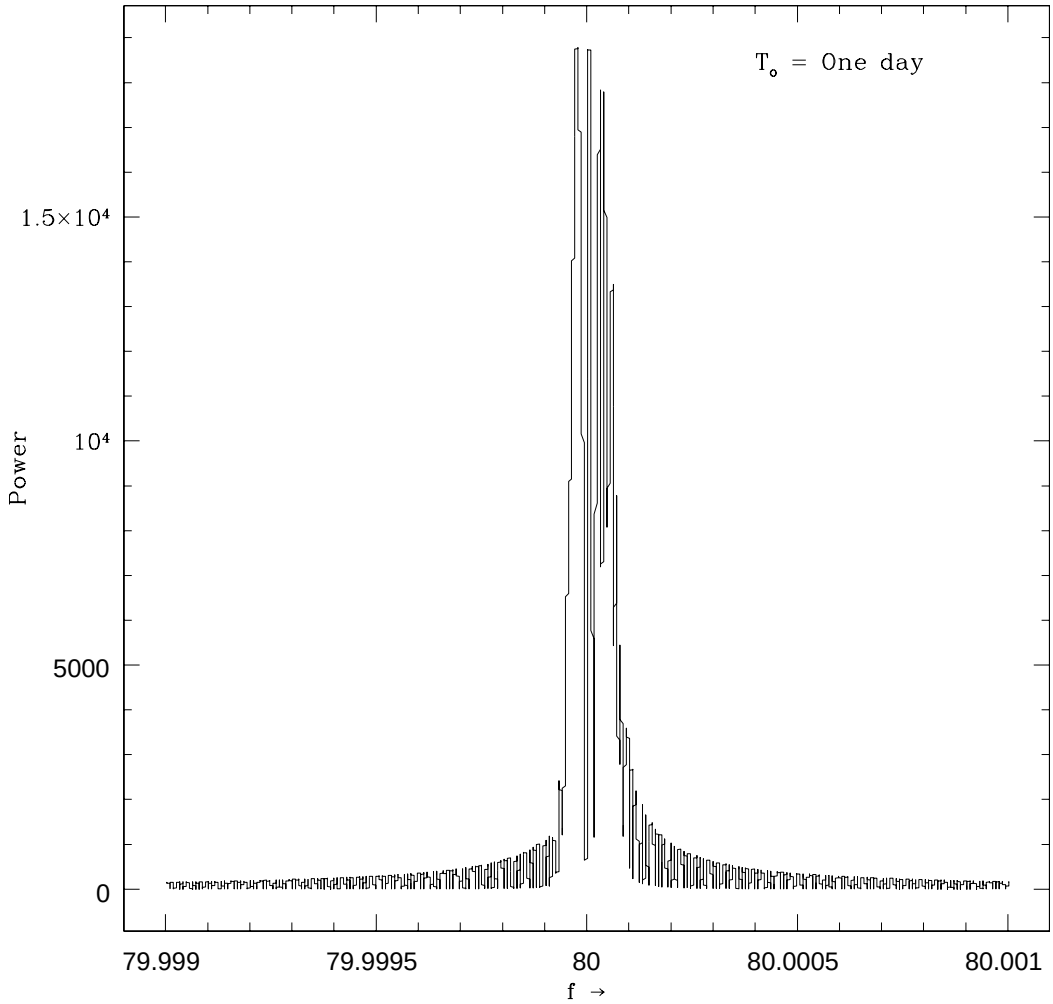

Figure 3.7: Power spectrum of a FM signal of a source located at $(\pi/36, \pi)$ with a resolution of 10^{-7}.

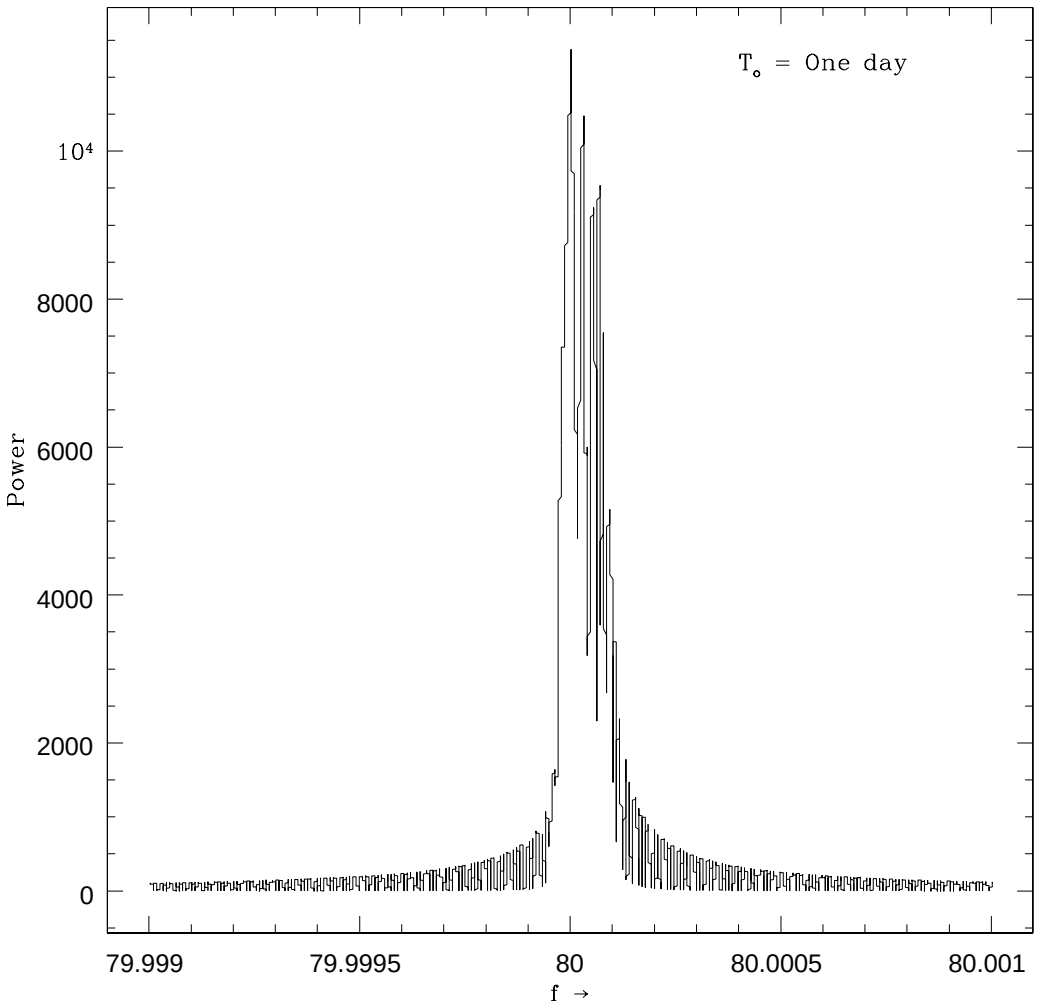

Figure 3.8: Power spectrum of the complete response of a Doppler modulated signal of a source located at $(\pi/36, \pi)$ with a resolution of 10^{-7}.

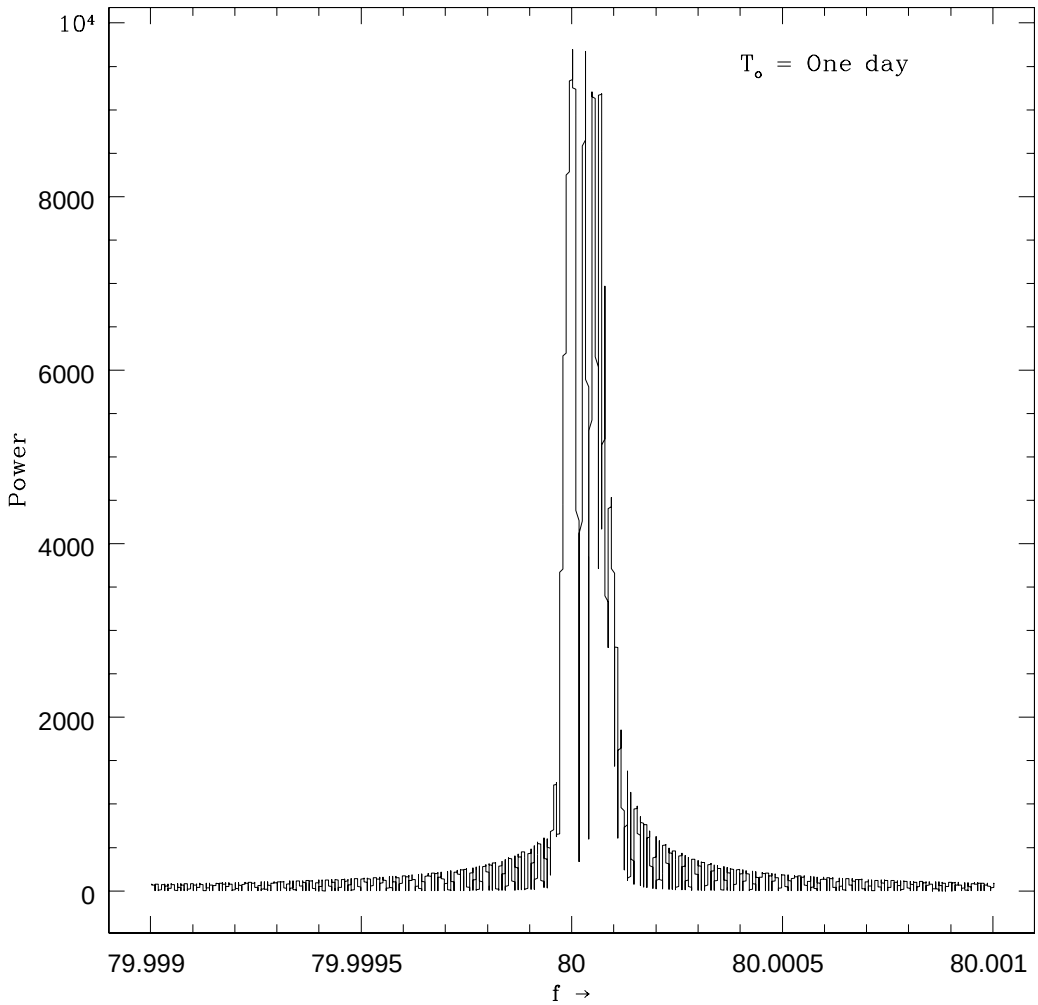

Figure 3.9: Power spectrum of a Doppler modulated signal at frequencies $f + 2f_{rot}$ of a source located at $(\pi/36, \pi)$ with a resolution of 10^{-7}.

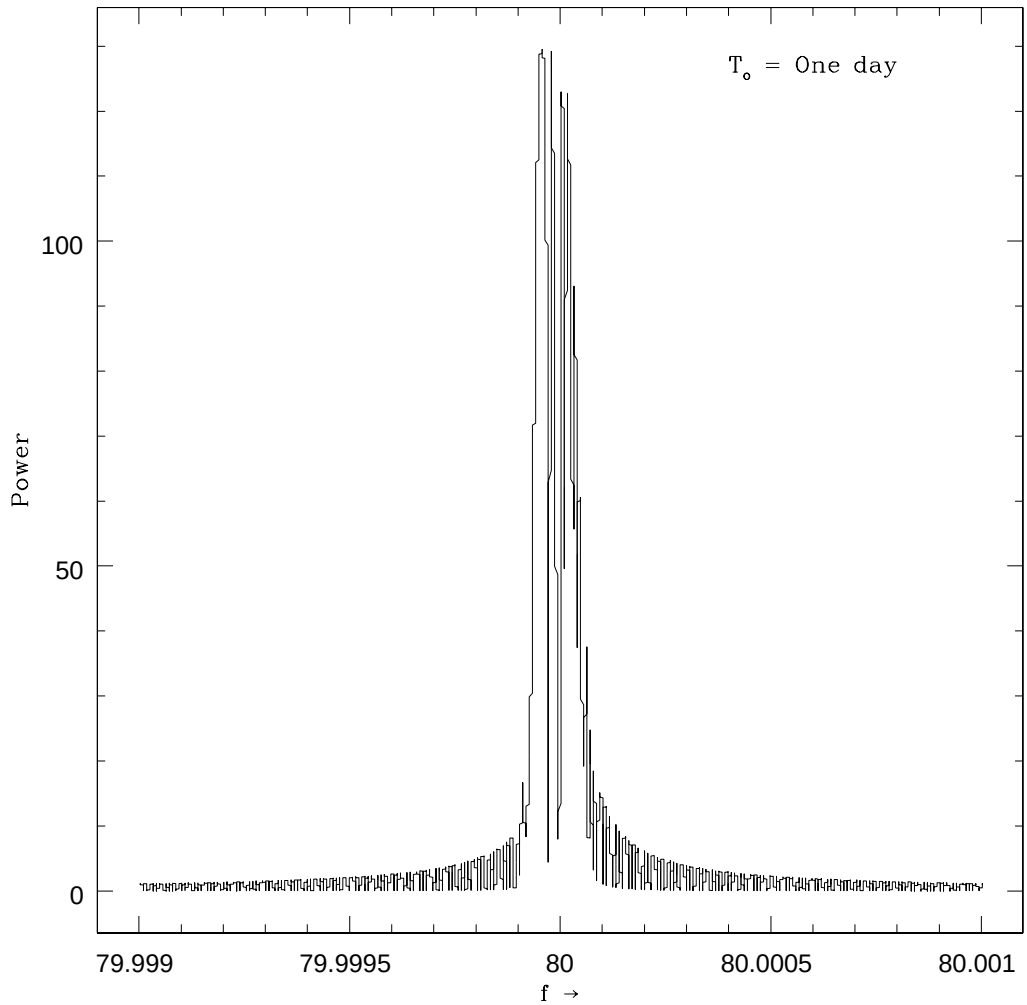

Figure 3.10: Power spectrum of a Doppler modulated signal at frequencies $f - 2f_{rot}$ of a source located at $(\pi/36, \pi)$ with a resolution of 10^{-7}.

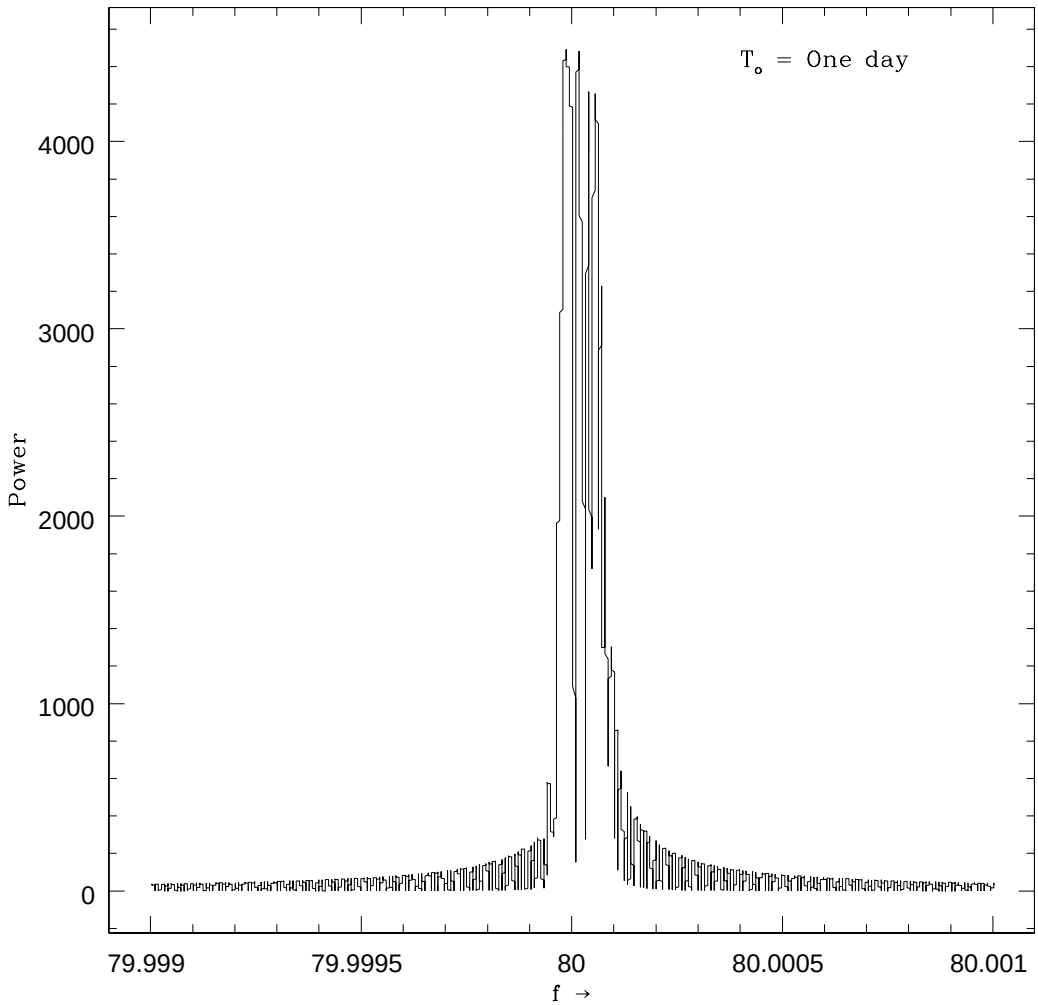

Figure 3.11: Power spectrum of a Doppler modulated signal at frequencies $f + f_{rot}$ of a source located at $(\pi/36, \pi)$ with a resolution of 10^{-7}.

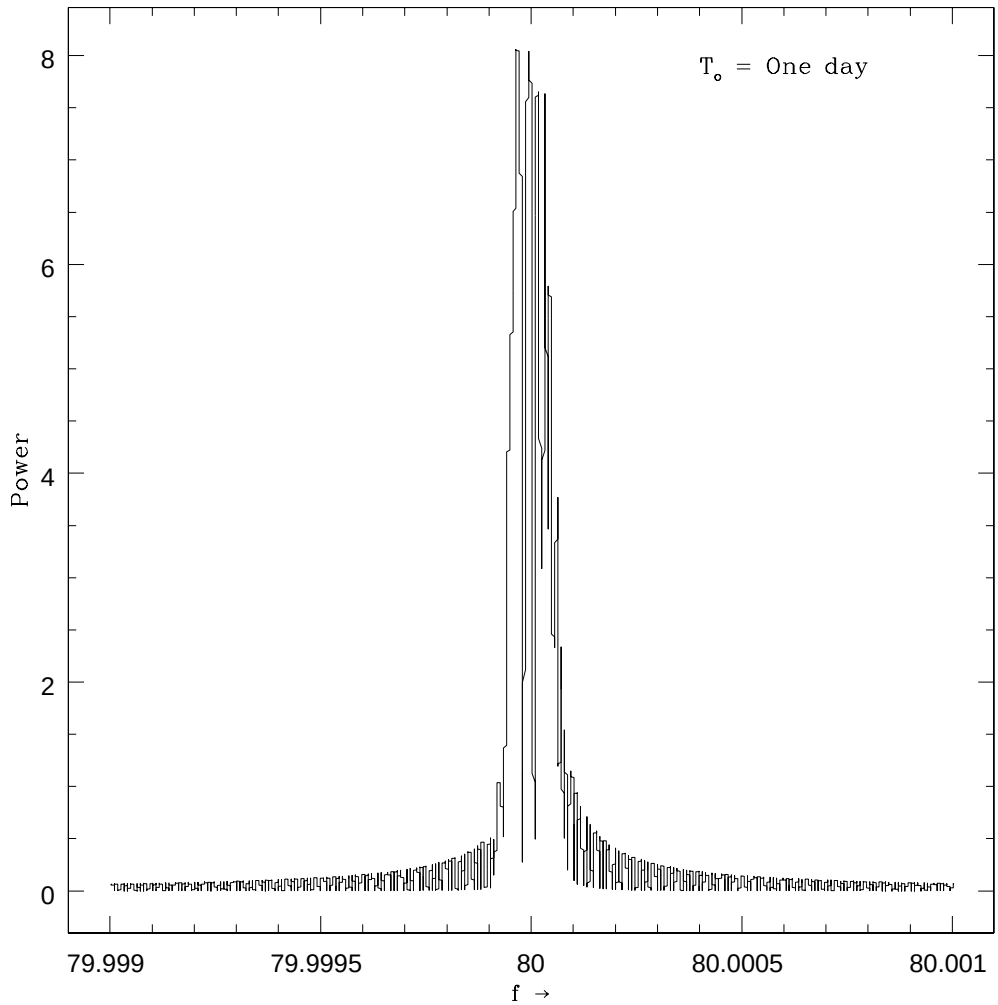

Figure 3.12: Power spectrum of a Doppler modulated signal at frequencies $f - f_{rot}$ of a source located at $(\pi/36, \pi)$ with a resolution of 10^{-7}.

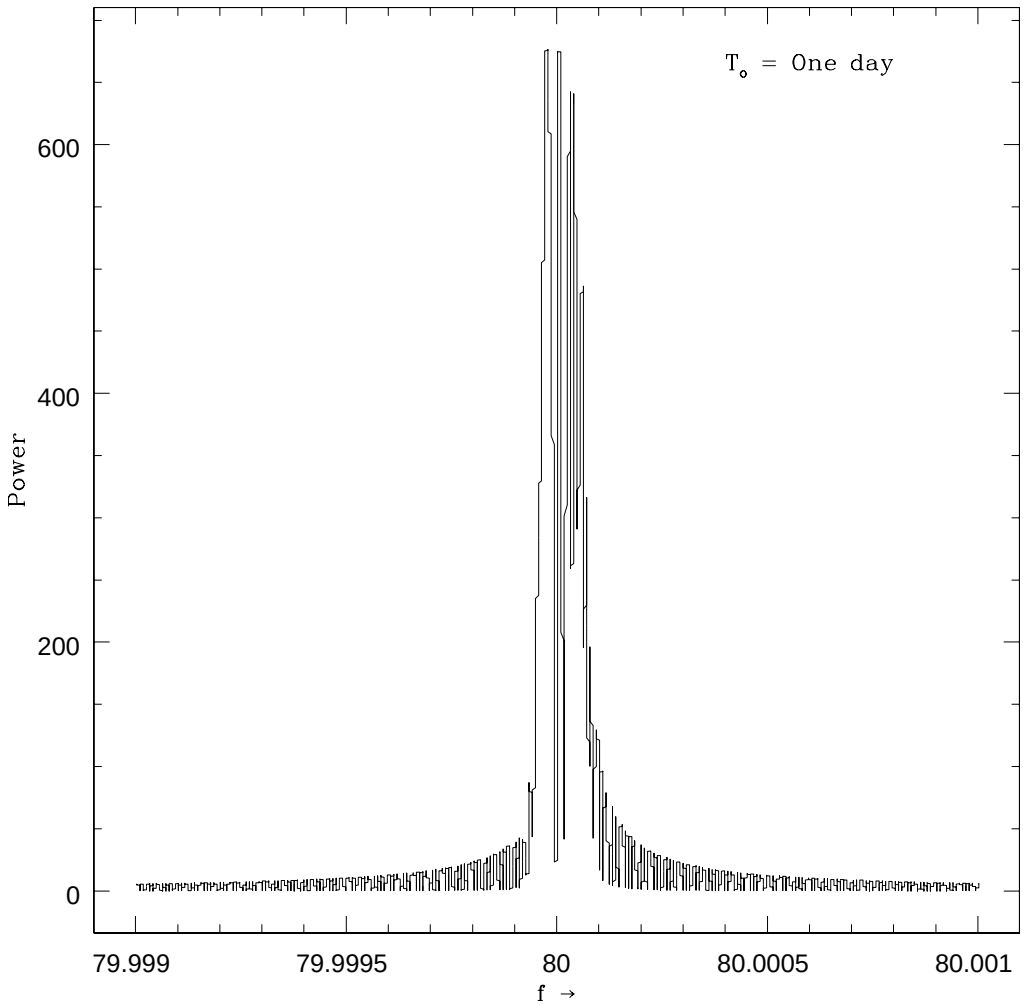

Figure 3.13: Power spectrum of a Doppler modulated signal at frequencies f of a source located at $(\pi/36, \pi)$ with a resolution of 10^{-7}.

3.5 Discussion

In this Chapter we have considered the effect of Earth's motion on the response of the detector through FT analysis. It can easily be inferred from Eqs. (3.52) and (3.42, 3.43) that the splitting of frequencies (i) in AM arise explicitly due to rotational motion and (ii) in FM arise due to rotational as well as orbital motion of earth. In view of the fact that the data output at the detector is available in discrete form, the analytical FT is not very convenient and one normally employs the popular FFT. However, FFT has resolution limited to $1/T_o$. Further, it is important to understand for how much time one can ignore the frequency shift arising due to Doppler effect. In fact, Schutz (1991) has demonstrated that these effects due to rotational motion are important after the time given by

$$T_{max} = \left(\frac{2c}{\omega_{rot}^2 f_o R_e}\right)^{1/2} \simeq 70 \left(\frac{f_o}{1kHz}\right)^{-1/2} min. \tag{3.53}$$

This means that for GW signal for frequency 80 Hz one has to take into account these effects after data time $\simeq$ 4 hours. The analytical FT studied in this Chapter leads to following inferences:

(i) FFT for one day observation data will not provide sufficient resolution as to represent the correct picture of the frequency splitting.

(ii) The adequate resolution required for one day observation $\simeq 10^{-6}$ Hz.

(iii) The frequency split due to FM for frequency $f_o = 80$ Hz and source at $(\theta, \phi) = (\pi/36, \pi)$ is $\simeq 2 \times 10^{-4}$ Hz and due to AM is $\simeq 4.64 \times 10^{-5}$ Hz.

(iv) The drop in amplitude due to FM alone is about 56%

(v) The drop in amplitude due to AM alone is about 18%.

(vi) The drop in amplitude for the complete response is about 74%.

(vii) The maximum power due to AM is associated with $f_o + 2f_{rot}$.

It is remarked that the drop of the amplitude in complete response is severe both due to AM and FM as the relevant frequency range lie in the same region [see conclusion (iii) above].

Finally, we would like to mention that we have presented the FT analysis assuming the phase of the GW to be zero at that instant $t = 0$. However, one may relax this condition and may obtain the results easily by taking into consideration the effects of change of the time origin.

Chapter 4

Data analysis of continuous gravitational wave: Fourier transform-II

4.1 Introduction

In previous Chapter we have presented Fourier analysis of one day observation data set of the response of a laser interferometer. We have seen that the amplitude and frequency modulations result into a large number of side bands about the signal frequency f_o. Consequently the maximum power lies in the frequency $f + 2f_{rot}$ with amplitude reduction by 74% to what one would have expected due to increased data interval. Hence, for GW detection it is desirable to obtain FT for larger data observation time interval. To begin with we present in the next section an analysis for data set of one year observation time. The analysis turns out to be simple in view of the observation that there exists correspondences and identifications to the analysis of previous Chapter to make them identical. We obtain in section 3 generalisations of the results for arbitrary observation time. To facilitate analogous modifications we have introduced corresponding quantities with tilde viz., $\tilde{\mathcal{C}}$ and $\tilde{\mathcal{D}}$ in place of $\mathcal{C}$ and $\mathcal{D}$. As an application of the results obtained here we consider spin down and N-component signal analysis respectively in sections 4 and 5. We

present discussion and conclusions in the last section.

4.2 Fourier transform for one year integration

4.2.1 Frequency modulation

Let us rewrite the expression for phase of the GW signal referring to Eqs. (3.27), (3.28) and (3.29)

$$\Phi(t) \;=\; 2\pi f_o t + \mathcal{Z}\cos(w_{orb}t - \phi) + \mathcal{N}\cos(w_{rot}t - \delta) - \mathcal{R} - \mathcal{Q} \quad (4.1)$$

The FT for one year observation time T_{obs} is given as

$$\left[\tilde{h}(f)\right]_y = \int_0^{\bar{a}T} \cos[\Phi(t)]e^{-i2\pi ft}dt \; ; \quad (4.2)$$

$$\bar{a} = a^{-1} = w_{rot}/w_{orb} \; ; \quad T = \; one\ sideral\ day \; ; \quad (4.3)$$

$$T_{obs} = \bar{a}T \simeq 3.14 \times 10^7 \; sec. \quad (4.4)$$

This may be splitted as usual into two terms as

$$\left[\tilde{h}(f)\right]_y = I_{\bar{\nu}_-} + I_{\bar{\nu}_+} \; ; \quad (4.5)$$

$$I_{\bar{\nu}_-} \;=\; \frac{1}{2w_{orb}}\int_0^{2\pi} e^{i\left[\bar{\xi}\bar{\nu}_- + \mathcal{Z}\cos(\bar{\xi}-\phi) + \mathcal{N}\cos(\bar{a}\bar{\xi}-\delta) - \mathcal{R} - \mathcal{Q}\right]}d\bar{\xi}\,, \quad (4.6)$$

$$I_{\bar{\nu}_+} \;=\; \frac{1}{2w_{orb}}\int_0^{2\pi} e^{-i\left[\bar{\xi}\bar{\nu}_+ + \mathcal{Z}\cos(\bar{\xi}-\phi) + \mathcal{N}\cos(\bar{a}\bar{\xi}-\delta) - \mathcal{R} - \mathcal{Q}\right]}d\bar{\xi}\,, \quad (4.7)$$

$$\bar{\nu}_\pm \;=\; \frac{f_o \pm f}{f_{orb}}; \quad \bar{\xi} \;=\; \xi_{orb} \;=\; w_{orb}t \quad (4.8)$$

Hereafter, we neglect the contribution of $I_{\bar{\nu}_+}$ to $\left[\tilde{h}(f)\right]_y$ as it oscillates rapidly and contributes very little and write $\bar{\nu}$ in place of $\bar{\nu}_-$. A careful comparison of Eq. (4.6) with (3.35) reveals that the integrand of the equations are identical with following identifications and correspondences.

$$\left.\begin{array}{ccc} \delta & \leftrightarrow & \phi\,, \\ \mathcal{Z} & \leftrightarrow & \mathcal{N}\,, \\ a & \leftrightarrow & \bar{a}. \end{array}\right\} \tag{4.9}$$

Hence, we may employ the results obtained there by introducing obvious corresponding quantities i.e. $\bar{\mathcal{B}}$, $\bar{\mathcal{C}}$, $\bar{\mathcal{D}}$ in place of $\mathcal{B}$, $\mathcal{C}$, $\mathcal{D}$ leaving $\mathcal{A}$ unchanged. Thus

$$\left[\tilde{h}(f)\right]_y \simeq \frac{\bar{\nu}}{2w_{orb}} \sum_{k=-\infty}^{k=\infty} \sum_{m=-\infty}^{m=\infty} e^{i\mathcal{A}} \bar{\mathcal{B}}[\bar{\mathcal{C}} - i\bar{\mathcal{D}}]\ ; \tag{4.10}$$

$$\left.\begin{array}{rcl} \mathcal{A} & = & \frac{(k+m)\pi}{2} - \mathcal{R} - \mathcal{Q}\,, \\ \bar{\mathcal{B}} & = & \frac{J_k(\mathcal{N})J_m(\mathcal{Z})}{\bar{\nu}^2-(\bar{a}k+m)^2}\,, \\ \bar{\mathcal{C}} & = & \sin 2\bar{\nu}\pi \cos(2\bar{a}k\pi - k\delta - m\phi) - \\ & & \frac{\bar{a}k+m}{\bar{\nu}}\{\cos 2\bar{\nu}\pi \sin(2\bar{a}k\pi - k\delta - m\phi) + \sin(k\delta + m\phi)\}\,, \\ \bar{\mathcal{D}} & = & \cos 2\bar{\nu}\pi \cos(2\bar{a}k\pi - k\delta - m\phi) + \\ & & \frac{k\bar{a}+m}{\bar{\nu}} \sin 2\bar{\nu}\pi \sin(2\bar{a}k\pi - k\delta - m\phi) - \cos(k\delta + m\phi) \end{array}\right\} \tag{4.11}$$

Now the FT of the two polarisation states can be written as

$$\begin{aligned} \left[\tilde{h}_+(f)\right]_y &= h_{o_+} \left[\tilde{h}(f)\right]_y \\ &\simeq \frac{\bar{\nu} h_{o_+}}{2w_{orb}} \sum_{k=-\infty}^{k=\infty} \sum_{m=-\infty}^{m=\infty} e^{i\mathcal{A}} \bar{\mathcal{B}}[\bar{\mathcal{C}} - i\bar{\mathcal{D}}] \end{aligned} \tag{4.12}$$

and

$$\begin{aligned} \left[\tilde{h}_\times(f)\right]_y &= -ih_{o_\times} \left[\tilde{h}(f)\right]_y \\ &\simeq \frac{\bar{\nu} h_{o_\times}}{2w_{orb}} \sum_{k=-\infty}^{k=\infty} \sum_{m=-\infty}^{m=\infty} e^{i\mathcal{A}} \bar{\mathcal{B}}[\bar{\mathcal{D}} - i\bar{\mathcal{C}}] \end{aligned} \tag{4.13}$$

The FT obtained contains double series of Bessel functions of the order k and m ranging from $-\infty$ to ∞. It is well known that Bessel functions decrease

rapidly as the order exceeds the argument. Hence possible range of k and m over which the summation of the series is to be considered depends on the arguments of Bessel functions i.e $\mathcal{Z}$ and $\mathcal{N}$. Referring to Eq. (3.28) it is found that

$$\left.\begin{aligned} \mathcal{Z}_{max} &= 3133215\left(\tfrac{f}{1\,KHz}\right) \\ \mathcal{N}_{max} &= 134\left(\tfrac{f}{1\,KHz}\right) \end{aligned}\right\} \tag{4.14}$$

The FT of a FM signal for

$$\left.\begin{array}{lll} f_o = 50\ Hz\,, & h_o = h_\times = 1 & \\ \alpha = \pi/4\,, & \beta_o = 0\,, & \gamma = \pi\,, \\ \theta = \pi/18\,, & \phi = 0\,, & \psi = \pi/4. \end{array}\right\} \tag{4.15}$$

is shown in Fig. (4.1). The spectrum has a resolution of $1/T_o \approx 3.17\times10^{-8}Hz$. The corresponding power spectrum is shown in Fig. (4.2). We have convinced ourselves by plotting the FT at higher resolutions that resolution of $1/T_o$ is sufficient to represent relevant peaks. We notice that the drop in amplitude is about 98%. This may be attributed to the presence of a very large number of side bands.

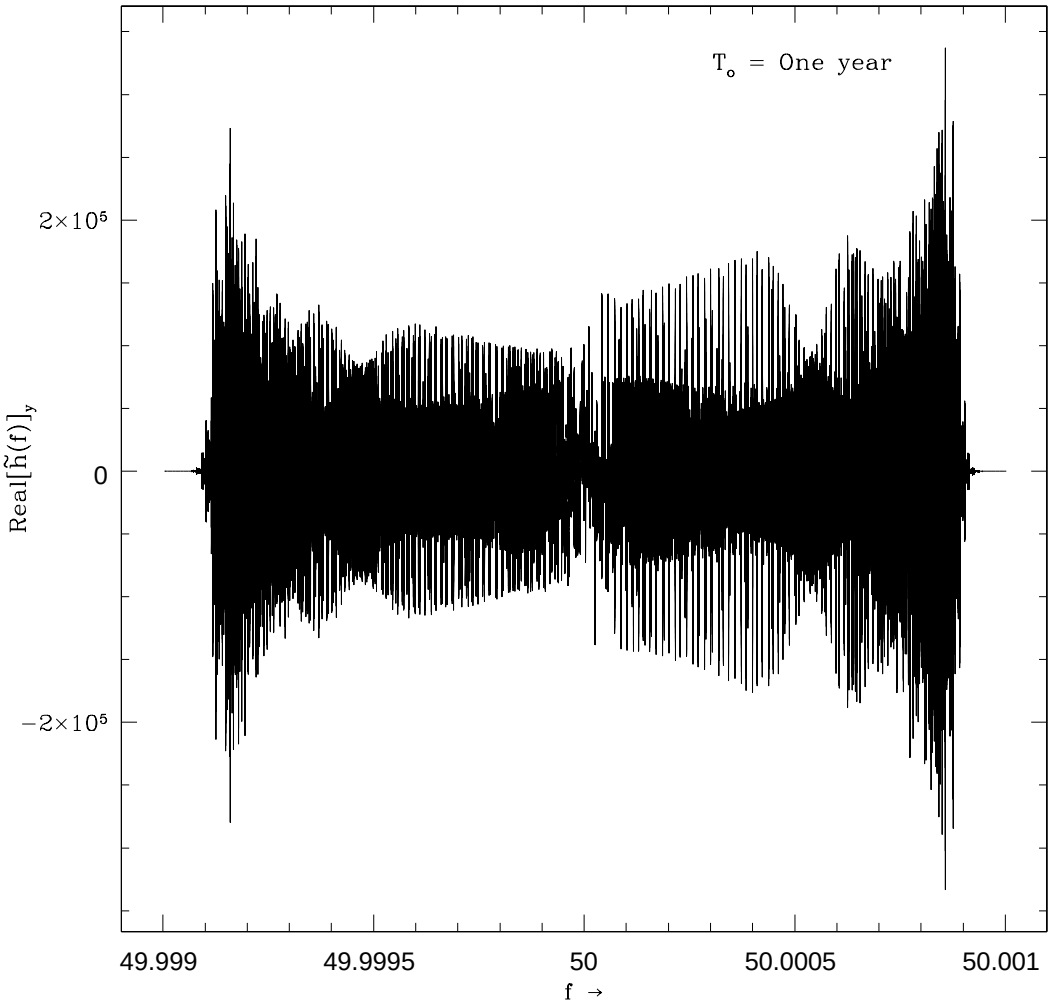

Figure 4.1: FT of a FM signal of a source located at $(\pi/18, 0)$ with a resolution of 3.17×10^{-8}.

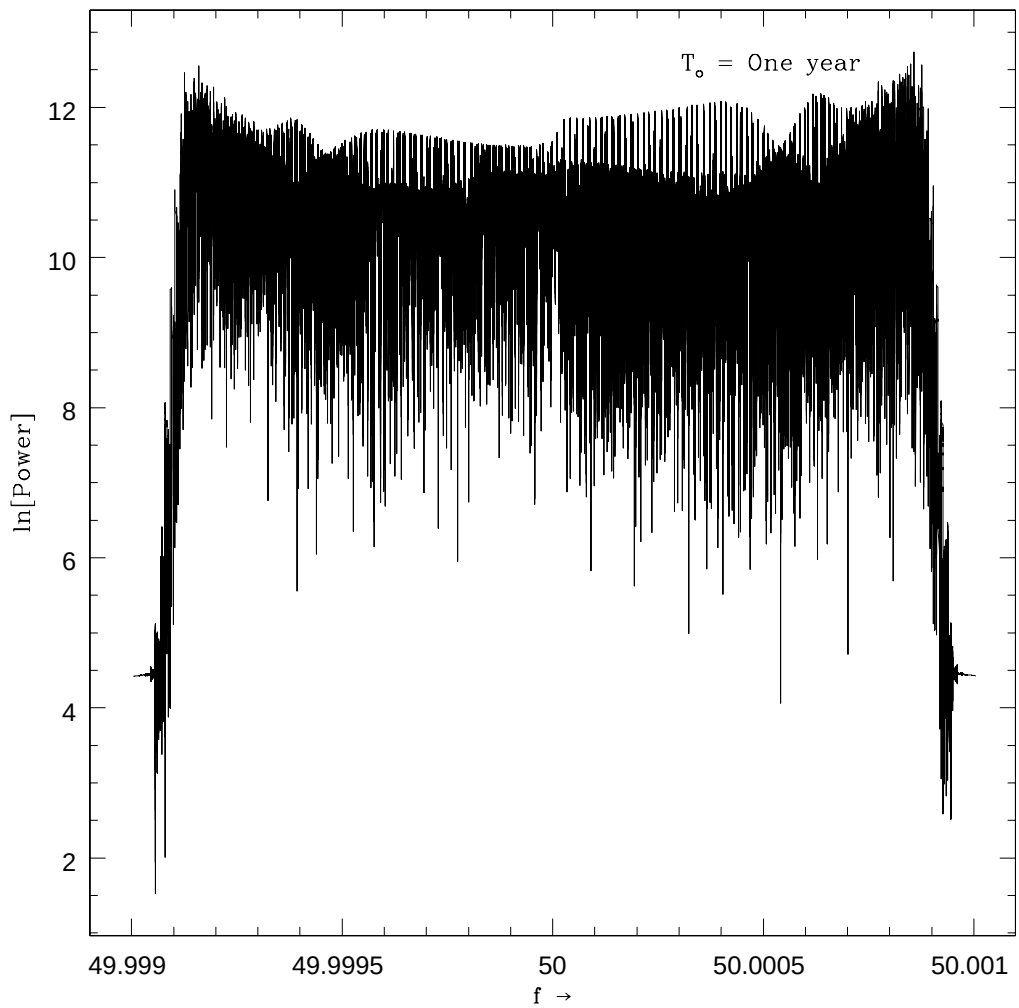

Figure 4.2: Power spectrum of a FM signal of a source located at $(\pi/18, 0)$ with a resolution of 3.17×10^{-8}.

4.2.2 Complete response

The complete response of the detector may be obtained employing Eqs. (4.12), (4.13), (3.46) and (3.47) and one gets

$$\begin{aligned}\left[\tilde{R}_+(f)\right]_y &= h_{o_+}\Big[e^{-i2\beta_o}(F_{1_+}+iF_{2_+})\left[\tilde{h}(f+2f_{rot})/2\right]_y + \\ &\quad e^{i2\beta_o}(F_{1_+}-iF_{2_+})\left[\tilde{h}(f-2f_{rot})/2\right]_y + \\ &\quad e^{-i\beta_o}(F_{3_+}+iF_{4_+})\left[\tilde{h}(f+f_{rot})/2\right]_y + \\ &\quad e^{i\beta_o}(F_{3_+}-iF_{4_+})\left[\tilde{h}(f-f_{rot})/2\right]_y + F_{5_+}\left[\tilde{h}(f)\right]_y\Big] \quad ;(4.16)\end{aligned}$$

$$\begin{aligned}\left[\tilde{R}_\times(f)\right]_y &= h_{o_\times}\Big[e^{-i2\beta_o}(F_{2_\times}-iF_{1_\times})\left[\tilde{h}(f+2f_{rot})/2\right]_y - \\ &\quad e^{i2\beta_o}(F_{2_\times}+iF_{1_\times})\left[\tilde{h}(f-2f_{rot})/2\right]_y + \\ &\quad e^{-i\beta_o}(F_{4_\times}-iF_{3_\times})\left[\tilde{h}(f+f_{rot})/2\right]_y - \\ &\quad e^{i\beta_o}(F_{4_\times}+iF_{3_\times})\left[\tilde{h}(f-f_{rot})/2\right]_y - iF_{5_\times}\left[\tilde{h}(f)\right]_y\Big] \quad (4.17)\end{aligned}$$

After rearranging these expressions we obtain

$$\begin{aligned}\left[\tilde{R}(f)\right]_y &= e^{-i2\beta_o}\left[\tilde{h}(f+2f_{rot})/2\right]_y\left[h_{o_+}(F_{1_+}+iF_{2_+})+h_{o_\times}(F_{2_\times}-iF_{1_\times})\right] + \\ &\quad e^{i2\beta_o}\left[\tilde{h}(f-2f_{rot})/2\right]_y\left[h_{o_+}(F_{1_+}-iF_{2_+})-h_{o_\times}(F_{2_\times}+iF_{1_\times})\right] + \\ &\quad e^{-i\beta_o}\left[\tilde{h}(f+f_{rot})/2\right]_y\left[h_{o_+}(F_{3_+}+iF_{4_+})+h_{o_\times}(F_{4_\times}-iF_{3_\times})\right] + \\ &\quad e^{i\beta_o}\left[\tilde{h}(f-f_{rot})/2\right]_y\left[h_{o_+}(F_{3_+}-iF_{4_+})-h_{o_\times}(F_{4_\times}+iF_{3_\times})\right] + \\ &\quad \left[\tilde{h}(f)\right]_y\left[h_{o_+}F_{5_+}-ih_{o_\times}F_{5_\times}\right] \quad (4.18)\end{aligned}$$

Figure (4.3) shows the power spectrum of the complete response of the Doppler modulated signal. We have kept here all parameters same as in FM. Figures (4.4), (4.5), (4.6), (4.7), and (4.8) are the power spectrum of complete response at frequencies $f+2f_{rot}$, $f-2f_{rot}$, $f+f_{rot}$, $f-f_{rot}$ and f. In this case also we observe that the maximum power is associated with $f+2f_{rot}$ and the least lies in $f-f_{rot}$.

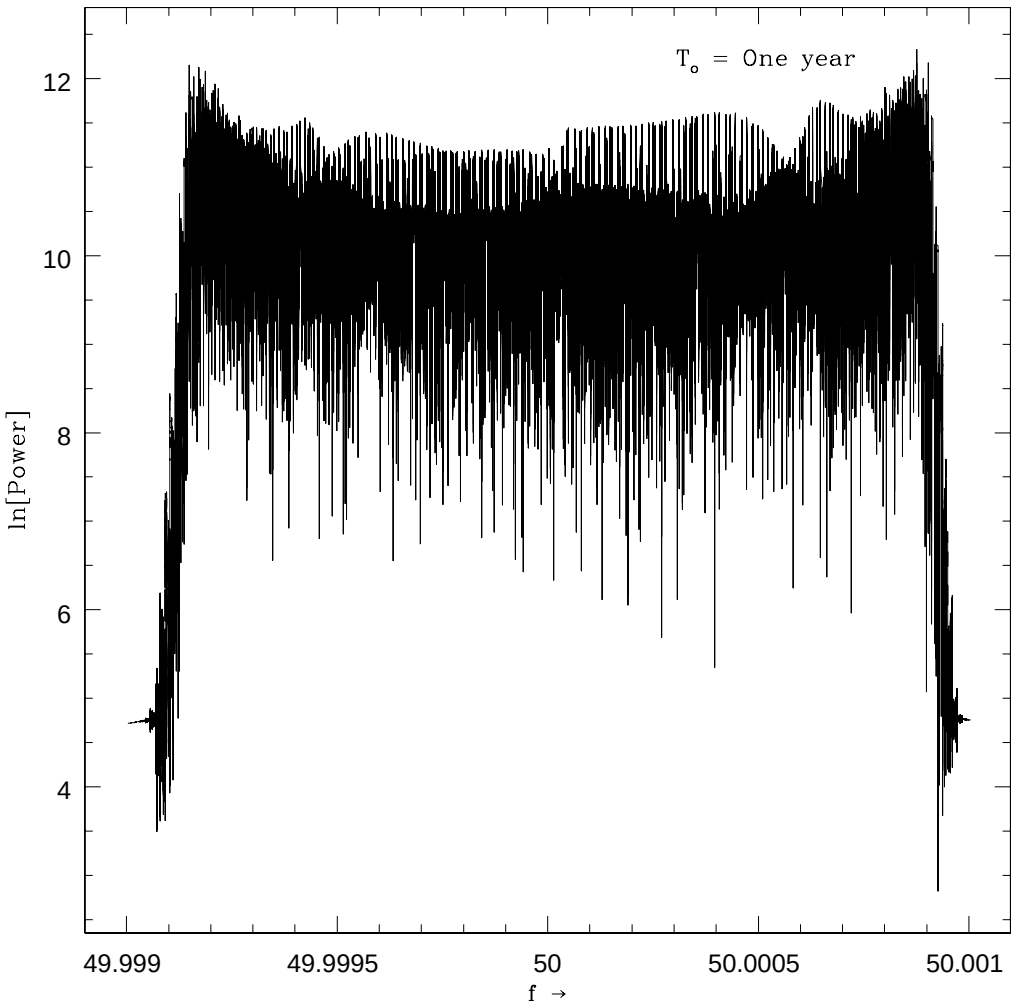

Figure 4.3: Power spectrum of the complete response of a modulated signal of a source located at $(\pi/18, 0)$ with a resolution of 3.17×10^{-8}.

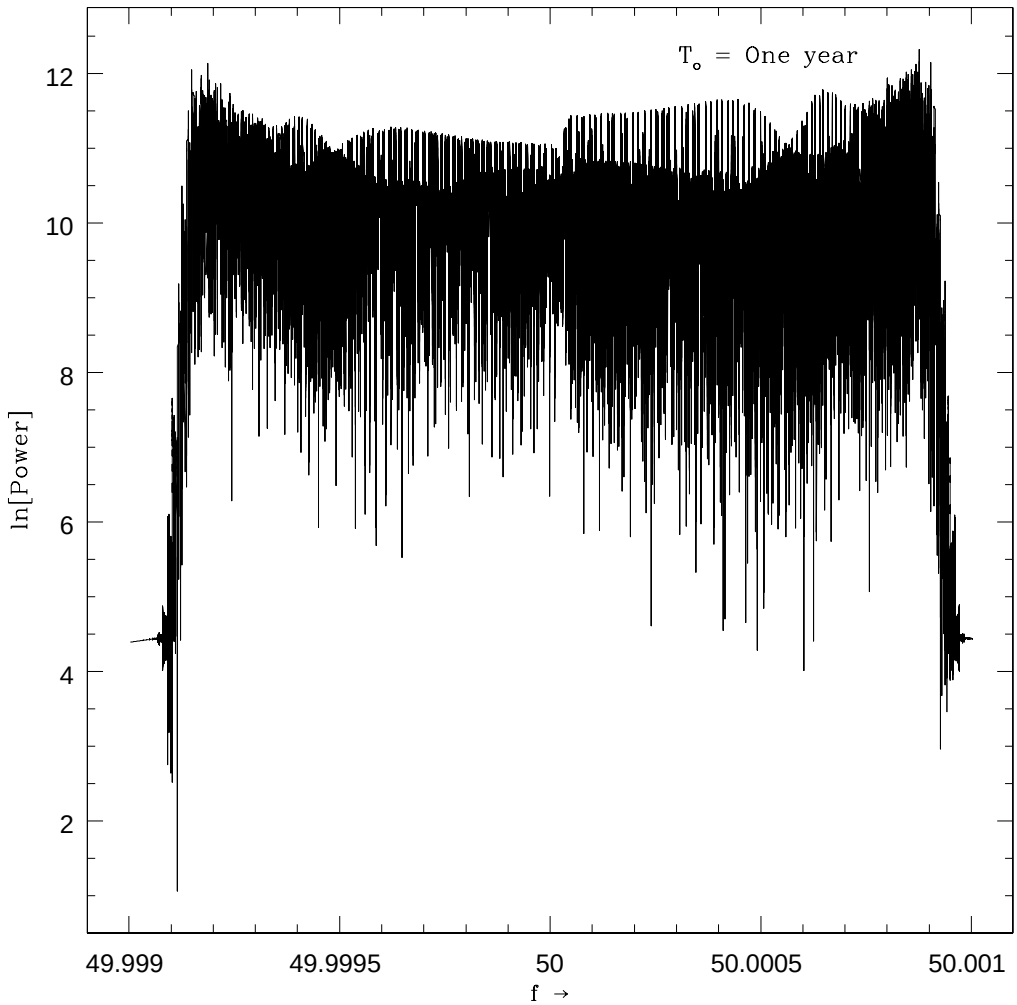

Figure 4.4: Power spectrum of a Doppler modulated signal at frequencies $f + 2f_{rot}$ of a source located at $(\pi/18, 0)$ with a resolution of 3.17×10^{-8}.

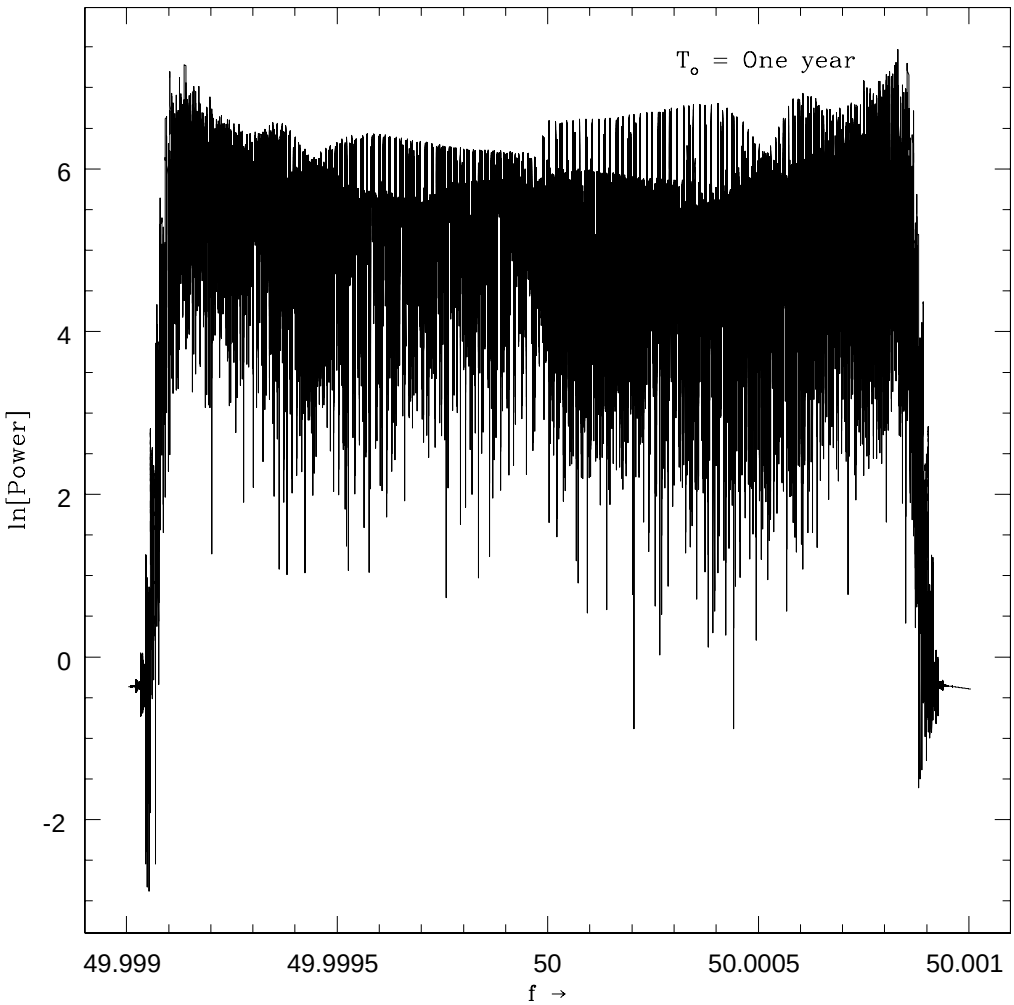

Figure 4.5: Power spectrum of a Doppler modulated signal at frequencies $f - 2f_{rot}$ of a source located at $(\pi/18, 0)$ with a resolution of 3.17×10^{-8}.

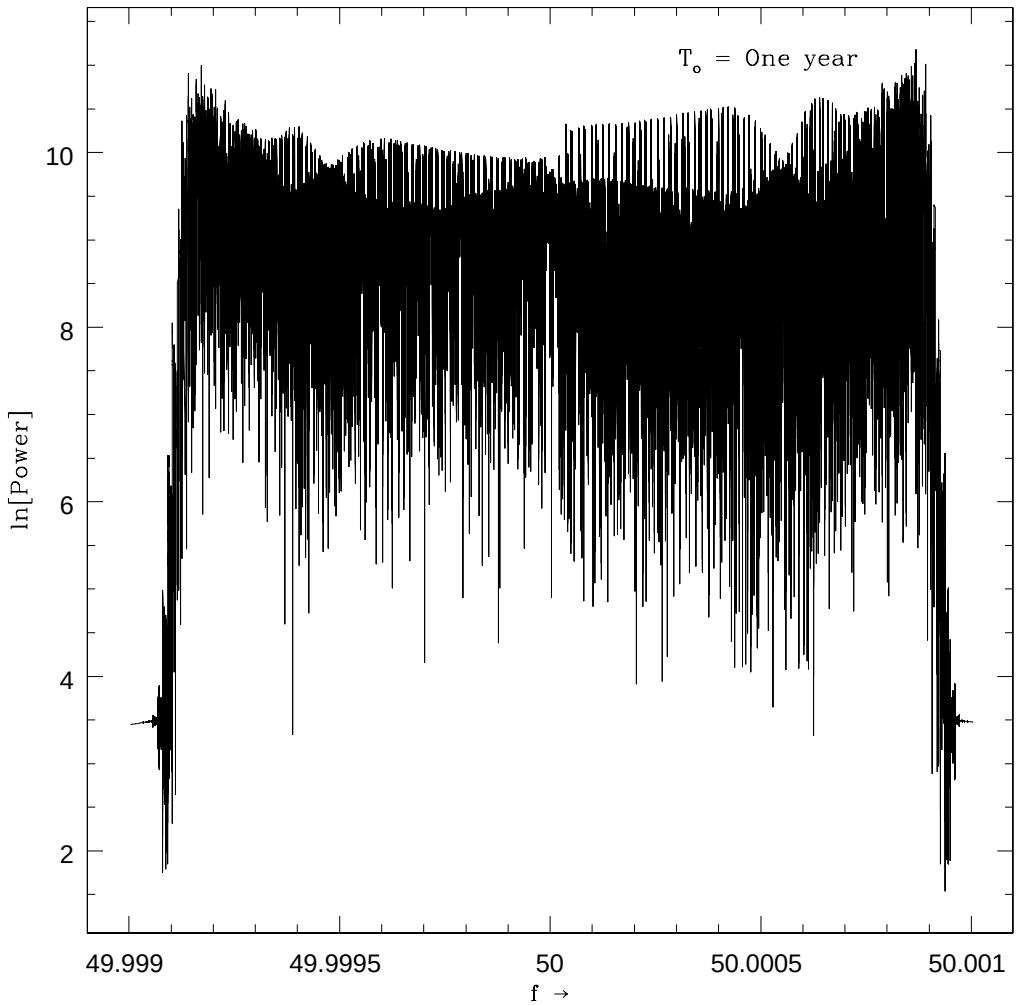

Figure 4.6: Power spectrum of a Doppler modulated signal at frequencies $f + f_{rot}$ of a source located at $(\pi/18, 0)$ with a resolution of 3.17×10^{-8}.

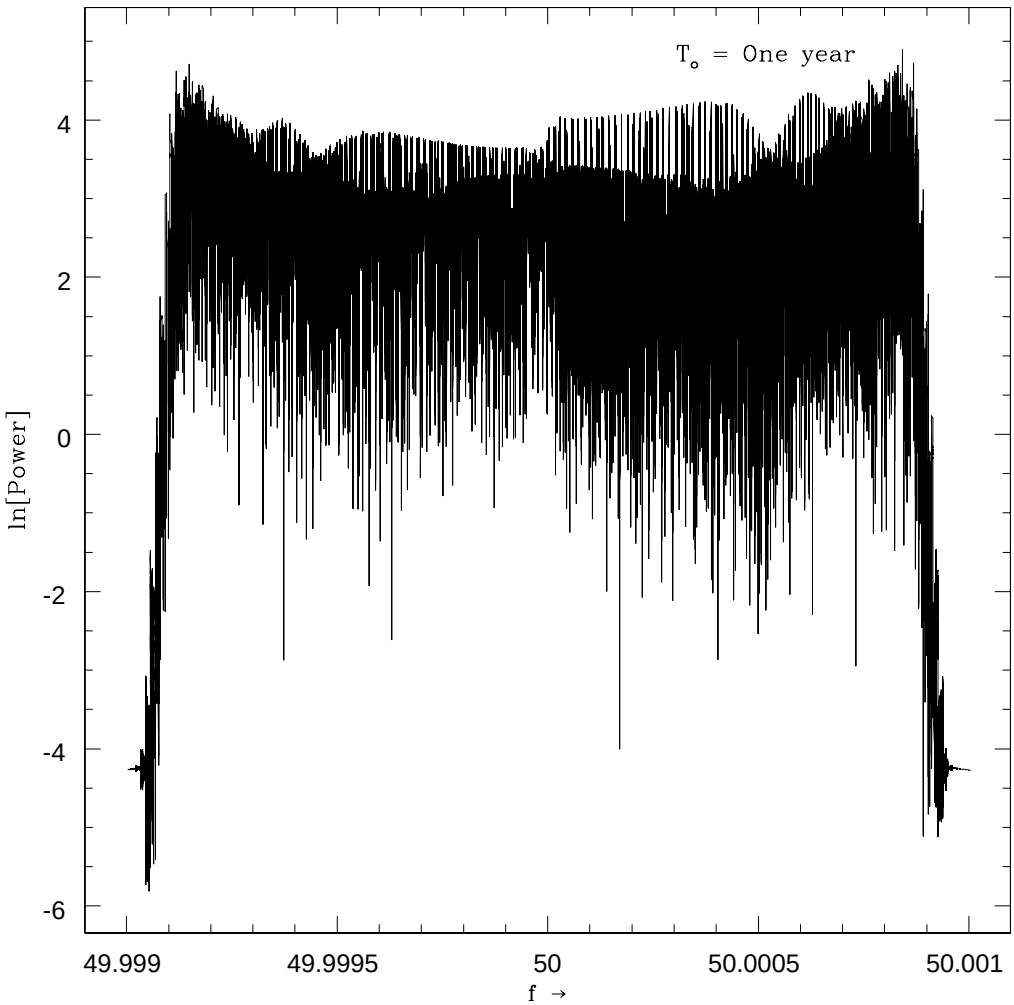

Figure 4.7: Power spectrum of a Doppler modulated signal at frequencies $f - f_{rot}$ of a source located at $(\pi/18, 0)$ with a resolution of 3.17×10^{-8}.

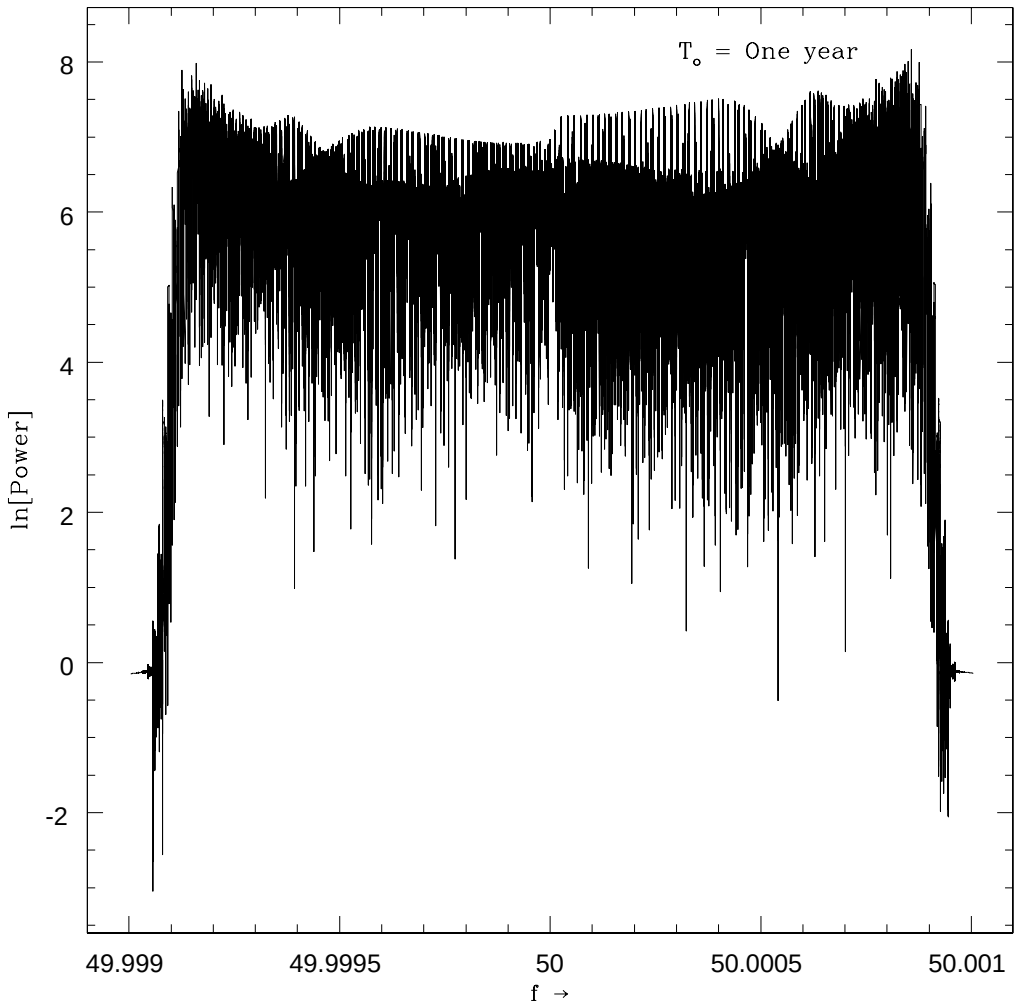

Figure 4.8: Power spectrum of a Doppler modulated signal at frequencies f of a source located at $(\pi/18, 0)$ with a resolution of 3.17×10^{-8}.

4.3 Fourier transform for arbitrary observation time

It is important to obtain the FT for arbitrary observation time. In this section we present this analysis. The results obtained will be employed to outline how spin down of a pulsar due to gravitational radiation back reaction or due to some other mechanism can be taken into account.

The FT for data of observation time T_o is given via

$$\tilde{h}(f) \;=\; \int_0^{T_o} \cos[\Phi(t)] e^{-i2\pi f t} dt \tag{4.19}$$

As usual, this splits into two terms as

$$\tilde{h}(f) \;= I_{\nu_-} + I_{\nu_+} \;; \tag{4.20}$$

$$I_{\nu_-} \;=\; \frac{1}{2w_{rot}} \int_0^{\xi_o} e^{i[\xi\nu_- + \mathcal{Z}\cos(a\xi-\phi) + \mathcal{N}\cos(\xi-\delta) - \mathcal{R} - \mathcal{Q}]} d\xi \,, \tag{4.21}$$

$$I_{\nu_+} \;=\; \frac{1}{2w_{rot}} \int_0^{\xi_o} e^{-i[\xi\nu_+ + \mathcal{Z}\cos(a\xi-\phi) + \mathcal{N}\cos(\xi-\delta) - \mathcal{R} - \mathcal{Q}]} d\xi \,, \tag{4.22}$$

$$\nu_\pm \;=\; \frac{f_o \pm f}{f_{rot}}; \quad \xi_o \;=\; w_{rot} T_o; \quad \xi \;=\; \xi_{rot} \;=\; w_{rot} t \tag{4.23}$$

As I_{ν_+} contributes very little to $\tilde{h}(f)$ we drop I_{ν_+} and write ν in place of ν_-. Using the identity (3.38) we get

$$\begin{aligned} \tilde{h}(f) \;\simeq\; & \frac{1}{2w_{rot}} e^{i(-\mathcal{R}-\mathcal{Q})} \int_0^{\xi_o} e^{i\nu\xi} \left[J_o(\mathcal{Z}) + 2\sum_{k=1}^{k=\infty} J_k(\mathcal{Z}) i^k \cos k(a\xi - \phi) \right] \\ & \times \left[J_o(\mathcal{N}) + 2\sum_{m=1}^{m=\infty} J_m(\mathcal{N}) i^m \cos m(\xi - \delta) \right] d\xi \end{aligned} \tag{4.24}$$

After performing the integration and proceeding in a straight forward manner we have

$$\tilde{h}(f) \simeq \frac{\nu}{2w_{rot}} \sum_{k=-\infty}^{k=\infty} \sum_{m=-\infty}^{m=\infty} e^{i\mathcal{A}} \mathcal{B}[\tilde{\mathcal{C}} - i\tilde{\mathcal{D}}] \; ; \tag{4.25}$$

$$\left.\begin{aligned}
\mathcal{A} &= \tfrac{(k+m)\pi}{2} - \mathcal{R} - \mathcal{Q} \\
\mathcal{B} &= \tfrac{J_k(\mathcal{Z}) J_m(\mathcal{N})}{\nu^2 - (ak+m)^2} \\
\tilde{\mathcal{C}} &= \sin \nu\xi_o \cos(ak\xi_o + m\xi_o - k\phi - m\delta) - \\
&\quad \tfrac{ak+m}{\nu} \{\cos \nu\xi_o \sin(ak\xi_o + m\xi_o - k\phi - m\delta) + \sin(k\phi + m\delta)\} \\
\tilde{\mathcal{D}} &= \cos \nu\xi_o \cos(ak\xi_o + m\xi_o - k\phi - m\delta) + \\
&\quad \tfrac{ka+m}{\nu} \sin \nu\xi_o \sin(ak\xi_o + m\xi_o - k\phi - m\delta) - \cos(k\phi + m\delta)
\end{aligned}\right\} \tag{4.26}$$

The FT of the two polarisation states of the wave can now be written as

$$\begin{aligned}
h_+(f) &= h_{o_+} \tilde{h}(f) \\
&\simeq \frac{\nu h_{o_+}}{2w_{rot}} \sum_{k=-\infty}^{k=\infty} \sum_{m=-\infty}^{m=\infty} e^{i\mathcal{A}} \mathcal{B}[\tilde{\mathcal{C}} - i\tilde{\mathcal{D}}] \; ;
\end{aligned} \tag{4.27}$$

$$\begin{aligned}
\tilde{h}_\times(f) &= -ih_{o_\times} \tilde{h}(f) \\
&\simeq \frac{\nu h_{o_\times}}{2w_{rot}} \sum_{k=-\infty}^{k=\infty} \sum_{m=-\infty}^{m=\infty} e^{i\mathcal{A}} \mathcal{B}[\tilde{\mathcal{D}} - i\tilde{\mathcal{C}}]
\end{aligned} \tag{4.28}$$

Now it is simple matter to obtain the FT of complete response. One gets

$$\begin{aligned}
\tilde{R}(f) &= e^{-i2\beta_o} \tilde{h}(f + 2f_{rot})/2 \left[h_{o_+}(F_{1_+} + iF_{2_+}) + h_{o_\times}(F_{2_\times} - iF_{1_\times})\right] + \\
& e^{i2\beta_o} \tilde{h}(f - 2f_{rot})/2 \left[h_{o_+}(F_{1_+} - iF_{2_+}) - h_{o_\times}(F_{2_\times} + iF_{1_\times})\right] + \\
& e^{-i\beta_o} \tilde{h}(f + f_{rot})/2 \left[h_{o_+}(F_{3_+} + iF_{4_+}) + h_{o_\times}(F_{4_\times} - iF_{3_\times})\right] + \\
& e^{i\beta_o} \tilde{h}(f - f_{rot})/2 \left[h_{o_+}(F_{3_+} - iF_{4_+}) - h_{o_\times}(F_{4_\times} + iF_{3_\times})\right] + \\
& \tilde{h}(f) \left[h_{o_+} F_{5_+} - ih_{o_\times} F_{5_\times}\right]
\end{aligned} \tag{4.29}$$

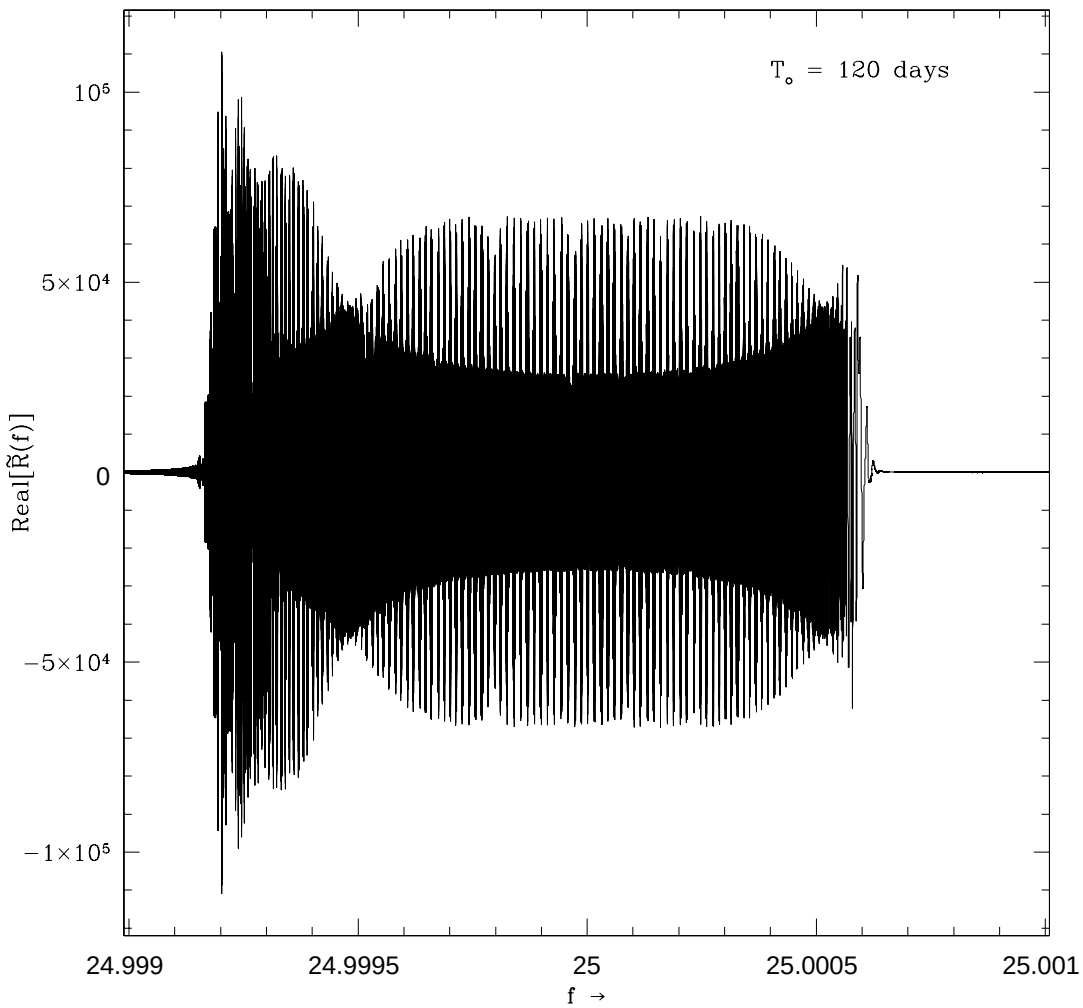

Figure 4.9: FT of a FM signal of a source located at $(\pi/9, \pi/4)$ with a resolution of 9.67×10^{-8}.

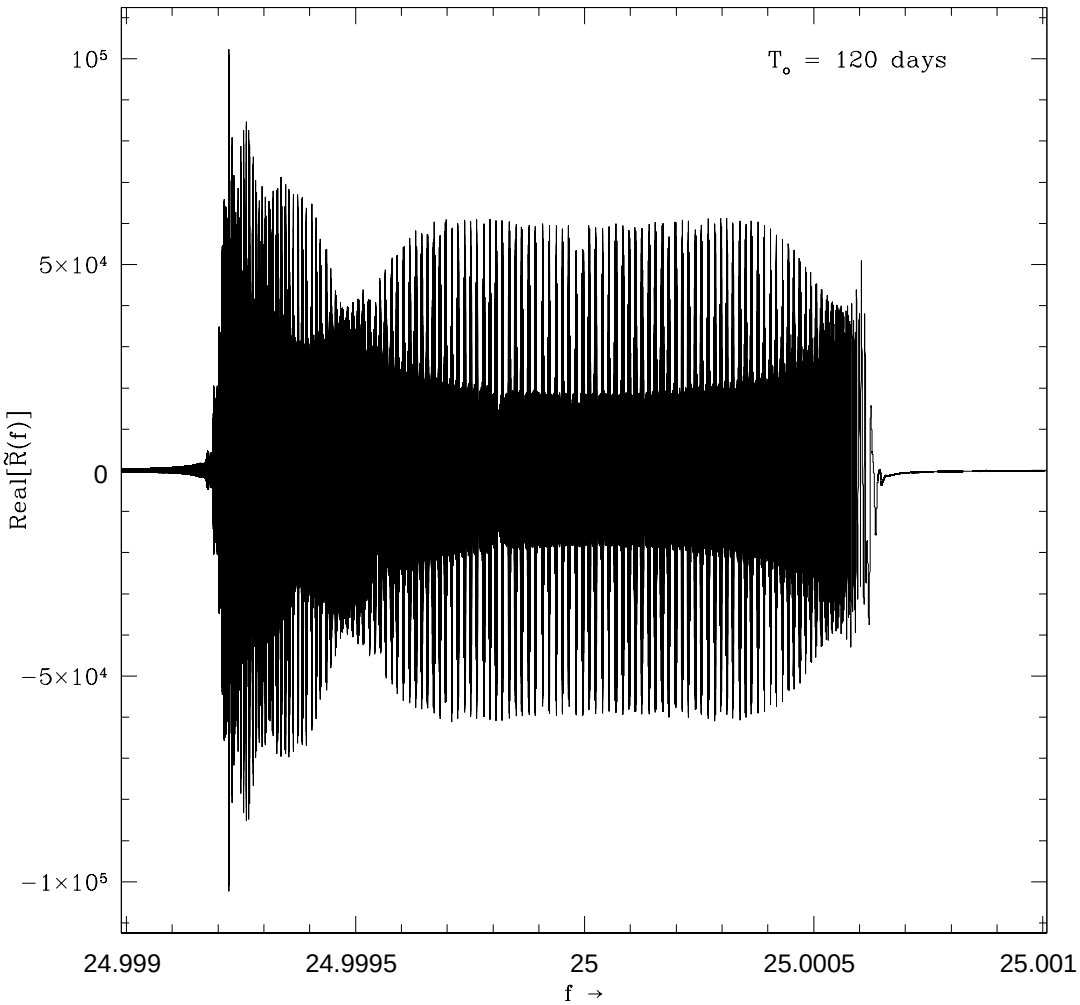

Figure 4.10: FT of the complete response of a Doppler modulated of a source located at $(\pi/9, \pi/4)$ with a resolution of 9.67×10^{-8}.

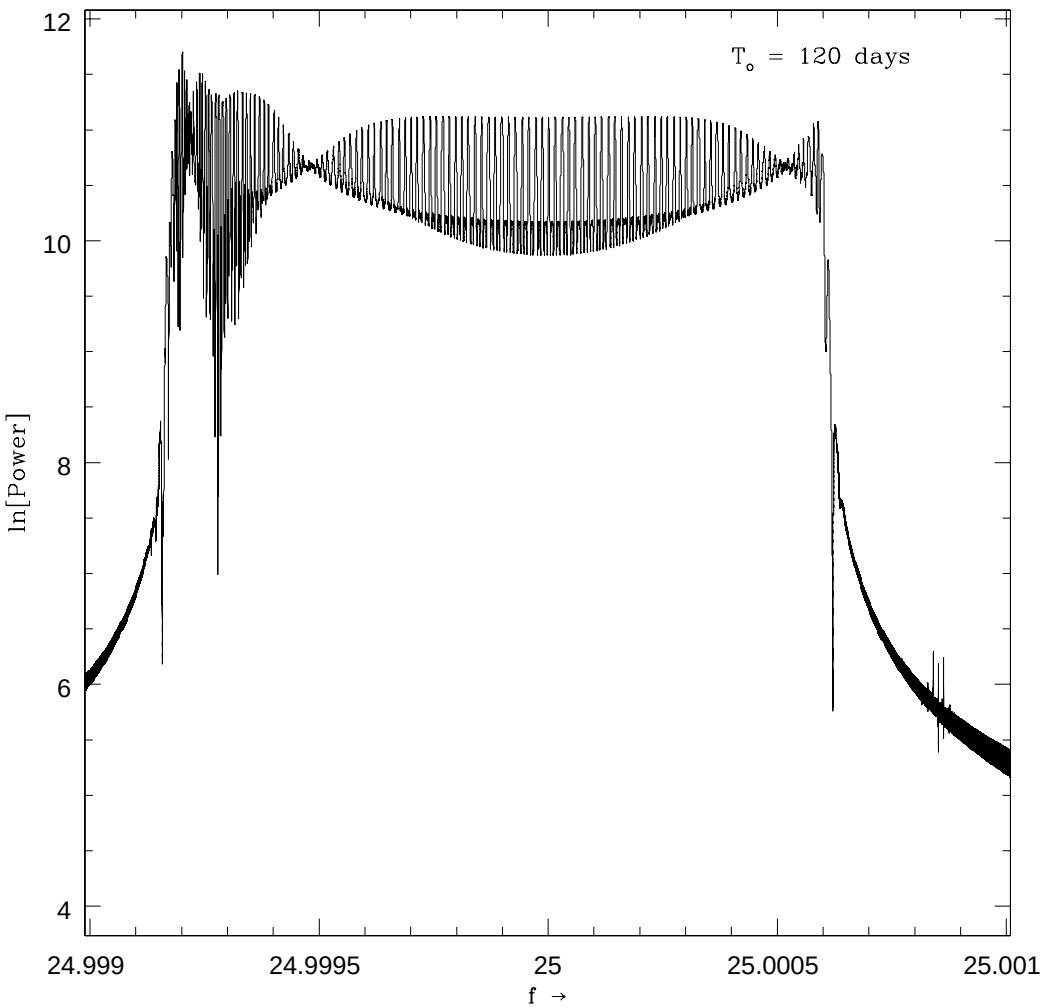

Figure 4.11: Power spectrum of a FM signal of a source located at $(\pi/9, \pi/4)$ with a resolution of 9.67×10^{-8}.

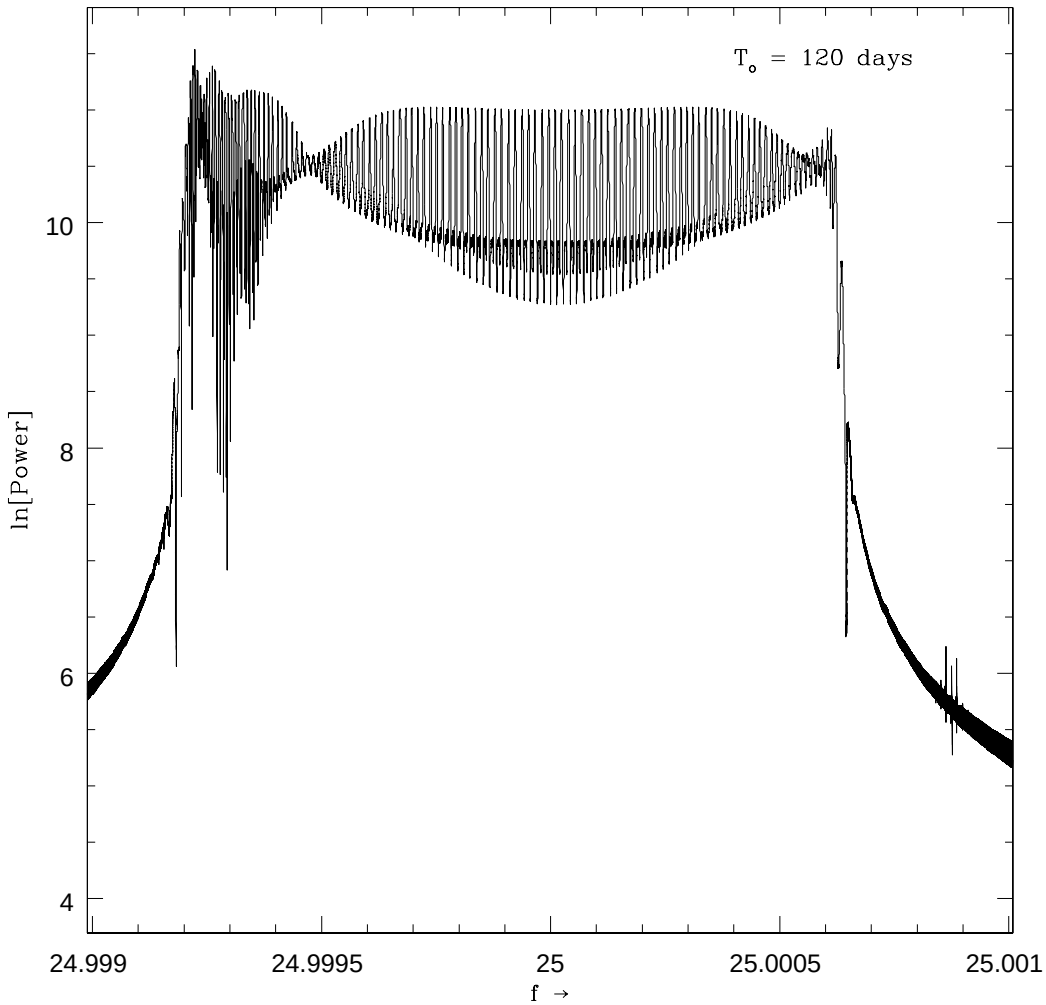

Figure 4.12: Power spectrum of the complete response of a Doppler modulated signal of a source located at $(\pi/9, \pi/4)$ with a resolution of 9.67×10^{-8}.

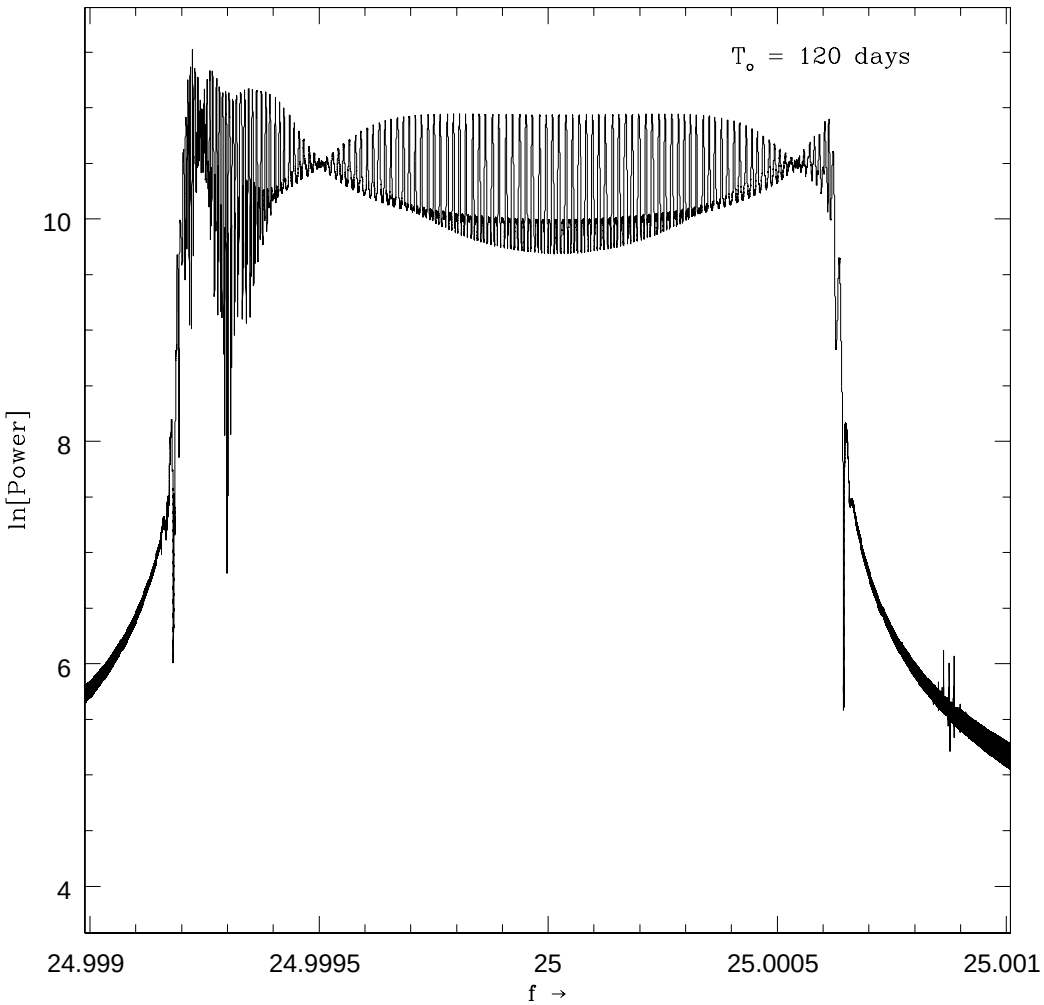

Figure 4.13: Power spectrum of a Doppler modulated signal at frequencies $f + 2f_{rot}$ of a source located at $(\pi/9, \pi/4)$ with a resolution of 9.67×10^{-8}.

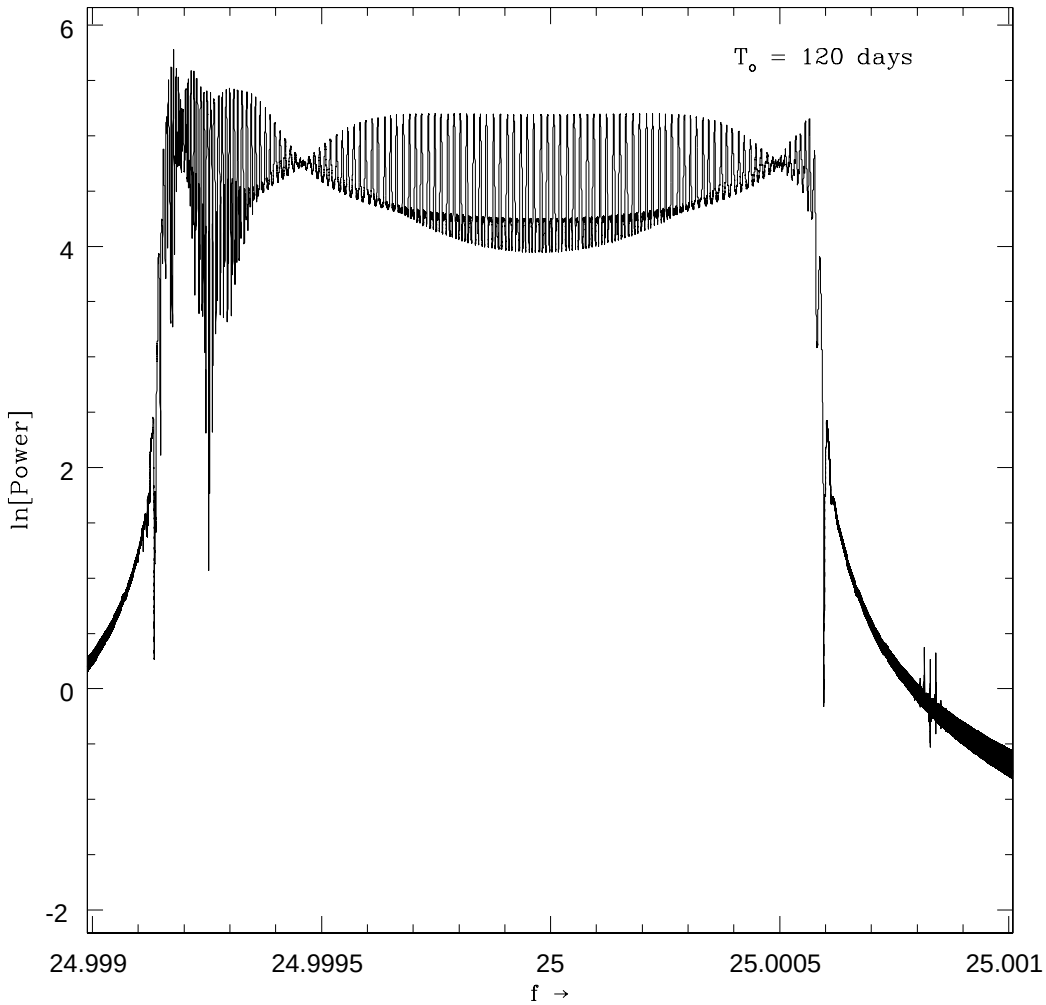

Figure 4.14: Power spectrum of a Doppler modulated signal at frequencies $f - 2f_{rot}$ of a source located at $(\pi/9, \pi/4)$ with a resolution of 9.67×10^{-8}.

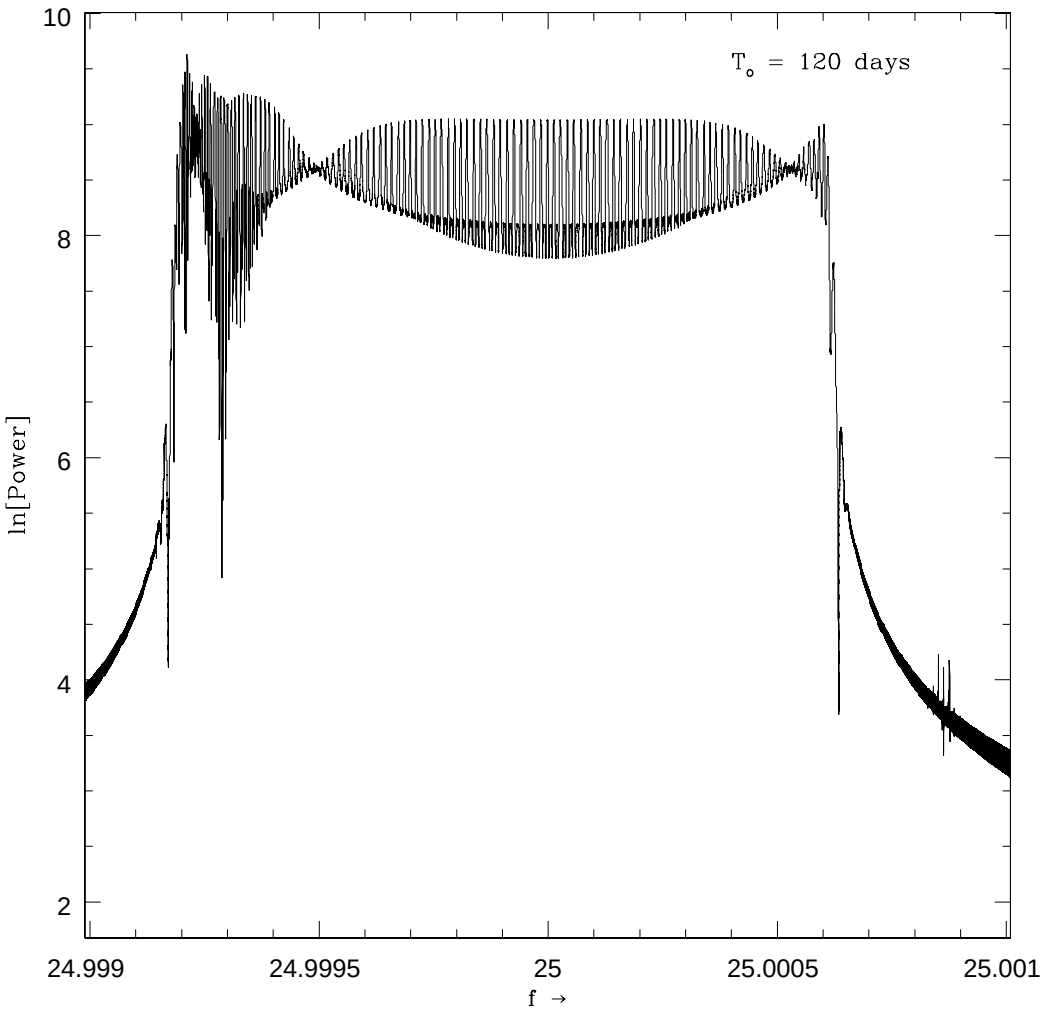

Figure 4.15: Power spectrum of a Doppler modulated signal at frequencies $f + f_{rot}$ of a source located at $(\pi/9, \pi/4)$ with a resolution of 9.67×10^{-8}.

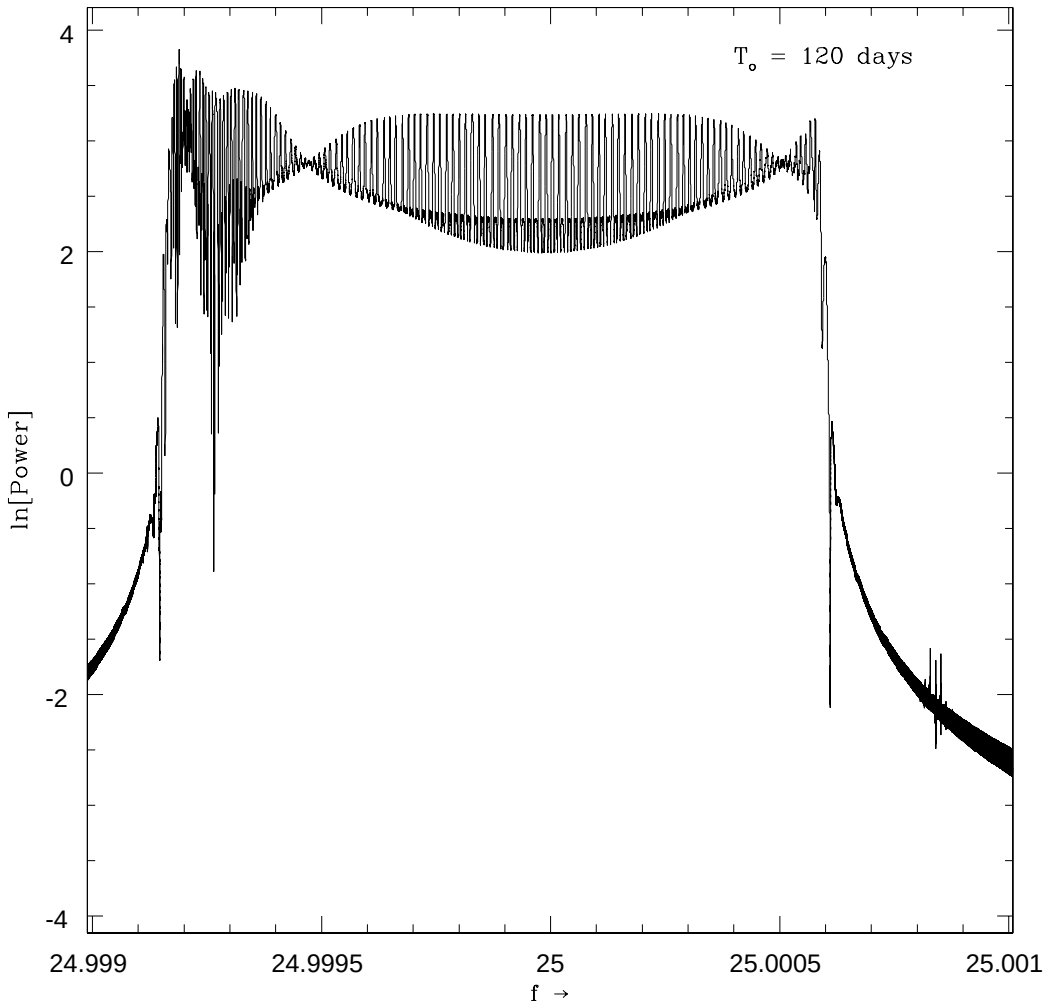

Figure 4.16: Power spectrum of a Doppler modulated signal at frequencies $f - f_{rot}$ of a source located at $(\pi/9, \pi/4)$ with a resolution of 9.67×10^{-8}.

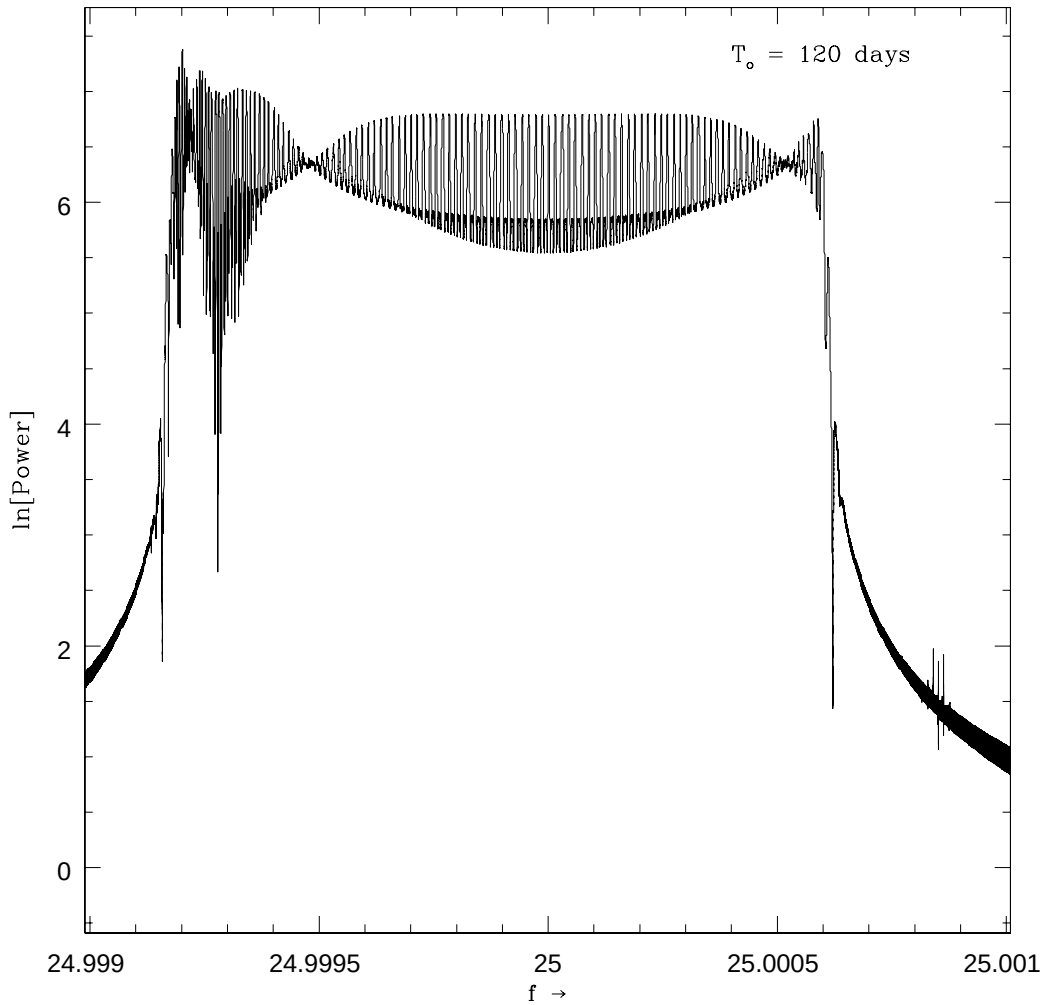

Figure 4.17: Power spectrum of a Doppler modulated signal at frequencies f of a source located at $(\pi/9, \pi/4)$ with a resolution of 9.67×10^{-8}.

The FT of FM and complete response of the detector for a data of 120 days and

$$\left.\begin{array}{lll} f_o = 25\ Hz\,, & h_o = h_\times = 1 & \\ \alpha = \pi/6\,, & \beta_o = \pi/3\,, & \gamma = 2\pi/3\,, \\ \theta = \pi/9\,, & \phi = \pi/4\,, & \psi = \pi/4. \end{array}\right\} \tag{4.30}$$

are plotted in Figs. (4.9) and (4.10) with a resolution of $1/2T_o \approx 9.67\times10^{-8}Hz$. The corresponding power spectra are plotted respectively in Figs. (4.11) and (4.12). Figs. (4.13), (4.14), (4.15) and (4.16) represent the power spectra of complete response of the detector at $f + 2f_{rot}$, $f - 2f_{rot}$, $f + f_{rot}$ and $f - f_{rot}$ whereas Fig. (4.17) shows the response of the detector at f. In this case also the most of the power of the signal lies in the frequency $f + 2f_{rot}$ and the least with $f - f_{rot}$. The codes for computing the frequency modulated signal and complete response of the detector, written in FORTRAN, are given in appendices A and B.

4.4 Spin down

Pulsars loose their rotational energy by processes like electro-magnetic breaking, emission of particles and emission of GW. Thus, the rotational frequency is not completely stable, but varies over a time scale which is of the order of the age of the pulsar. Typically, younger pulsars have the largest spin down rates. Current observations suggest that spin down is primarily due to electro-magnetic breaking (Manchester, 1992 and Kulkarni, 1992). Over the entire observing time T_o the frequency drift would be small but it may be taken into account for better sensitivity. To account this aspect we consider the evaluation of FT in a sequence of time windows by splitting the interval $0 - T_o$ in M equal parts, each of interval $\triangle t$ ($T_o = M \triangle t$) such that the

signal over a window may be treated as monochromatic. The strategy is to evaluate the FT over the window and finally to add the result. This process has been suggested by Brady and Creighton (2000) and Schutz (1998) in numerical computing and has been termed as *stacking* and *tracking*. For any such window let the time interval of data under consideration corresponds to $t = t_o + n \triangle t$ and $t = t_o + (n+1) \triangle t$ where t_o is the instant representing the start of the data set and $0 \leq n \leq M-1$. The window under consideration is the n_{th} window. Now we have

$$\begin{aligned} I &= \int_{t_o+n\triangle t}^{t_o+(n+1)\triangle t} h(\bar{t}) e^{-i2\pi f \bar{t}} d\bar{t} \\ &= \int_0^{\triangle t} h(t + t_o \ + n \triangle t) e^{-i2\pi f (t+t_o+n\triangle t)} dt \ ; \qquad (4.31) \\ \bar{t} &= t + t_o + n \triangle t \qquad (4.32) \end{aligned}$$

Hence, the FT to account spin down is given via

$$\left[\tilde{h}(f)\right]_s = \int_0^{\triangle t} \cos[\Phi(t + t_o + n \triangle t)] e^{-i2\pi f (t+t_o+n\triangle t)} dt \qquad (4.33)$$

Taking the initial time of the data set

$$t_o = 0 \qquad (4.34)$$

and proceeding in the same manner as in previous section the FT is obtained as

$$\begin{aligned} \left[\tilde{h}(f)\right]_s \simeq \ & \frac{1}{2w_{rot}} e^{i[2\pi n(f_o - f)\triangle t - \mathcal{R} - \mathcal{Q}]} \int_0^{\triangle t} e^{i\nu\xi} \left[J_o(\mathcal{Z}) + \right. \\ & \left. 2 \sum_{k=1}^{k=\infty} J_k(\mathcal{Z}) i^k \cos k(a\xi - \lambda) \right] \times \\ & \left[J_o(\mathcal{N}) + 2 \sum_{m=1}^{m=\infty} J_m(\mathcal{N}) i^m \cos m(\xi - \zeta) \right] d\xi \qquad (4.35) \end{aligned}$$

After integration we get,

$$\left[\tilde{h}(f)\right]_s = \frac{\nu}{2w_{rot}} \sum_{k=-\infty}^{k=\infty} \sum_{m=-\infty}^{m=\infty} e^{i\mathcal{A}_s} \mathcal{B} \left[\mathcal{C}_s - i\mathcal{D}_s\right] \tag{4.36}$$

where

$$\left.\begin{aligned}
\mathcal{A}_s &= \tfrac{(k+m)\pi}{2} + 2\pi n \triangle t(f_o - f) - \mathcal{R} - \mathcal{Q} \\
\mathcal{B} &= \tfrac{J_k(\mathcal{Z}) J_m(\mathcal{N})}{\nu^2 - (ak+m)^2}\,, \\
\mathcal{C}_s &= \sin(\nu\tau)\cos(ak\tau + m\tau - k\lambda - m\zeta) \\
&\quad -\tfrac{ak+m}{\nu}\{\cos(\nu\tau)\sin(ak\tau + m\tau - k\lambda - m\zeta) \\
&\quad + \sin(k\lambda + m\zeta)\}\,, \\
\mathcal{D}_s &= \cos(\nu\tau)\cos(ak\tau + m\tau - k\lambda - m\zeta) \\
&\quad + \tfrac{ak+m}{\nu}\sin(\nu\tau)\sin(ak\tau + m\tau - k\lambda - m\zeta) \\
&\quad - \cos(k\lambda + m\zeta)\,, \\
\lambda &= \phi - an\tau_o\,, \quad \zeta = \delta - n\tau_o\,, \quad \tau = \xi_o = w_{rot}T_o\,, \\
\tau_o &= w_{rot} \triangle t\,, \quad n = 0, 1, 2, 3, ..., M-1.
\end{aligned}\right\} \tag{4.37}$$

The FT of the complete response would now be given via

$$\begin{aligned}
\left[\tilde{R}(f)\right]_s = {} & e^{-i2\beta_o}\left[\tilde{h}(f + 2f_{rot})/2\right]_s \left[h_{o_+}(F_{1_+} + iF_{2_+}) + h_{o_\times}(F_{2_\times} - iF_{1_\times})\right] + \\
& e^{i2\beta_o}\left[\tilde{h}(f - 2f_{rot})/2\right]_s \left[h_{o_+}(F_{1_+} - iF_{2_+}) - h_{o_\times}(F_{2_\times} + iF_{1_\times})\right] + \\
& e^{-i\beta_o}\left[\tilde{h}(f + f_{rot})/2\right]_s \left[h_{o_+}(F_{3_+} + iF_{4_+}) + h_{o_\times}(F_{4_\times} - iF_{3_\times})\right] + \\
& e^{i\beta_o}\left[\tilde{h}(f - f_{rot})/2\right]_s \left[h_{o_+}(F_{3_+} - iF_{4_+}) - h_{o_\times}(F_{4_\times} + iF_{3_\times})\right] + \\
& \left[\tilde{h}(f)\right]_s \left[h_{o_+}F_{5_+} - ih_{o_\times}F_{5_\times}\right]
\end{aligned} \tag{4.38}$$

4.5 N-component signal

The FT in Eqs. (4.25) and (4.29) are for a pulsar which emits GW signal at single frequency f_o. But there are known physical mechanisms which generate GW signals consisting of many components. An axially symmetric pulsar undergoing free precession, emits quadrupole GW at two frequencies, one equal

to the sum of the spin frequency and the precession frequency, and the other twice of it (Zimmermann, 1979, 1980). The quadrupole GW from a triaxial ellipsoid rotating about one of its principal axes consists of one component only (Thorne, 1987). In this case the signal has frequency about twice the spin frequency of the star. In general, if a star is non-axisymmetric and precesses, the GW signal consists of more than two components. For the case of triaxial ellipsoid and small wobble angle there is a third component with frequency equal to twice the spin frequency of the star (Zimmermann, 1979, 1980). Recently, new mechanisms e.g. r-mode instability of spinning neutron stars (Anderson, 1998; Lindblom et al., 1998; Owen, et al., 1998) and temperature asymmetry in the interior of the neutron star with miss-aligned spin axis (Bildsten, 1998) have been discussed in the literature.

In view of the above discussion CGW signal may consists of frequencies which are multiple of some basic frequencies. An analysis of the GW data of N-component of signal has been made recently by Jaranowski and Królak (2000). We in this section present Fourier analysis of N-component CGW signal. We model the N-component signal as

$$h(t) = \sum_{l=1}^{N} h_l(t) \; ; \tag{4.39}$$

$$h_{l+}(t) = h_{o_{l+}} \cos[\Phi_l(t)] \tag{4.40}$$

$$h_{l\times}(t) = h_{o_{l\times}} \sin[\Phi_l(t)] \qquad l = 1, 2, ..., N \; ; \tag{4.41}$$

$$\Phi_l(t) = 2\pi f_l \left[t + \mathcal{Z}_l \cos(a\xi_{rot} - \phi) + \mathcal{N}_l \cos(\xi_{rot} - \delta_l) - \mathcal{R}_l - \mathcal{Q}_l\right] \tag{4.42}$$

where f_l represent the component frequency of the signal. Let us write

$$h_l(t) = \cos[\Phi_l(t)] \tag{4.43}$$

It is trivial matter to obtain $\tilde{h}_l(f)$, $\tilde{R}_l(f)$ and to get

$$\tilde{h}_N(f) = \sum_l \tilde{h}_l(f) \qquad and \tag{4.44}$$

$$\tilde{R}_N(f) = \sum_l \tilde{R}_l(f) \tag{4.45}$$

We do not continue this analysis as the requisite formalism is analogous to what we have presented in Chapter 3 and earlier sections of the present Chapter.

4.6 Discussion and conclusions

The analysis and results obtained in earlier Chapter regarding FT of the response of a Laser Interferometer have been generalised in the present Chapter. In this context following points must be noted.

1. For longer observation time, say, 120 days the resolution provided by FFT (equal to $1/T_o$) is sufficient to represent the structure of side bands.

2. Although in every case discussed, it turned out that the maximum power lies in the frequency $f + 2f_{rot}$. However, this is not established conclusively whether this result is generic. In any case, for any given detector location, we can know in advance if similar type of behaviour is obtained.

3. The computer time required in computing analytical FT depends on the orientation of the source and is independent of time interval of the observation data set. In contrast to this the computation cost increases for FFT with increase of the data set.

4. Throughout our analysis in Chapters 3 and 4 we have employed following conditions.

   (i) The phase of the wave is zero at $t = 0$.

(ii) The observation time of the data set is from $t = 0$ to $t = T_o$.

5. As remarked in Chapter 3 the requirement 4-(i) may be acheived by translation of time-origin. Now let us see how the condition 4(ii) can be relaxed. Let the data set is taken for

$$t = t_i \quad to \quad t = t_i + T_o \tag{4.46}$$

Eqs. (4.31), (4.32), (4.33) and (4.34) reveal that the results obtained there corresponds to data set

$$t = n \triangle t \quad to \quad t = (n+1) \triangle t \tag{4.47}$$

To obtain the sought generalisation we set

$$t_i = n \triangle t \quad and \quad T_o = \triangle t \tag{4.48}$$

and may use the results of section (4.3) by noting that for the present case we have

$$\lambda = \phi - n w_{orb} \triangle t \quad \Longrightarrow \quad \lambda = \phi - w_{orb} t_i \tag{4.49}$$

$$\zeta = \delta - n w_{rot} \triangle t \quad \Longrightarrow \quad \zeta = \delta - w_{rot} t_i \tag{4.50}$$

Chapter 5

All sky search: Study of templates

5.1 Introduction

Gravitational wave Laser Interferometer antennas are essentially omni - directional with their response better than 50% of the average over 75% of the whole sky (Grishchuk et al., 2000). Hence the data analysis systems will have to carry out all sky searches for the sources. We know that the amplitude of intense GW believed bathing Earth is very small, as compared to the sensitivity of GW detectors and is further masked by the dominant noise. In these circumstances, CGW sources are of prime importance because for such sources we can achieve enhanced SNR by investigating longer observation data set. However, a long observation time introduces modulation effects, arising due to relative motion of detector and the source. As a consequence, there results distribution of power in a forest of sidebands to such an extent that there is reduction to the tune of 90% of the expected power due to AM. The problem of all sky search gains another dimension in view of the fact that there are reasons to believe the presence of intense GW sources whose locations and even frequencies are not known. Amongst such sources pulsars occupy an important position. Similar to all sky search one will also have to do all frequency search.

All sky all frequency search is the holy grail of gravitation pulsar astronomy. In this Chapter we confine ourselves to the problem of all sky search.

Search of CGW without a priori knowledge appears to be computationally quite demanding even by the standard computers expected to be available in near future. For example, in the case of bandwidth 10^3 Hz, observation time 10^7 sec. and star's minimum decay time of 100 years one would require $10^{14}\,Tflops$ computer (Frasca, 2000). Very fast computer and large memories with ample amount of disk space seems inevitable. However, choice of optimal data processing and clever programming is also integral part of solution to this problem. Amongst these the pre-correction of time series due to Doppler modulation before the data is processed may be a method, which will reduce computational requirements. In reference to this, Schutz (1991) has introduced the concept of patches in the sky defined as the region of space for which similar Doppler corrections would be required. He has also demonstrated that the number of patches required for 10^7 sec. observation data set and one KHz signal would be about 1.3×10^{13} if one takes into account the rotational motion of Earth. However, the size of the patch would also depend on the data analysis technique being employed.

Matched filtering is the most suitable technique for detection of signals from sources viz., pulsars whose wave form is known. The wave forms are used to construct a bank of templates, which represent expected signal wave form with all possible ranges of its parameters. The time of arrival, source location, frequency of the signal, ellipticity of the source and its spin down represent important parameters of GW emitted by a pulsar. For detection of GW we set a criterion to judge if the cross correlation of the templates with the corresponding data set exceeds the preassigned threshold. We would perform the data analysis employing the criterion of the *FF*.

5.2 Matched filter analysis: Templates

The bank of templates will be matched to only a discrete set of signals from among the continuum of possible signals. Consequently, it is natural that all signals will not get detected with equal probability. However, it is possible to choose judiciously the set of templates so that all signals of a given amplitude are detected with a given minimum detection probability. The standard measure for deciding what class of wave form is good enough is the FF (Apostolatos, 1995). It quantitatively describes the closeness of the true signals to the template manifold in terms of the reduction of SNR due to cross correlation of a signal outside the manifold with all the templates lying inside the manifold. If the FF of a template family is unity the signal lies in the manifold. If the FF is less than unity the signal lies outside manifold.

Even if the signal discrete templates lies within the template manifold it would be unlikely that any of the actual templates used would correspond to the signal. The parameters describing the search template (source location, ellipticity, etc.) can vary continuously through out a finite range of values. The set of templates characterised by the continuously varying parameters is ofcourse infinite. However, in practice the interferometer output must be cross correlated with a finite subset of the templates whose parameter values vary in discrete steps from one template to the next. This subset ("the discrete template family") has measure zero on the manifold of the full set of possible templates ("the continuous template family"), so the template which most closely match a signal will generally lie in between the signal and the nearest of the discrete template family. The mismatch between the signal and the nearest of the discrete templates will cause some reduction in SNR. This would mean that the members of the discrete template family must be chosen so as

to render acceptable loss of SNR.

The study of templates has been made by many research workers in time domain [Schutz (1991), Królak (1997), Brady et. al. (1998), Brady and Creighton (2000), Jaranowski et al. (1998) and Jaranowski and Królak (2000)]. However, the analysis in frequency domain has the advantage of incorporating interferometer's spectral noise density. In order to determine the number of templates required to perform matched filtering analysis let us rewrite the formula expressing FF [Eq. (2.12)] as

$$FF(\theta,\phi) \;=\; \max_{\theta,\phi} \frac{\langle h(f)|h_T(f;\theta_T,\phi_T)\rangle}{\sqrt{\langle h_T(f;\theta_T,\phi_T)|h_T(f;\theta_T,\phi_T)\rangle\langle h(f)|h(f)\rangle}} \tag{5.1}$$

where, $h(f)$ and $h_T(f;\theta_T,\phi_T)$ represent respectively the FTs of the actual signal wave form and the templates. The template parameter θ_T and ϕ_T are chosen differing from the actual orientation of the source in discrete steps.

We have seen in earlier Chapters that the AM of CGW data output results into redistribution of power at four additional frequencies $f \pm 2f_{rot}$, $f \pm f_{rot}$ in accordance with the FM. Hence it is sufficient for the analysis of FF to consider only the frequency modulated FT. The results obtained in Chapter 4 regarding FT of frequency modulated data output [Eq. (4.25)] may be arranged using the symmetry property of the Bessel functions and one may write

$$\begin{aligned}\tilde{h}(f) \;\simeq\; & \frac{\nu}{w_{rot}}\Bigg[\frac{J_o(\mathcal{Z})J_o(\mathcal{N})}{2\nu^2}\left[\{\sin(\mathcal{R}+\mathcal{Q})-\sin(\mathcal{R}+\mathcal{Q}-\nu\xi_o)\}+\right.\\ & \left. i\,\{\cos(\mathcal{R}+\mathcal{Q})-\cos(\mathcal{R}+\mathcal{Q}-\nu\xi_o)\}\right] \;+\\ & J_o(\mathcal{Z})\sum_{m=1}^{m=\infty}\frac{J_m(\mathcal{N})}{\nu^2-m^2}\left[(\mathcal{YU}-\mathcal{XV})-i(\mathcal{XU}+\mathcal{YV})\right] \;+\\ & \sum_{k=1}^{k=\infty}\sum_{m=-\infty}^{m=\infty} e^{i\mathcal{A}}\mathcal{B}\left[\tilde{\mathcal{C}}-i\tilde{\mathcal{D}}\right] \;;\end{aligned} \tag{5.2}$$

$$\left.\begin{array}{rcl}\mathcal{X} & = & \sin(\mathcal{R}+\mathcal{Q}-m\pi/2) \\ \mathcal{Y} & = & \cos(\mathcal{R}+\mathcal{Q}-m\pi/2) \\ \mathcal{U} & = & \sin\nu\xi_o\cos m(\xi_o-\delta)-\frac{m}{\nu}\cos\nu\xi_o\sin m(\xi_o-\delta)-\sin m\delta \\ \mathcal{V} & = & \cos\nu\xi_o\cos m(\xi_o-\delta)+\frac{m}{\nu}\sin\nu\xi_o\sin m(\xi_o-\delta)-\cos m\delta\end{array}\right\} \quad (5.3)$$

Now it is straight forward to compute FF. To understand the procedure let us assume that there is a source at the location $(\theta, \phi) = (25^o, 30^o)$ emitting frequency $f_o = 0.5$ Hz. We wish to analyze the data set for $T_o =$ one sidereal day. We first fix the template parameter ϕ for the whole set given by $\phi_T = \phi = 30^o$ and vary θ_T in discrete steps over its entire range i.e. 0° to 180°. The results obtained are plotted graphically in Fig. (5.1). It is remarked that in order to compute the inner product defined via Eq. (2.9) one would require to integrate the expression over the band width of Doppler modulated signal. This may be determined either analytically by computing the maximum value of the Doppler shift in accordance with Eq. (3.25) or may be taken as represented by the frequency spectrum of the FT. In the present case we have taken the band width equal to 0.002 Hz. In a similar manner one may fix the $\theta-$parameter of the template set and obtain the variation of FF with template parameter ϕ_T. Figures (5.2) and (5.3) represent respectively the behaviour for $f_o = 25$ Hz, $\theta = \theta_T = 1^o$, $T_o =$ one sidereal day for source orientation $\phi = 35^o$ and 220°.

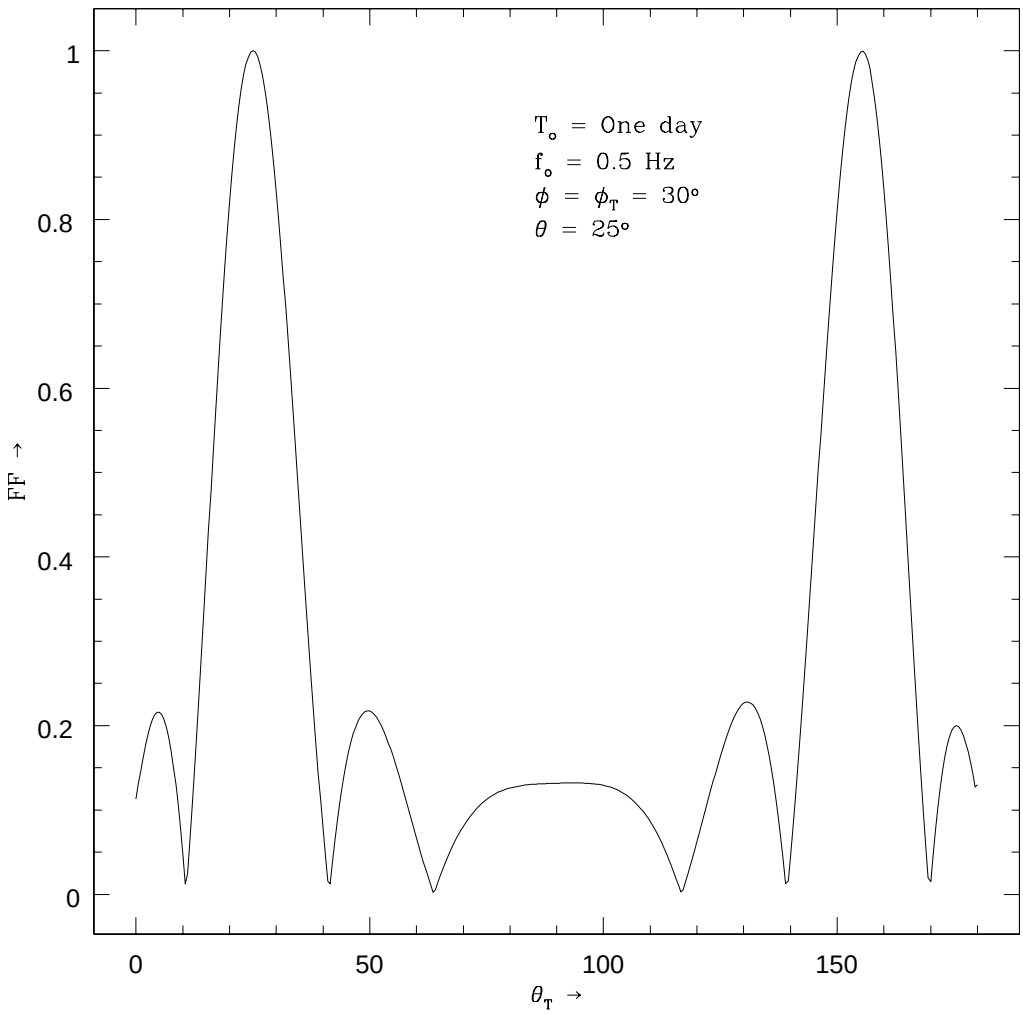

Figure 5.1: Variation of FF with θ_T.

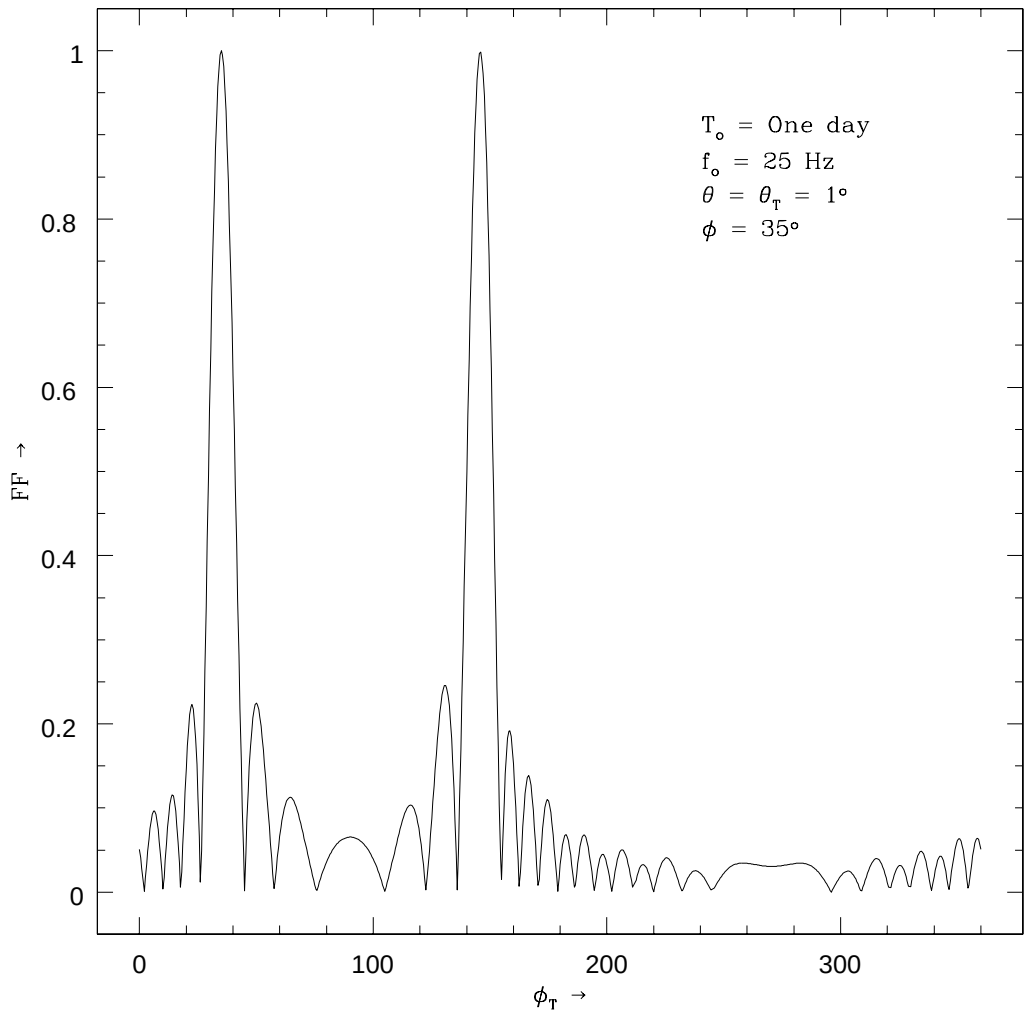

Figure 5.2: Variation of FF with ϕ_T.

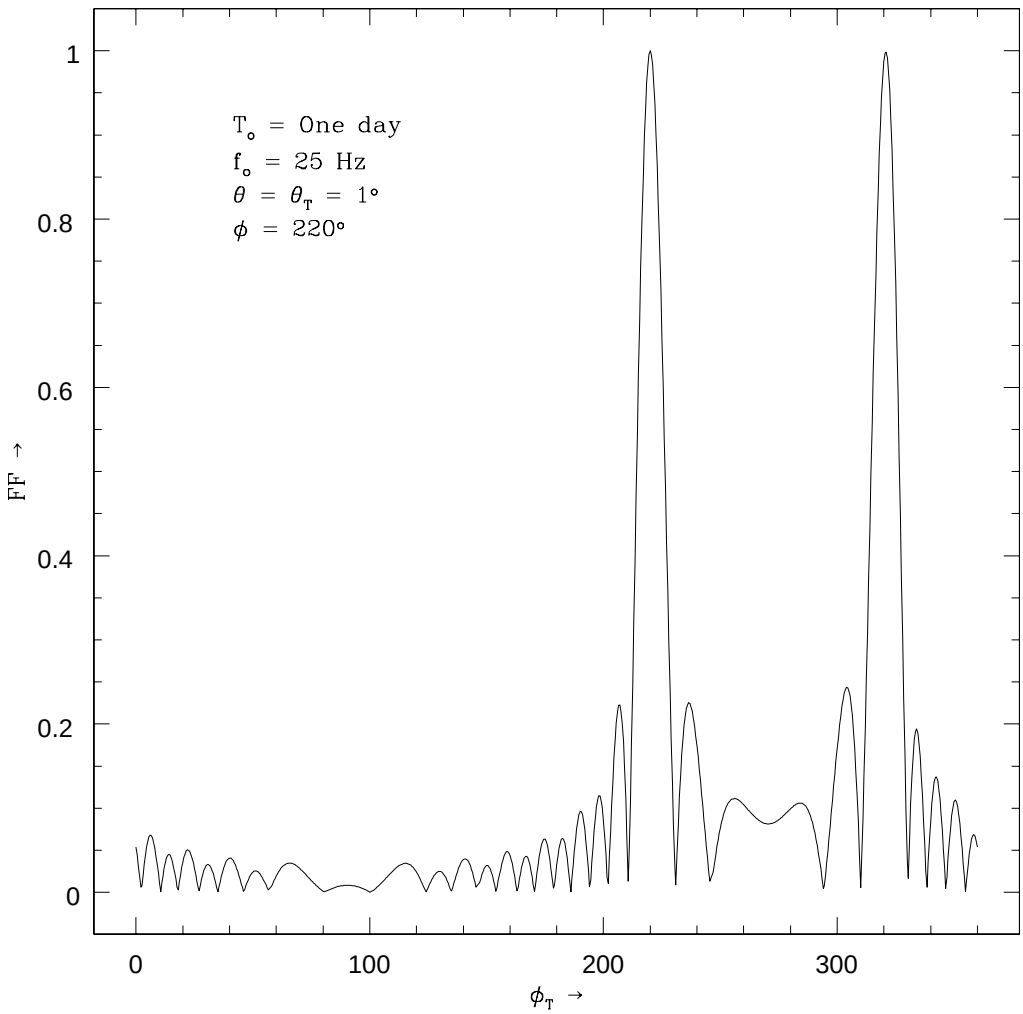

Figure 5.3: Variation of FF with ϕ_T.

The following points in reference to these plots may be noted.

(i) The FF is unity for $\theta_T = 25^o$, 155° [Fig (5.1] for $\phi_T = 35^o$, 145° [Fig (5.2)] and for $\phi_T = 220^o$, 320° [Fig (5.3)].

(ii) It is observed that FF decreases exponentially with template variables θ_T and ϕ_T. The specific relations are found numerically to be

$$FF = e^{0.047(\theta_T \sim \theta)^2} \tag{5.4}$$

$$FF = e^{0.06(\phi_T \sim \phi)^2} \tag{5.5}$$

(iii) The oscillatory behaviours do not represent any real situation as it arise because of the improper choice of numerical integration technique. However, we are content with the technique we have employed as the region of such artificial facets fall in the region of the $FF < 0.25$.

Finally, we conclude this section by noting the symmetry property of the template parameters. A closer look of the graphs and the remark (i) above reveal the following symmetry property. The FF is symmetrical under following transformations.

$$\theta_T \longrightarrow \pi - \theta_T \qquad 0 \leq \theta_T \leq \pi \tag{5.6}$$

$$\phi_T \longrightarrow \pi - \phi_T \qquad 0 \leq \phi_T \leq \pi \tag{5.7}$$

$$\phi_T \longrightarrow 3\pi - \phi_T \qquad \pi \leq \phi_T \leq 2\pi \tag{5.8}$$

Let us note that these symmetry properties are based on our results for one sidereal day observation time. The generic nature of the symmetries may be established only after studying the variation of FF with T_o. Unfortunately, we could not make this analysis because of our limitations on computational facilities.

5.3 Number of Templates

It is important to study the problem of number of templates for all sky search in the light of FF. The results of previous section reveal that the grid spacing $\triangle\theta$ in the $\theta-$parameter of templates may be expressed symbolically as a function of FF, f_o, and T_o i.e.

$$\triangle\,\theta = \mathcal{F}(FF, f_o, T_o) \tag{5.9}$$

Similarly, we have

$$\triangle\,\phi = \mathcal{G}(FF, f_o, T_o) \tag{5.10}$$

In view of this, Equations (5.4) and (5.5) may be equivalently expressed as

$$\mathcal{F}(FF, 0.5, T) = (0.047)^{-1}\ln(FF) \tag{5.11}$$

$$\mathcal{G}(FF, 25, T) = (0.06)^{-1}\ln(FF) \tag{5.12}$$

For any chosen value of FF one can determine $\triangle\theta$ and $\triangle\phi$. But there is no unique choice for it. Our interest would be in the assignment of $\triangle\theta$ and $\triangle\phi$ such that the spacing are maximum resulting into the least number of templates. As we have mentioned earlier there is stringent requirement on reducing computer time. Accordingly, there is serious need of adopting some procedure/formalism to achieve this. For example, one may adopt the method of hierarchical search given by Mohanty and Dhurandhar (1996) and Mohanty (1998). This search is carried out in two steps. At the first level one would start with template bank with a coarse spacing in the parameter space but with a lower threshold. In the next level a more finely spaced set of templates and a higher threshold would be used but only around those templates of the previous level which crossed the previous threshold.

However, an important issue related to the problem of number of templates is regarding the study of the behaviour of number of templates with FF for

different f_o and T_o. We have made investigations of this aspect. We assume a source location $(\theta, \phi) = (1^o, 30^o)$. We choose some value of FF, say 0.995. Now taking $\phi_T = 30^o$ we determine the spacing $\triangle\theta$ to yield the selected FF. In the case under investigation $\triangle\theta$ is found to equal 4.5×10^{-5}. Thereafter, we introduce spacing $\triangle\phi$ in the so obtained bank of templates and determine the resulting FF. The results obtained may be expressed in the form of a graph such as shown in Figs. (5.4) and (5.5). Interestingly the nature of these curves are similar. We have obtained a best fit to the graphs and obtain the relation.

$$N_{Templates} = \exp[a - bx + cx^2 - dx^3 + ex^4] \; ; \quad x = FF \, , \tag{5.13}$$

$$0.85 \leq x \leq 0.99$$

where a, b, c, d and e are constants. The values of these constants are given in Table (5.1).

Let us note from the graphs, for sake of comparison, that the number of templates required for FF equal to 0.97 are respectively 1.44×10^{10}, 3.5×10^{10} and 5.5×10^{10} for observation data set of 30, 120 and 365 days and $f_o = 50$ Hz. Similarly the number of templates required to analyse the observation data set of 120 days of GW frequencies 20, 50 and 100 Hz are respectively 1.22×10^{10}, 2.16×10^{10} and 5×10^{10}. It is observed that higher FF requires exponentially increasing large number of templates.

f_o (Hz)	T_o (days)	a $\times 10^{-2}$	b $\times 10^{-4}$	c $\times 10^{-5}$	d $\times 10^{-6}$	e $\times 10^{-7}$
50	30	2138.05	2071.43	7225.73	6239.43	2036.14
	180	2317.05	−71.3155	1746.61	2146.55	944.931
	365	2382.96	216.917	2464.42	2464.42	1031.54
20	120	2047.55	−794.473	3564.56	4650.68	1945.87
50		2266.59	4269.44	15655.0	17509.5	6484.51
100		2360.23	−206.906	1158.27	1491.01	733.520

Table 5.1: Coefficients of the best fit graphs obtained for the number of templates.

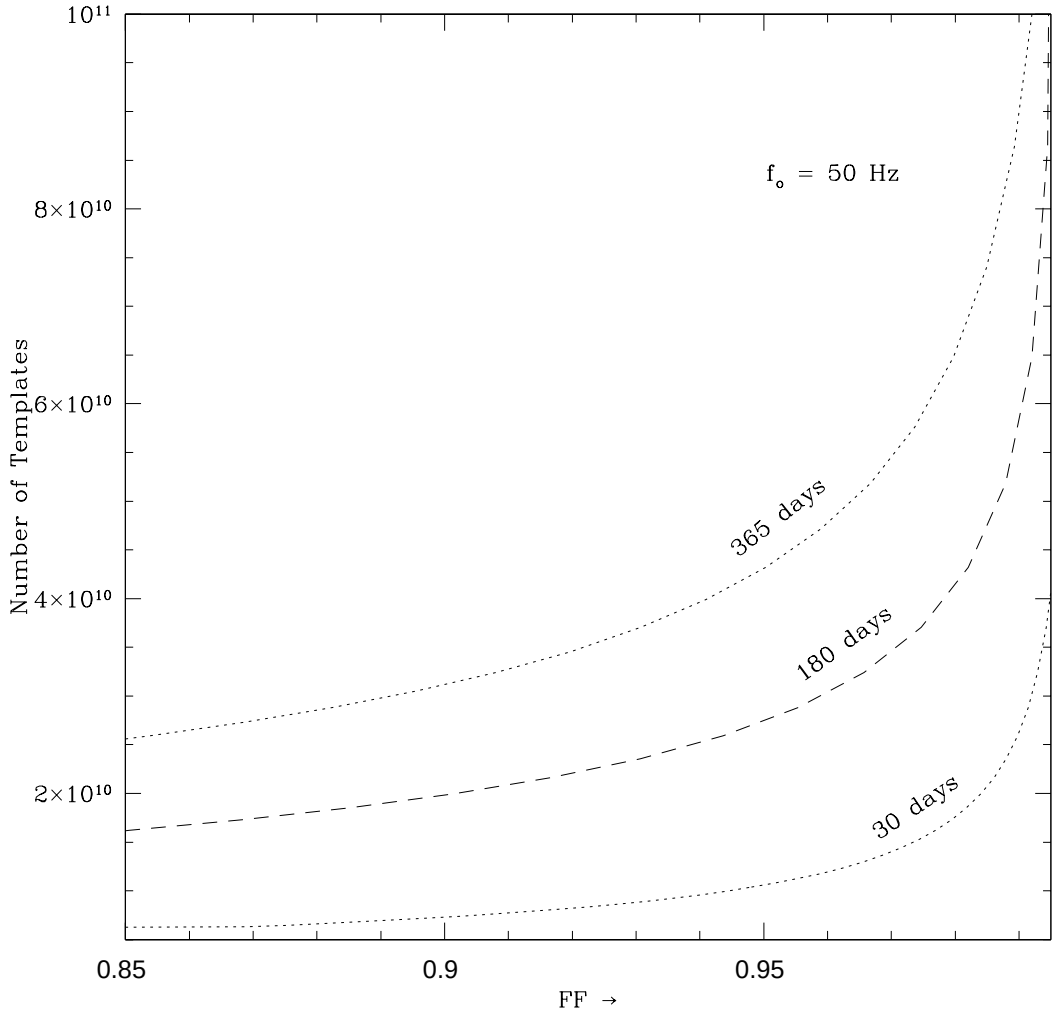

Figure 5.4: Variation of number of templates with FF for fixed f_o at different T_o.

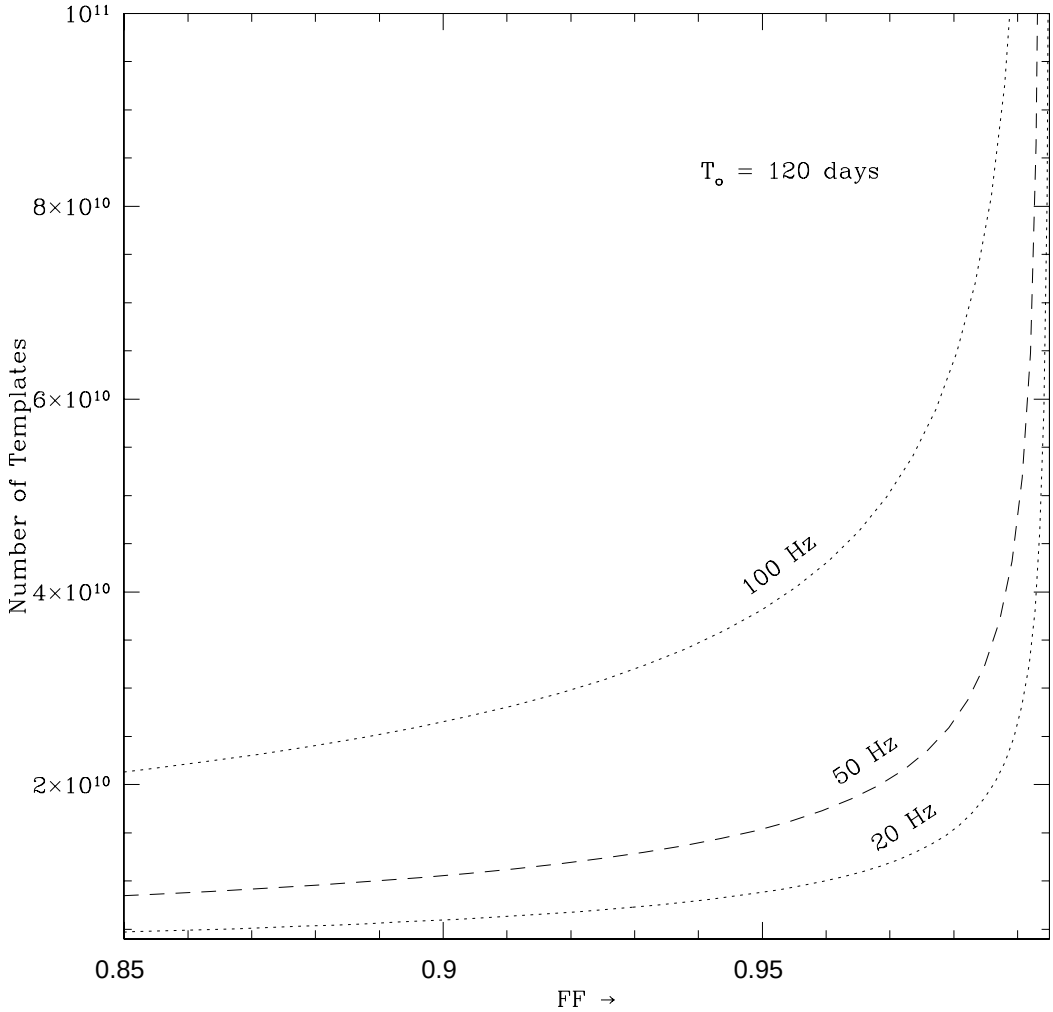

Figure 5.5: Variation of number of templates with FF for fixed T_o and of frequencies.

5.4 Discussion

In view of the complexity of the FT which contains exponential as well as Bessel functions; one has to be careful in computing FF. We have found useful to employ the Romberg integration using Padé approximation. We have used (i) QROMO of numerical recipes instead of QROMB as the former takes care of singularities, and (ii) RATINT routine for Padé approximation. The basic structure of the code is given in the appendix A and C (FM.F & TEM.F).

To compute FF the code has been written in FORTRAN. The Bessel functions are computed using the routine BESSJ0(X), BESSJ1(X) and BESSJ(N,X) of numerical recipes (Press et al. 1986). The BESSJ0(X) and BESSJ1(X) compute the Bessel function of first kind of zeroth and first order respectively for any value of X, while BESSJ(N,X) computes the Bessel function of first kind of arbitrary integeral order N for any value of X.

We have noticed marked symmetries in all sky search in both θ and ϕ space for one day observation time. It has been found that any FF corresponds to two values each in θ_T and ϕ_T. Accordingly, computation burden will be reduced by a factor of four. However, it is not clear whether the symmetry property can be established analytically as well. The source location, because of the symmetry, is uncertain. Some other analysis is to be adopted for getting the exact location.

We have computed the number of templates required for all sky search for matched filtering assuming the noise power spectral density $S_n(f)$ to be flat. However, for realistic situation, the effect of the noise have to be taken into consideration.

The issues of optimum template parameterization and placement, and the

related computational burden have been discussed in literature by several authors notably by Sathyaprakash and Dhurandhar (1991), Dhurandhar and Sathyaprakash (1994), Owen (1996), Apostolatos (1995, 1996), Mohanty and Dhurandhar (1996), Mohanty (1998), Owen and Sathayaprakash (1999). The question of possible efficient interpolated representation of the correlators is a problem of current interest and remains still unsolved.

Appendix A

Source code of the frequency modulated signal: *FM.F*

```
C       FT of the frequency modulated signal
        FUNCTION hfm(fnu,dtheta,dphi)
        IMPLICIT none
        INTEGER k,m,ms,ks
        REAL t,f0,fnu,dtheta,dphi,dalpha,dbeta0
C       [t = T_o, f0 = f_o, fnu = ν, dtheta = θ^o, dphi = φ^o, dalpha = α^o,
     * dbeta0 = β_o^o]
        PARAMETER (t = 86164.0, f0 = 25.0, dalpha = 75.0,
        dbeta0 = 60.0, ks = 720, ms = 8)
C       ['ks' & 'ms' are the values of 'k' & 'm' respectively]
        REAL h,z,bessj0,bessj1,bessj,bsh(-ms:ms),bsz(0:ks)
        REAL*8 pi,fr,pfr,a,u,rc,rad,theta,phi,epsilon,alpha,beta0,
     * sth,sal,sbe0,sph,sep,cth,cal,cbe0,cph,cep,p,q,r,delta,crq,
     * srq,bs0,fnn,cfnn,sfnn,rqf,fnu2,rplusq
        REAL*8 dm(1:ms),dmu(1:ms),rqm(1:ms),cmud(1:ms), smud(1:ms),
     * smd(1:ms),cmd(1:ms),crqm(1:ms),srqm(1:ms),wmn(1:ms),vmn(1:ms)
     * akd(1:ks,-ms:ms),rqk(1:ks,-ms:ms),skm(1:ks,-ms:ms),
     * pmd(1:ks,-ms:ms),akm(1:ks,-ms:ms),ckmu(1:ks,-ms:ms),
     * skmu(1:ks,-ms:ms),ckmr(1:ks,-ms:ms),ckm(1:ks,-ms:ms),
     * skmr(1:ks,-ms:ms)
        COMPLEX sum1,sum2,hfm
C       [hfm ⟶ Spectrum of the frequency modulated signal.]
```

```
EXTERNAL bessj0,bessj1,bessj

pi = 4.d0*datan(1.d0)
fr = 1.d0/86164.d0
pfr = 2.d0*pi*fr
a = 1.d0/365.2572d0
u = 2.d0*pi*fr*t
rc = 2.d0*pi*f0*0.0637/3.d0
rad = pi/180.d0
theta = rad*dtheta
phi = rad*dphi
epsilon = rad*23.45d0
alpha = rad*75.d0
beta0 = rad*60.d0
sth = dsin(theta)
sal = dsin(alpha)
sbe0 = dsin(beta0)
sph = dsin(phi)
sep = dsin(epsilon)
cth = dcos(theta)
cal = dcos(alpha)
cbe0 = dcos(beta0)
cph = dcos(phi)
cep = dcos(epsilon)
p = rc*sal*(cbe0*(sth*cep*sph + cth*sep) - sbe0*sth*cph)
q = rc*sal*(sbe0*(sth*cep*sph + cth*sep) + cbe0*sth*cph)
z = 2.d0*pi*f0*1496.d0/3.d0*sth
r = z*cph
rplusq = r + q
delta = datan(p/q)
h = dsqrt(p*p + q*q)
crq = dcos(rplusq)
srq = dsin(rplusq)
bsz(0) = bessj0(z)
```

```
      bsh(0) = bessj0(h)
      bsz(1) = bessj1(z)
      bsh(1) = bessj1(h)
      bsh(-1) = - bsh(1)
      bs0 = bsz(0)*bsh(0)
         DO 10 m = 2,ms
      bsh(m) = bessj(m,h,bsh(0),bsh(1))
      bsh(-m) = (-1)**m*bsh(m)
10     CONTINUE
         DO 20 k = 2,ks
      bsz(k) = bessj(k,z,bsz(0),bsz(1))
20     CONTINUE
         DO 30 m = 1,ms
      dm(m) = m*delta
      dmu(m) = m*(u-delta)
      rqm(m) = rplusq - m*pi/2.d0
      cmud(m) = dcos(dmu(m))
      smud(m) = m*dsin(dmu(m))
      smd(m) = m*dsin(dm(m))
      cmd(m) = dcos(dm(m))
      crqm(m) = dcos(rqm(m))
      srqm(m) = dsin(rqm(m))
30     CONTINUE
         DO 40 m = -ms,ms
            DO 50 k = 1,ks
      akd(k,m) = a*k*u+m*u-k*phi - m*delta
      rqk(k,m) = (k + m)*pi/2.d0 - rplusq
      pmd(k,m) = k*phi+m*delta
      akm(k,m) = k*a + m
      ckmu(k,m) = dcos(akd(k,m))
      skm(k,m) = akm(k,m)*dsin(pmd(k,m))
      skmu(k,m) = akm(k,m)*dsin(akd(k,m))
      ckmr(k,m) = dcos(rqk(k,m))
      ckm(k,m) = dcos(pmd(k,m))
```

```
      skmr(k,m) = dsin(rqk(k,m))
50       CONTINUE
40    CONTINUE
      fnn = fnu*u
      fnu2 = fnu*fnu
      cfnn = dcos(fnn)
      sfnn = dsin(fnn)
      rqf = rplusq - fnn
      sum1 = cmplx(0.0,0.0)
      sum2 = cmplx(0.0,0.0)
         DO 60 m = 1,ms
      wmn(m) = sfnn*cmud(m) - (cfnn*smud(m) + smd(m))/fnu
      vmn(m) = cfnn*cmud(m) + sfnn*smud(m)/fnu - cmd(m)
      sum1 = sum1 + bsz(0)*bsh(m)/(fnu2 - m*m)*
     * cmplx((wmn(m)*crqm(m) - vmn(m)*srqm(m)),
     * - (wmn(m)*srqm(m) + vmn(m)*crqm(m)))
60    CONTINUE
         DO 70 m = - ms,ms
            DO 80 k = 1,ks
      sum2 = sum2 + bsz(k)*bsh(m)/(fnu2 - (a*k+m)**2)*
     * cmplx((sfnn*ckmu(k,m) - (skm(k,m) + skmu(k,m)*cfnn)/fnu),
     * - (cfnn*ckmu(k,m) - ckm(k,m) + skmu(k,m)*
     * sfnn/fnu))*cmplx(ckmr(k,m),skmr(k,m))
80       CONTINUE
70   CONTINUE
      hfm = fnu/pfr*(bs0/(2.0*fnu2)*cmplx((srq - dsin(rqf)),
     * (crq - dcos(rqf))) + sum1 + sum2)
         RETURN
            END
```

Appendix B

Source code of the noise free complete response of the detector: *CR.F*

```
C       FT of the nosie free complete response of the detector
        IMPLICIT none
        INTEGER k,m,n,ms,ks,j,l
        PARAMETER (ks = 27225,ms = 15,j = 174)
C       [ j ⟶ Number of frequencies bins in the spectrum
C       of the complete response.]
        REAL t,f0,f,dtheta,dphi,dalpha,dbeta0,dgamma,dpsi,h0_p,
     * h0_c,res_n,z,h,bessj0,bessj1,bessj
        PARAMETER (t = 86164.0, f0 = 50.0, f = 49.9995, dtheta = 10.0,
     * dphi = 0.0, dalpha = 46.45, dbeta0 = 0.0, dgamma = 171.8,
     * dpsi = 45.0, h0_p = 1.0, h0_c = 1.0, res_n = 2.0*t)
C       [dgamma = γ^o, dpsi = ψ^o, h0_p & h0_c ⟶ Amplitude of the plus
C       and cross polarisation of the signal respectively and
C       res_n ⟶ resolution of the spectrum.]
        REAL*8 pi,rad,fr,pfr,a,u,rc,theta,phi,epsilon,alpha,
     * psi,beta0,sth,sal,sbe0,sph,sep,cth,cal,cbe0,cph,cep,gamma,ssi,csi
     * ,s2ep,c2ep,s2gm,c2gm,al,am,an,ap,aq,ar,ag,ah,ai,aj,f1_p,f2_p,f3_p
     * ,f4_p,f5_p,sph_c,cph_c,al_c,am_c,an_c,ap_c,aq_c,ar_c,ag_c,ah_c,
     * ai_c,aj_c,f1_c,f2_c,f3_c,f4_c,f5_c,p,q,r,rplusq,delta,crq,srq,fn(0:j)
C       [fn ⟶ frequency bins of the complete response.]
```

```
      REAL*8 bsh(-ms:ms),bsz(0:ks),bs0,dm(1:ms),dmu(1:ms),
     * rqm(1:ms),cmud(1:ms),smud(1:ms),smd(1:ms),cmd(1:ms),crqm(1:ms),
     * srqm(1:ms),akd(1:ks,-ms:ms),rqk(1:ks,-ms:ms),pmd(1:ks,-ms:ms),
     * akm(1:ks,-ms:ms),ckmu(1:ks,-ms:ms),skm(1:ks,-ms:ms),
     * skmu(1:ks,-ms:ms),ckmr(1:ks,-ms:ms), ckm(1:ks,-ms:ms),
     * skmr(1:ks,-ms:ms),fnu(-2:2,0:j),fnn(-2:2,0:j),
     * cfnn(-2:2,0:j),sfnn(-2:2,0:j),rqf(-2:2,0:j),wmn(1:ms,-2:2),
     * vmn(1:ms,-2:2)
      COMPLEX fp2fr,fm2fr,fpfr,fmfr,sum1(-2:2,0:j),sum2(-2:2,0:j),
     * hfm(-2:2,0:j),crp2f(0:j),crp1f(0:j),cr0f(0:j),crm1f(0:j),
     * crm2f(0:j),cr(0:j)
C     [cr ⟶ complete response of the detector and crp2f, crp1f, cr0f,
C     crm2f & crm1f ⟶ complete response at f + 2f_r, f + f_r, f,
C     f − 2f_r & f − f_r respectively.]
      EXTERNAL bessj0,bessj1,bessj

      pi = 4.d0*datan(1.d0)
      rad = pi/180.d0
      fr = 1.d0/86164.d0
      pfr = 2.d0*pi*fr
      a = 1.d0/365.2572d0
      u = 2.d0*pi*fr*t
      rc = 2.d0*pi*f0*0.0637d0/3.d0
      theta = rad*dtheta
      phi = rad*dphi
      epsilon = rad*23.45d0
      alpha = rad*dalpha
      psi = rad*dpsi
      beta0 = rad*dbeta0
      sth = dsin(theta)
      sal = dsin(alpha)
      sbe0 = dsin(beta0)
      sph = dsin(phi)
      sep = dsin(epsilon)
```

```
      cth = dcos(theta)
      cal = dcos(alpha)
      cbe0 = dcos(beta0)
      cph = dcos(phi)
      cep = dcos(epsilon)
      gamma = rad*dgamma
      ssi = dsin(psi)
      csi = dcos(psi)
      s2ep = dsin(2.d0*epsilon)
      c2ep = dcos(2.d0*epsilon)
      s2gm = dsin(2.d0*gamma)
      c2gm = dcos(2.d0*gamma)

C     Beam pattern for plus polarisation

      al = csi*cph - cth*sph*ssi
      am = csi*sph + cth*cph*ssi
      an = - ssi*cph - cth*sph*csi
      ap = - ssi*sph + cth*cph*csi
      aq = sth*sph
      ar = sth*cph
      ag = ((al*aq + am*ar)*sep - (al*an - am*ap)*cep)/2.d0
      ah = ((an*an - ap*ap)*cep*cep - (al*al - am*am) +
     * (aq*aq - ar*ar)*sep*sep - (an*aq + ap*ar)*s2ep)/2.d0
      ai = ((aq*aq - ar*ar)*(s2ep) - (an*an - ap*ap)*s2ep -
     * 2.d0*(an*aq + ap*ar)*c2ep)/2.d0
      aj = ((al*aq + am*ar)*cep + (al*an - am*ap)*sep)/2.d0
      f1_p = h0_p*(ah*s2gm*(cal*cal + 1) - 4.d0*ag*cal*c2gm)/2.d0
      f2_p = h0_p*(ah*cal*c2gm + ag*s2gm*((cal)**2 + 1.d0))
      f3_p = h0_p*(ai*sal*c2gm + aj*dsin(2.d0*alpha)*s2gm)
      f4_p = h0_p*(4.d0*aj*sal*c2gm - ai*dsin(2.d0*alpha)*s2gm)/2.d0
      f5_p = h0_p*sal*sal*s2gm*(ah + al*al - am*am)*3.d0/2.d0

C     Beam pattern for cross polarisation
```

```
      sph_c = dsin(phi - pi/4.d0)
      cph_c = dcos(phi - pi/4.d0)
      al_c = csi*cph_c - cth*sph_c*ssi
      am_c = csi*sph_c + cth*cph_c*ssi
      an_c = - ssi*cph_c - cth*sph_c*csi
      ap_c = -ssi*sph_c + cth*cph_c*csi
      aq_c = sth*sph_c
      ar_c = sth*cph_c
      ag_c = ((al_c*aq_c + am_c*ar_c)*sep - (al_c*an_c -
     * am_c*ap_c)*cep)/2.d0
      ah_c = ((an_c*an_c - ap_c*ap_c)*cep*cep -
     * (al_c*al_c - am_c*am_c) +(aq_c*aq_c - ar_c*ar_c)*sep*sep -
     * (an_c*aq_c + ap_c*ar_c)*s2ep)/2.d0
      ai_c = ((aq_c*aq_c - ar_c*ar_c)*(s2ep) - (an_c*an_c - ap_c*ap_c)*
     * s2ep - 2.d0*(an_c*aq_c + ap_c*ar_c)*c2ep)/2.d0
      aj_c = ((al_c*aq_c + am_c*ar_c)*cep + (al_c*an_c -
     * am_c*ap_c)*sep)/2.d0
      f1_c = h0_c*(ah_c*s2gm*(cal*cal + 1) - 4.d0*ag_c*cal*c2gm)/2.d0
      f2_c = h0_c*(ah_c*cal*c2gm+ag_c*s2gm*((cal)**2 + 1.d0))
      f3_c = h0_c*(ai_c*sal*c2gm + aj_c*dsin(2.d0*alpha)*s2gm)
      f4_c = h0_c*(4.d0*aj_c*sal*c2gm -
     * ai_c*dsin(2.d0*alpha)*s2gm)/2.d0
      f5_c = h0_c*sal*sal*s2gm*(ah_c + al_c*al_c - am_c*am_c)*3.d0/2.d0

C     Both polarisations are suitably arrange to compute
C     complete response

      fp2fr = cmplx((f1_p + f2_c), (f2_p - f1_c))/2.d0
      fm2fr = cmplx((f1_p - f2_c), (- f2_p - f1_c))/2.d0
      fpfr = cmplx((f3_p + f4_c), (f4_p - f3_c))/2.d0
      fmfr = cmplx((f3_p - f4_c), (- f4_p - f3_c))/2.d0

C     Computation for frequncy modulation
```

```
      p = rc*sal*(cbe0*(sth*cep*sph + cth*sep) - sbe0*ar)
      q = rc*sal*(sbe0*(sth*cep*sph + cth*sep) + cbe0*ar)
      z = 2.d0*pi*f0*1496.d0/3.d0*sth
      r = z*cph
      rplusq = r + q
      delta = datan(p/q)
      h = dsqrt(p*p + q*q)
      crq = dcos(rplusq)
      srq = dsin(rplusq)
      bsz(0) = bessj0(z)
      bsh(0) = bessj0(h)
      bsz(1) = bessj1(z)
      bsh(1) = bessj1(h)
      bsh(-1) = - bsh(1)
      bs0 = bsz(0)*bsh(0)
         DO 10 m = 2,ms
      bsh(m) = bessj(m,h,bsh(0),bsh(1))
      bsh(-m) = (-1)**m*bsh(m)
10    CONTINUE
         DO 20 k = 2,ks
      bsz(k) = bessj(k,z,bsz(0),bsz(1))
20    CONTINUE
         DO 30 m = 1,ms
      dm(m) = m*delta
      dmu(m) = m*(u-delta)
      rqm(m) = rplusq - m*pi/2.d0
      cmud(m) = dcos(dmu(m))
      smud(m) = m*dsin(dmu(m))
      smd(m) = m*dsin(dm(m))
      cmd(m) = dcos(dm(m))
      crqm(m) = dcos(rqm(m))
      srqm(m) = dsin(rqm(m))
30    CONTINUE
```

```
      DO 40 m = - ms,ms
          DO 50 k = 1,ks
  akd(k,m) = a*k*u+m*u - k*phi - m*delta
  rqk(k,m) = (k + m)*pi/2.d0 - rplusq
  pmd(k,m) = k*phi + m*delta
            akm(k,m) = k*a + m
  ckmu(k,m) = dcos(akd(k,m))
  skm(k,m) = akm(k,m)*dsin(pmd(k,m))
  skmu(k,m) = akm(k,m)*dsin(akd(k,m))
  ckmr(k,m) = dcos(rqk(k,m))
  ckm(k,m) = dcos(pmd(k,m))
  skmr(k,m) = dsin(rqk(k,m))
50    CONTINUE
40 CONTINUE
      DO 60 n = 0,j
  fn(n) = f + n/res_n
60 CONTINUE
      DO 70 n = 0,j
          DO 80 l = - 2,2
  fnu(l,n) = (f0 - fn(n))/fr + l
  fnn(l,n) = fnu(l,n)*u
  cfnn(l,n) = dcos(fnn(l,n))
  sfnn(l,n) = dsin(fnn(l,n))
  rqf(l,n) = rplusq - fnn(l,n)
  sum1(l,n) = cmplx(0.0,0.0)
  sum2(l,n) = cmplx(0.0,0.0)
      DO 90 m=1,ms
  wmn(m,l) = sfnn(l,n)*cmud(m) - (cfnn(l,n)*smud(m) +
 * smd(m))/fnu(l,n)
  vmn(m,l) = cfnn(l,n)*cmud(m) + sfnn(l,n)*
 * smud(m)/fnu(l,n) - cmd(m)
  sum1(l,n) = sum1(l,n) + bsz(0)*bsh(m)/(fnu(l,n)**2 - m*m)*
 * cmplx((wmn(m,l)*crqm(m) - vmn(m,l)*srqm(m)), -
 * (wmn(m,l)*srqm(m) + vmn(m,l)*crqm(m)))
```

```
90    CONTINUE
          DO 100 m = - ms,ms
              DO 110 k = 1,ks
      sum2(l,n) = sum2(l,n) + bsz(k)*bsh(m)/(fnu(l,n)**2 -
     * (a*k + m)**2)*
     * cmplx((sfnn(l,n)*ckmu(k,m) - (skm(k,m) + skmu(k,m)*cfnn(l,n))/
     * fnu(l,n)), - (cfnn(l,n)*ckmu(k,m) - ckm(k,m)+skmu(k,m)*
     * sfnn(l,n)/fnu(l,n)))*cmplx(ckmr(k,m),skmr(k,m))
110         CONTINUE
100   CONTINUE
      hfm(l,n) = fnu(l,n)/pfr*(bs0/(2.d0*fnu(l,n)**2)*
     * cmplx((srq - dsin(rqf(l,n))),(crq - dcos(rqf(l,n)))) +
     * sum1(l,n) + sum2(l,n))
80        CONTINUE
70    CONTINUE

C       Computation for complete response

          DO 120 n=0,j
      crp2f(n) = fp2fr*hfm(2,n)
      crp1f(n) = fpfr*hfm(1,n)
      cr0f(n) = (cmplx(f5_p,f5_c))*hfm(0,n)
      crm1f(n) = fm2fr*hfm(-1,n)
      crm2f(n) = fmfr*hfm(-2,n)
      cr(n) = crp2f(n) + crp1f(n) + cr0f(n) + crm1f(n) + crm2f(n)
      write(10,*) fn(n),cabs(cr(n)),cabs(crp2f(n))),cabs(crp1f(n))
      write(20,*) fn(n),cabs(crm2f(n)),cabs(crm1f(n))),cabs(cr0f(n))
120   CONTINUE
          STOP
              END
```

Appendix C

Source code for the estimation of templates for all sky search: *TEM.F*

```
C       Estimation of templates for all sky search
        IMPLICIT none
        INTEGER n,nt
        PARAMETER (nt = 721)
        REAL*8 fr,pi
        REAL x,y,f0,st,sig,dtheta,dphi,tdtheta,tdphi(1:nt),sigsig,ff(1:nt),
     * sigtem(1:nt),temtem(1:nt),tem_theta,tem_phi(1:nt),skytem(1:nt)
C       [ff = Fitting Factor, skytem = Number of templates for all sky search]
C       FREQUENCY AND SOURCE LOCATION
        PARAMETER (f0 = 1.0, dtheta = 1.0, tdtheta = 0.999955,
     * dphi = 35.0)
        EXTERNAL st,qromo,sig

        pi = 4.d0*datan(1.d0)
        fr = 1.d0/86164.d0
        x = (f0 - 0.999998d0)/fr
        y = (f0 - 1.000002d0)/fr
        CALL qromo(sig,x,y,dtheta,dphi,dtheta,dphi,sigsig)
        tem_theta = 180.0/(dtheta - tdtheta)
          DO 10 n = 0,nt
```

```
      tdphi(n) = 0.5*float(n)
      tem_phi(n) = abs(360.d0/(dphi + 0.1e-4 - tdphi(n)))
      CALL qromo(sig,x,y,tdtheta,tdphi(n),tdtheta,tdphi(n),temtem(n))
      CALL qromo(st,x,y,dtheta,dphi,tdtheta,tdphi(n),sigtem(n))
      ff(n) = abs(sigtem(n)/(sqrt(sigsig*temtem(n))))
      skytem(n) = tem_theta*tem_phi(n)
      write(10) sngl(ff(n)),skytem(n)
 10   CONTINUE
        STOP
          END


      SUBROUTINE qromo(func,a,b,dtheta,dphi,tdtheta,tdphi,ss)
      INTEGER JMAX,JMAXP,K,KM
      REAL a,b,func,ss,EPS,dtheta,dphi,tdtheta,tdphi
      EXTERNAL func
      PARAMETER (EPS = 1.e-6, JMAX = 14, JMAXP = JMAX+1,
     *K = 5, KM = K-1)
C     USES ratint,midpnt
      INTEGER j
      REAL dss,h(JMAXP),s(JMAXP)
      h(1) = 1.
        DO 10 j = 1,JMAX
      CALL midpnt(func,a,b,dtheta,dphi,tdtheta,tdphi,s(j),j)
        IF (j.ge.K) THEN
      CALL ratint(h(j - KM),s(j - KM),K,0.,ss,dss)
        IF (abs(dss).le.EPS*abs(ss)) RETURN
        ENDIF
      s(j+1) = s(j)
      h(j+1) = h(j)/9.
 10   CONTINUE
      PAUSE 'too many steps in qromo'
        END
```

```
      SUBROUTINE midpnt(func,a,b,dtheta,dphi,tdtheta,tdphi,s,n)
      INTEGER n
      REAL a,b,s,func,dtheta,dphi,tdtheta,tdphi
      EXTERNAL func
      INTEGER it,j
      REAL ddel,del,sum,tnm,x
         IF (n.eq.1) THEN
      s = (b - a)*func(0.5*(a + b),dtheta,dphi,tdtheta,tdphi)
         ELSE
      it = 3**(n - 2)
      tnm = it
      del = (b - a)/(3.*tnm)
      ddel = del + del
      x = a + 0.5*del
      sum = 0.
         DO 10 j=1,it
      sum = sum + func(x,dtheta,dphi,tdtheta,tdphi)
      x = x + ddel
      sum = sum + func(x,dtheta,dphi,tdtheta,tdphi)
      x = x + del
10    CONTINUE
      s = (s + (b - a)*sum/tnm)/3.
         ENDIF
         RETURN
             END


      SUBROUTINE ratint(xa,ya,n,x,y,dy)
      INTEGER n,NMAX
      REAL dy,x,y,xa(n),ya(n),TINY
      PARAMETER (NMAX = 10,TINY = 1.e-25)
      INTEGER i,m,ns
      REAL dd,h,hh,t,w,c(NMAX),d(NMAX)
```

```
      ns = 1
      hh = abs(x - xa(1))
         DO 10 i = 1,n
      h = abs(x - xa(i))
         IF (h.eq.0.) THEN
      y = ya(i)
      dy = 0.0
         RETURN
         ELSE IF (h.lt.hh) THEN
      ns = i
      hh = h
         ENDIF
      c(i) = ya(i)
      d(i) = ya(i) + TINY
10    CONTINUE
      y = ya(ns)
      ns = ns - 1
         DO 20 m = 1,n - 1
             DO 30 i = 1,n - m
      w = c(i + 1) - d(i)
      h = xa(i + m) - x
      t = (xa(i) - x)*d(i)/h
      dd = t - c(i + 1)
         IF(dd.eq.0.)PAUSE 'failure in ratint'
      dd = w/dd
      d(i) = c(i + 1)*dd
      c(i) = t*dd
30      CONTINUE
         IF (2*ns.lt.n - m) THEN
      dy = c(ns + 1)
         ELSE
      dy = d(ns)
      ns = ns - 1
         ENDIF
```

```
      y = y + dy
20    CONTINUE
         RETURN
            END

      FUNCTION sig(fnu,dtheta,dphi)
      REAL sig,fnu,dtheta,dphi
      COMPLEX hfm
      EXTERNAL hfm
      sig = real(hfm(fnu,dtheta,dphi)*conjg(hfm(fnu,dtheta,dphi)))
         RETURN
            END

      FUNCTION st(fnu,dtheta,dphi,tdtheta,tdphi)
      REAL st,fnu,dtheta,dphi,tdtheta,tdphi
      COMPLEX hfm
      EXTERNAL hfm
      st = real(hfm(fnu,dtheta,dphi)*conjg(hfm(fnu,tdtheta,tdphi)))
         RETURN
            END
```

Bibliography

[1] Abramovici, A., Althouse, W.E., Drever, R.W.P., Gürsel,Y., Kanwamura, S., Raab, F.J. Shoemaker, D., Sievers, L., Spero, R.E., Thorne, K.S., Vogt, R.E., Weiss, R., Whitcomb, S.E., and Zucker, Z.E., Sciences **256**, 325, (1992).

[2] Abrmowitz, M. and Stegun, I.A., in *Handbook of Mathematical Functions,* (Dover Publication, New York, 10th printing with corrections of first edition, 1972).

[3] Allen, B., Preprint gr-qc/9607075 (1996).

[4] Allen, B., in *Relativistic Gravitation and Gravitational Radiation,* eds. Marck, J.A. and Lasota, J.P, (Cambridge: Cambridge University Press, 1997).

[5] Andersson, N., Astrophys. J **502**, 708 (1998).

[6] Apostolatos, T.A., Phys. Rev. D **52**, 605, (1995).

[7] Apostolatos, T.A., Phys. Rev. D **54**, 2421, (1996).

[8] Astone, P., Bassan, M., Bonifazi, Carelli, P., Coccia, E., Castellano, M.G., Cavallari, G., Coccia, E., Cosmelli, C., Fafone, V., Frasca, S., Majorana, E., Modena, I., Pallottino, G.V., Pizzella, G., Rapagnami, Ricce, F., and Visco, M., Phys. Rev. D **47**, 362 (1993).

[9] Astone, P., Bassan M., Bonifazi, Carelli, P., Coccia, E., Castellano, Cosmelli, C., Fafone, V., Federici, G., Marini, A., Minenkov, Y., Modena, I., Modestino, G., Moleti, A., Pallottino, G.V., Pizzella, G., Quintieri, L.,

Ronga, F., Terenzi, R., Visco, M. and Votano, L., Preprint gr-qc/0007055 (2000).

[10] Astone, P., Borkowski, K.M., Jaranowski, P. and Królak, A., Preprint gr-qc/0012108 (2000).

[11] Atkinson, K.E., *An Introduction to Numerical Analysis,* (John Wiley & Sons, NewYork, 1978).

[12] Balasubramanian, R. and Dhurandhar, S.V., Phys. Rev. D **50**, 6080 (1994).

[13] Bildsten, L., Astrophys. J. Lett., **501**, L89 (1998).

[14] Blair, D., and Ju, L., Monthly Not. RAS , **283**, 648 (1996).

[15] Blair, D.G., in *Gravitational Wave Data Analysis,* ed. Schutz, B.F., (Kluwer Dordrecht, 1989).

[16] Blair, D.G., in *The Detection of Gravitational Waves,* ed. Blair, D.G., (Cambridge University Press, Cambridge, England, 1991).

[17] Blair, D.G., Ivanov, E.N., Tobaar, M.E. Turner, P.J., Kann, F. and Heng, I.S., Phys. Rev. Lett. **74**, 1908 (1995).

[18] Blanchet, L. and Damour, T., Phil. Tran. R. Soc. London A **320**, 379 (1986).

[19] Blanchet, L. and Damour, T., Pro. Tran. R. Soc. London A **409**, 383 (1987).

[20] Blanchet, L. and Damour, Phys. Rev. D **37**, 1410 (1988).

[21] Blanchet, L. and Damour, T., Ann. Inst. Henri Poincare **50**, 277 (1989).

[22] Blanchet, L. and Damour, Phys. Rev. D **46**, 4304 (1992).

[23] Bonazzola, S. and Gourgoulhon, E., Astron. and Astrophys. **312**, 675 (1996).

[24] Bonazzola, S. and Gourgoulhon, E., in *Relativistic Gravitation and Gravitational Radiation,* ed. Marck, J.A. and Lasota, J.P. (Cambridge University Press, Cambridge, 1996).

[25] Boughn, S.P., Fairbank, W.M., Giffard, R.P., Hlloenhorst, J.N., Mapoles, E.R., McAshan, M.S., Michelson, P.F., Paik, H.J. and Taber, R.C., Astrophy. J. **126**, L19 (1982).

[26] Bracewell, Ron., *The Fourier Transform and Its Application,* (McGraw-Hill, NewYork, 1984), 2nd revised edition.

[27] Bradaschia, C., et al., Nucl. Instum. Methods Phys. Res. A, **289**, 518 (1990).

[28] Brady, P.R., Creighton, T., Cutler, C. and Schutz, B.F., Phys. Rev. D **57**, 2101 (1998).

[29] Brady, P.R. and Creighton, T., Phys. Rev. D **61**, 82001 (2000).

[30] Brigham, E.O., *The Fast Fourier Transform and its Application,* (Prentice-Hall International, 1988).

[31] Brillet, A. et al., VIRGO Final Conceptual Design, INFIN, Pisa (1992).

[32] Clark, J.P.A., and Eardley, D.M. Astrophy. J., **215**, 315 (1977).

[33] Croce, R.P., Demma, Th., Postiglione, F., Pierro, V. and Pinto, I.M., in *2nd TAMA Workshop on Gravitational Wave Detection, Tokyo, Japan* (1999).

[34] Cutler, C., Apostolatos, Bildsten, L., Finn, L.S., Flanagan, E.E., Kennefick, D., Markovic, D.M., Ori, A., Poisson, E., Sussman, G.J. and Thorne, K.S., Phys. Rev. Lett. **70** 2984 (1993).

[35] Cutler, C. and Flanagan, E., Phys. Rev. D **49**, 2658 (1994).

[36] Damour, T., *Three Hundred Years of Gravitation*, (Ed. Hawking, S.W. and Israel, W., (Cambridge University Press, Cambridge, England, 1987).

[37] Damour, T., in *Gravitation in Astrophysics*, eds. Carter, B. and Hartle, J.B. (Plenum: NewYork, 1987b).

[38] Damour, T., in *Gravitational Radiation*, eds. Deruelle, N. and Piran, T., (North-Holland, Amsterdam, 1983).

[39] Damour, T. and Iyer, B.R., Ann. Inst. H. Poincare, Phys. Theor., **54(2)**, 115 (1991).

[40] Damour, T. and Taylor, J.H., Astrophy. J **356**, 501 (1991).

[41] Damour, T. and Taylor, Phys. Rev. D **45**, 1840 (1992).

[42] Damour, T. and Gibbons, G. and Taylor, J.H., Phys. Rev. Lett. **61**, 1151 (1988).

[43] Danzmann, K., in *Gravitational Wave Experiment,* eds. Coccia, E., Pizzela, G., and Ronga, F., (World Scientific Publishing Co. Pte. Ltd., Singapore, 1995).

[44] Davis, M.M.A., in *Gravitational Wave Data Analysis,* ed. Schutz, B.F., (Kluwer Academic Publishers, 1989).

[45] Dhurandhar, S.V., Proceedings of the Fourth International Conference on Gravitation and Cosmology, Pramana J. Phys. **55**, 545 (2000).

[46] Dhurandhar, S.V. and Sathyaprakash, B.S., Phys. Rev. D **49**, 1707 (1994).

[47] Dhurandhar, S.V. and Tinto, M., Monthly Not. RAS **234**, 663 (1998).

[48] Drever, R.W.P., *Gravitational Radiation,* eds. Deruelle, N. and Piran, T., (North-Holland, Amsterdam, 1983).

[49] Einstein, A., Preuss. Akad. Wiss. Berlin, Sitzungaberichte der physikalisch-mathemamatischen Klass, p. 688 (1916).

[50] Einstein, A., Preuss. Akad. Wiss. Berlin, Sitzungaberichte der physikalisch-mathemamatischen Klass, p. 154 (1918).

[51] Epstein, R. and Wagoner, R.V., Astrophy. J., **197**, 717 (1975).

[52] Frasca, S., International Journal of Modern Physics D **9**, 369 (2000).

[53] Freund, J.E. and Walpole, R.E., in *Mathematical Statistics,* (Prientice Hall of India Pvt. Ltd, New Delhi, 1987).

[54] Gertsenshtein, M.E. and Pustovoit, V.I., Soviet Physics - JETP **16**, 433 (1962).

[55] Gürsel, Y. and Tinto, M., Phys. Rev. D **40**, 3884 (1989).

[56] Giazotto, A. in *Gravitational Wave Experiments,* Coccia, E., Pizzella, G. and Ronga, F., (World Scientific Publishing Co. Pte. Ltd., Singapore, 1995) p. 86.

[57] Giazotto, A., Bonazzola and Gourgoulhon, E., Phys. Rev. D , **55**, 2014 (1997).

[58] Goldstein, H., *Classical Mechanics* (Addison-Wesley New York, 1980), p. 143.

[59] Green, R.M., *Spherical Astronomy,* (Cambridge University Press, Cambridge, England, 1985), p. 40.

[60] Grishchuk, L.P., Class. Quant. Gravity **14**, 1445 (1997).

[61] Grishchuk, L.P., Lipunov, V.M., Postnov, K.A., Prokhorov and Sathyaprakash, B.S., Preprint astro-ph/0008481 (2000).

[62] Helstrom, C.W., *Statistical Theory of Signal Detection,* 2nd ed. (Pergamon Press, London, 1968).

[63] Hulse, R.A. and Taylor J.H., Astrophy. J. Lett. **195**, L51-53 (1975).

[64] Jaranowski, P. and Królak, A., Phys. Rev. D **49**, 1723 (1994).

[65] Jaranowski, P., Królak, A., and Schutz, B.F., Phys. Rev. D **58**, 063001 (1998).

[66] Jaranowski, P. and Królak, A., Phys. Rev. D **59**, 063003 (1999).

[67] Jaranowski, P. and Królak, A., Phys. Rev. D **61**, 062001 (2000).

[68] Jotania, K. and Dhurandhar, S.V., Bull. Astron. Soc. India, **22**, 303 (1994).

[69] Jotania, K., *Some Aspects of Gravitational Waves Signal Analysis from Coalescing Binaries and Pulsars,* Ph.D. thesis, unpublished (1994).

[70] Jotania K. and Dhurandhar, S.V., Astron. and Astrophys. **306**, 317-325, (1996).

[71] Jotania, K., Wagh, S.M. and Dhurandhar, S.V., Phys. Rev. D **46**, 2507, (1992).

[72] Królak, A., Preprint gr-qc/9704044 (1997).

[73] Królak, A., Preprint gr-qc/9903099 (1999).

[74] Królak, A. in *Gravitational Wave Data Analysis,* ed. Schutz, B.F., (Kluwer, Dordrecht, 1989), p. 59.

[75] Królak, A., Lobo, J.A. and Meers, B.J., Phys. Rev. D **43**, 2470 (1991).

[76] Kulkarni, S.R., Philos. Trans. R. Soc. London **341**, 77 (1992).

[77] Landau, L.D., and Lifshitz, E.M., *Mechanics,* (Oxford, England: Pergamon Press, 1969).

[78] Landau, L.D., and Lifshitz, E.M., *The classical theory of fields,* (Oxford, England: Pergamon Press, 1975).

[79] Levine, J. and Garwin, R., Phys. Rev. Lett. **33**, 794 (1974).

[80] Lindblom, L., Owen, B.J. and Morsink, S.M., Phys. Rev. Lett. **80**, 4843 (1998).

[81] Lincoln, C.W., and Will, C.M., Phys. Rev. D **42**, 1123 (1990).

[82] Livas, J.C., *Upper limits for Gravitational Radiation from Astrophysical Sources,* Ph.D. Thesis, MIT, Cambridge (1987).

[83] Manchester, R.N., Philos. Trans. R. Soc. London **341**, 3 (1992).

[84] Mauceli, E., Geng, Z.K., Hamilton, W.O., Johnson, W.W., Merkowitz, S., Morse, A., Price, B. and Solomonson, N., Phys. Rev. D **54**, 1264 (1996).

[85] Mauceli, E., McHugh, M.P., Hamilton, W.O., Johnson, W.W., and Morse, A., Preprint gr-qc/0007023 (2000).

[86] Misner, C.W., Thorne, K.S., Wheeler, J.A. *Gravitation,* (San Francisco: W.H. Freeman and Company, 1973).

[87] Mohanty, S.D. and Dhurandhar, S.V., Phys. Rev. D **54**, 7108 (1996).

[88] Mohanty, S.D., Phys. Rev. D **57**, 630 (1998).

[89] Narayan, R., Piran, T., Shemi, A., *Astrophys. J. Lett.* **379**, L17 (1991).

[90] Newman, E.T. and Penrose, R., J. Math. Phy. **3**, 566 (1962).

[91] Owen, B.J., Phys. Rev. D **53**, 6749 (1996).

[92] Owen, B.J., Lindblom, L., Cutler, C., Schutz, B.F., Vecchio, A. and Andersson, N., Phys. Rev. D **58**, 084020 (1998).

[93] Owen, B.J. and Sathyaprakash, B.S., Phys. Rev. D **60**, 022002 (1999).

[94] Papoulis, A., *Signal Analysis,* (McGraw-Hill Inc., Singapore, 1977).

[95] Phinney, E.S., *Astrophys. J. Lett.*, **330**, L17 (1991).

[96] Press, W.H., Flannery, B.P., Teukolsky, S.A. and Vetterling, W.T., *Numerical Recipes, The Art of Scientific Computing,* (Cambridge University Press, Cambridge, England, 1986).

[97] Richard, J.P. and Folkner, W.M., in *The Detection of Gravitational Waves,* ed. Blair, D.G., (Cambridge University Press, Cambridge, England, 1991).

[98] Sathyaprakash, B.S., Preprint gr-qc/0012014 (2000).

[99] Sathyaprakash, B.S., Phys. Rev. D **50**, R7111 (1994).

[100] Sathyaprakash, B.S. in *Relativistic Gravitation and Gravitational Radiation,* eds. Marck, J.A. and Lasota, J.P, (Cambridge: Cambridge University Press, 1997).

[101] Sathyaprakash, B.S., in *Black Holes, Gravitational Radiation and the Universe,* eds. Iyer, B.R. and Bhawal, B., (Kluwer Academic Publishers, Dordrecht, 1999).

[102] Sathyaprakash, B.S. and Dhurandhar, S.V., Phys. Rev. D **44**, 3819 (1991).

[103] Sathyaprakash, B.S. and Dhurandhar, S.V., J. Computational Phys. **109**, 215 (1993).

[104] Saulson, P.R., *Fundamentals of Interfeometric Gravitational Wave Detectors,* (World Scientific Publishing Co. Pte. Lts., 1994).

[105] Schutz, B.F., *A First Course in General Relativity,* (Cambridge University Press, Cambridge, England, 1989).

[106] Schutz, B.F., Nature **323**, 310 (1986).

[107] Schutz, B.F., Class. Quant. Gravity **6**, 1761 (1989b).

[108] Schutz, B.F., in *Gravitational Wave Data Analysis,* ed. Schutz, B.F., (Kluwer, Dordrecht, 1989).

[109] Schutz, B.F., in *The Detection of Gravitational Waves,* ed. Blair, D.G., (Cambridge University Press, Cambridge, England, 1991).

[110] Schutz, B.F., Class. Quant. Gravity **10**, S135 (1993b).

[111] Schutz, B.F., in *Relativistic Gravitation and Gravitational Radiation,* eds. Marck, J.A. and Lasota, J.P, (Cambridge University Press, Cambridge, England, 1996).

[112] Schutz, B.F., Preprint gr-qc/9802020 (1998).

[113] Schutz, B.F., Class. Quant. Gravity **16**, A131 (1999).

[114] Schutz, B.F., Preprint gr-qc/9911034 (1999).

[115] Schutz, B.F., and Papa, M.A., Preprint gr-qc/9905018 (1999).

[116] Schutz, B.F., and Tinto, M., Monthly Not. RAS **224**, 131 (1987).

[117] Shanmugam, K.S., Breiphol, A.M., *Random Signals: Detection, Estimation and Data Analysis,* (Willey, NewYork, 1989).

[118] Shapiro, S.L. and Teukolsky, S.A., black Holes, White Dwarfs and Neutron Stars, (Willey-interscience: NewYork, 1985).

[119] Smart, W.M., in *Textbook on Spherical Astronomy*, (Cambridge University Press, Cambridge, 1977).

[120] Taylor, J.H., Fowler, L.A and McCulloch, P.M., Nature **227**, 437 (1979).

[121] Taylor, J.H., Wesberg, J.H., Astrophy. J. **253**, 908 (1982), Astrophy. J. **345**, 434, (1989).

[122] Taylor, J.H., Wlaszczan, Damour, T. and Weisber, J.M., Nature **355**, 132 (1992).

[123] Thorne, K.S., in *Three Hundred Years of Gravitation.* eds. Hawking, S.W., Israel, W., (Cambridge University Press, Cambridge, 1987).

[124] Thorne, K.S., Rev. Mod. Phy. **52**, 285 (1980a).

[125] Thorne, K.S., Rev. Mod. Phy. **52**, 299 (1980b).

[126] Thorne, K.S., Preprint gr-qc/9506086 (1995).

[127] Tsubona, K., et al., in *Gravitational Wave Detection,* Proceeding of the TAMA International Workshop on Gravitational Wave Detection eds. Tsubono, K., Fujimoto, M.K. and Kuroda, K., (Universal Academy. Tokyo, 1997).

[128] Vinet, J.Y., Meers, B.J., Mann, C.N. and Brillet, A., Phys. Rev. D **38**, 433 (1998).

[129] Wagoner, R.V. and Will C.M., Astrophy. J. **210**, 764 (1976).

[130] Wagoner, R.V., Astrophy. J. **278**, 345 (1984).

[131] Wainstein, L.A. and Zubakov, L.D., *Extraction of Signals from noise,* (Prentice-Hall, Englewood, NJ, 1962).

[132] Weber, J., *General Relativity and Gravitational Waves* (New York: Interscience, 1961).

[133] Weber, J., Phys. Rev. **117**, 306 (1960).

[134] Weber, J., Phys. Rev. Lett. **18**, 498 (1967).

[135] Weber, J., Phys. Rev. Lett. **18**, 1302 (1969).

[136] Weber, J., Phys. Rev. Lett. **22**, 1320 (1969).

[137] Weiss, R., Quarterly Progress report of the Research Laboratory of Electronics of the Masachusetts Institute of technology **105**, 54 (1972).

[138] Weiss, R., Reviews of Modern Physics **71**, S187 (1999).

[139] Weyl, H., *Space-Time-Matter,* (Methuen: London, 1992).

[140] Williams, P.R., and Schutz, B.F., Preprint gr-qc/9912029 (1999).

[141] Wiseman, A.G., Phys. Rev. D **46**, 1517 (1992).

[142] Woosley, S.E. and Weaver, T.A., Ann. Rev Astron. Astrophy, **24**, 205 (1986).

[143] Zimmermann, M. and Szedenits, E., Phys. Rev. D **20**, 351 (1979).

[144] Zimmermann, M., Phys. Rev. D **21**, 891 (1980).